

DEFENCE



DÉFENSE

Design and Optimization of a Wideband Printed-Dipole Array

B.G. Duffley
Royal Military College of Canada

G.A. Morin
Defence Research Establishment Ottawa

Y.M.M. Antar
Royal Military College of Canada

DISTRIBUTION STATEMENT A
Approved for Public Release
Distribution Unlimited

DEFENCE RESEARCH ESTABLISHMENT OTTAWA

TECHNICAL REPORT
DREO TR 1999-122
November 1999



National
Defence

Défense
nationale

Canada

DTIC QUALITY INSPECTED 1

20000118 140



Design and Optimization of a Wideband Printed-Dipole Array

B.G. Duffley
Royal Military College of Canada

G.A. Morin
*MIL SAT Communications Group
Space Systems & Technology Section*

Y.M.M. Antar
Royal Military College of Canada

DEFENCE RESEARCH ESTABLISHMENT OTTAWA

TECHNICAL REPORT
DREO TR 1999-122
November 1999

Project
5CA12

ABSTRACT

Modern satellite and mobile communications systems continue to push the bandwidth requirement of antenna subsystems. Printed microstrip architectures have been widely investigated and are attractive for their conformability, small size and cost effectiveness. While vigorous research activity over the past two decades has improved the bandwidth of microstrip elements to upwards of 30%, this may not be adequate for the future system demands of multipurpose antennas. In this report, printed-dipole arrays are investigated. They have the advantage of large bandwidths, up to 100%. Arrays of this type were described in the literature, however, no detailed analysis or measurements were provided. For this report, a 32-element wideband printed-dipole array was fabricated, analyzed from 4 to 20 GHz and successfully optimized for improved bandwidth performance in excess of an octave. The important design parameters were extracted and their effect on performance were demonstrated.

RÉSUMÉ

Les systèmes modernes de télécommunication par satellite et des services mobiles imposent aux sous-systèmes d'antenne des exigences de plus en plus grandes en matière de largeur de bande. Les architectures microruban imprimé ont fait l'objet de nombreuses études, et elles sont intéressantes en raison de leur conformabilité, de leur petite taille et de leur efficacité en fonction du coût. Bien que les travaux intensifs de recherche menés au cours des deux dernières décennies aient permis d'accroître la largeur de bande des éléments microruban à plus de 30 %, il se peut que cet accroissement ne soit pas suffisant pour permettre aux antennes polyvalentes de répondre aux exigences des systèmes futurs. Le présent rapport traite des réseaux de doublets imprimés. Ceux-ci ont l'avantage d'offrir de grandes largeurs de bandes pouvant atteindre jusqu'à 100 %. La littérature contient des descriptions de réseaux de ce type, mais elle ne mentionne pas d'analyses approfondies ni de mesures exhaustives. Aux fins du présent rapport, un réseau de doublets imprimés à large bande comprenant 32 éléments a été fabriqué, analysé entre 4 et 20 GHz et optimisé efficacement pour donner une largeur de bande accrue de plus d'un octave. Les paramètres de conception importants ont été isolés et leur effet sur la performance a été démontré.

EXECUTIVE SUMMARY

Modern satellite and mobile communications systems continue to push the bandwidth capabilities of antenna subsystems. Printed microstrip architectures have been widely investigated and are attractive for their conformability, small size and cost effectiveness. While vigorous research activity over the past two decades has improved the bandwidth of microstrip elements to upwards of 30%, this may not be adequate for the future system demands of multipurpose antennas. An architecture, which can meet these difficult bandwidth requirements, is undergoing a resurgence in research interest, that being the double-sided printed-dipole.

Though not truly a microstrip device, due to its relatively large ground plane spacing and balanced feed line, it shares many similarities with the classic microstrip structure. Primarily, they are both printed devices. However, unlike the more common microstrip antenna element, which is severely limited by its bandwidth, the double-sided printed-dipole possesses an exceptionally wide operational bandwidth. Configurations using arrays of this type of structure were described in the literature, however, no detailed analysis or comprehensive measurements were provided. The starting point was therefore to consider and analyze a recently reported topology of double-sided printed-dipoles.

A 32-element wideband printed-dipole array was fabricated, analyzed from 4 to 20 Ghz and successfully optimized for improved bandwidth performance in excess of an octave. Various aspects of the architecture, which control the performance of the antenna, have been investigated including the wideband balun and launcher system. A double-ended balun test arrangement was devised which yielded return losses less than 15 dB and provided an indication of frequency dependant conductive losses. The array's height over the ground-plane was determined to have the greatest effect on maximum bandwidth as the $1/2\lambda$ boresight null actually began to have significant effect before the height approached $3/8\lambda$. Simulations using vertically fed elements in *IE3D*[™] yielded excellent correlation between simulated and measured radiation patterns and also indicated that mutual coupling was not significant, while identifying that most current resides on the sides of the rectangular dipole elements. The software was also used to develop an improved wideband antenna element for future exploitation. This simulation effort also indicated the general insensitivity of the element's performance to dimensional changes which is a very positive feature for mass production.

Range measurements indicated that optimization of element spacing could yield improved radiation efficiency. Pattern measurements demonstrated very good cross-pol in excess of -30 dB as well as acceptable side lobe levels from 4 to 14 Ghz.

Duffley, B.G., Morin, G.A., Antar, Y.M.M., Design and Optimization of a Wideband Printed-Dipole Array, Defence Research Establishment Ottawa, DREO TM 1999-122. November 1999.

SOMMAIRE

Les systèmes modernes de télécommunication par satellite et des services mobiles imposent aux sous-systèmes d'antenne des exigences de plus en plus grandes en matière de largeur de bande. Les architectures microruban imprimé ont fait l'objet de nombreuses études, et elles sont intéressantes en raison de leur conformabilité, de leur petite taille et de leur efficacité en fonction du coût. Bien que les travaux intensifs de recherche menés au cours des deux dernières décennies aient permis d'accroître la largeur de bande des éléments microruban à plus de 30 %, il se peut que cet accroissement ne soit pas suffisant pour permettre aux antennes polyvalentes de répondre aux exigences des systèmes futurs. Une architecture qui peut satisfaire à ces exigences élevées en matière de largeur de bande, soit le doublet imprimé double face, connaît un nouvel essor dans le domaine de la recherche.

Bien qu'il ne soit pas réellement un dispositif microruban, en raison des dimensions relativement importantes de l'espacement entre la masse et la ligne d'alimentation symétrique, ce type de doublet présente un grand nombre de similitudes avec la structure microruban classique. La principale similitude des deux types de structures est qu'elles sont toutes deux des dispositifs imprimés. Cependant, contrairement à l'antenne élémentaire microruban plus courante, qui est fortement limitée par sa largeur de bande, le doublet imprimé double face possède une largeur de bande opérationnelle exceptionnellement étendue. La littérature contient des descriptions de configurations à réseaux de ce type, mais elle ne mentionne pas d'analyses approfondies ni de mesures exhaustives. Le point de départ consistait donc à prendre en considération et à analyser une topologie de doublets imprimés double face dont on a récemment fait mention.

Un réseau de doublets imprimés à large bande comprenant 32 éléments a été fabriqué, analysé entre 4 et 20 GHz et optimisé efficacement pour donner une largeur de bande accrue de plus d'un octave. Divers aspects de l'architecture, qui déterminent la performance de l'antenne, ont été étudiés, y compris le balun à large bande et l'adaptateur coaxial. On a conçu un montage d'essai de deux baluns bout-à-bout donnant un affaiblissement des courants réfléchis inférieur à 15 dB et fournissant une indication des pertes par conduction dépendantes de la fréquence. On a déterminé que la hauteur du réseau par rapport à la masse était le facteur qui influait le plus sur la largeur de bande maximale, étant donné que le zéro de l'axe de pointage normal dû à une hauteur de $1/2 \lambda$ commençait en réalité à exercer un effet appréciable avant que la hauteur s'approche de $3/8 \lambda$. Des simulations faisant appel à des éléments à alimentation verticale et effectuées à l'aide du logiciel *IE3D^{mc}* ont donné une excellente corrélation entre les diagrammes de rayonnement simulés et les diagrammes mesurés. Elles ont également montré que le couplage mutuel n'était pas important et que la plus grande partie du courant se retrouvait sur les côtés des éléments de doublets rectangulaires. On s'est aussi servi du logiciel pour mettre au point une antenne élémentaire à large bande améliorée à des fins d'exploitation

future. Ces travaux de simulation ont aussi montré que la performance des éléments était en général indépendante des variations dimensionnelles, ce qui constitue un avantage pour la production en série.

Des mesures en chambre anéchoïde ont montré que l'optimisation de l'espacement des éléments pouvait se traduire par un meilleur rendement de rayonnement. Des mesures de diagrammes ont montré une très bonne polarisation croisée, dépassant -30 dB, de même que des niveaux de lobes secondaires acceptables entre 4 et 14 GHz.

Duffley, B.G., Morin, G.A., Antar, Y.M.M., Design et Optimisation d'un Réseau d'Antenne à Large-Bande Fait de Dipôles Imprimés, Le Centre de recherches pour la défense Ottawa, DREO TM 1999-122, novembre 1999. (en anglais)

TABLE OF CONTENTS

ABSTRACT	III
RÉSUMÉ.....	III
EXECUTIVE SUMMARY	V
SOMMAIRE	VI
TABLE OF CONTENTS	IX
LIST OF FIGURES.....	XIII
LIST OF TABLES.....	XV
ABBREVIATIONS.....	XVII
1. INTRODUCTION	1
1.1 INTRODUCTION	1
1.2 THESIS OBJECTIVES.....	2
1.3 ORGANIZATION OF REPORT	2
2. PRINTED WIDEBAND ANTENNAS	5
2.1 GENERAL	5
2.2 BANDWIDTH DEFINITIONS	5
2.3 APPLICATIONS FOR WIDEBAND ANTENNAS	6
2.3.1 <i>GPS and GLONASS</i>	6
2.3.2 <i>SAR</i>	6
2.3.3 <i>Satellite Communications – Direct Broadcast Satellite (DBS)</i>	7
2.3.4 <i>Electronic Support Measures (ESM)</i>	7
2.4 VARIOUS WIDEBAND ENHANCEMENT TECHNIQUES	7
2.4.1 <i>Impedance matching</i>	8
2.4.2 <i>Coplanar matching networks</i>	8
2.4.3 <i>Series capacitance</i>	9
2.4.4 <i>Multiple resonances</i>	10
2.4.5 <i>Strip-Slot-Foam-Inverted-Patch (SSFIP) Antenna</i>	11
2.4.6 <i>Annular rings</i>	12
2.4.7 <i>Aperture coupled parallel resonators</i>	12
2.4.8 <i>U-slot rectangular patch</i>	13
2.4.9 <i>Loading and losses</i>	14
2.4.10 <i>End loading</i>	14
2.4.11 <i>Other structures</i>	15
2.5 DESIGN AND FABRICATION ISSUES	15
2.6 DISCUSSION OF <i>IE3D</i> SOFTWARE	16
2.6.1 <i>Theory of operation</i>	16
3. WIDEBAND PRINTED-DIPOLE ARRAYS.....	17
3.1 GENERAL	17
3.2 BASIC DIPOLE THEORY	17
3.3 HORIZONTAL DIPOLE OVER A GROUND-PLANE	18
3.4 ARRAY CONSIDERATIONS.....	19

3.5	THICK DIPOLE THEORY	20
3.6	THE WIDEBAND PRINTED-DIPOLE	20
3.7	COMPONENTS OF THE WIDEBAND PRINTED-DIPOLE ARRAY	21
3.7.1	<i>Microstrip to coax transition</i>	21
3.7.2	<i>The K Connector™</i>	24
3.7.3	<i>Connector to antenna interface</i>	25
3.7.4	<i>Wideband balun</i>	27
3.7.5	<i>Balanced transmission line</i>	28
3.7.6	<i>Feed network</i>	29
3.8	PRINTED-DIPOLES – DIFFERENCE FROM CLASSICAL MICROSTRIP	29
4.	ANALYSIS OF U OF B PRINTED-DIPOLE ARRAY	31
4.1	INTRODUCTION	31
4.2	PHYSICAL DESCRIPTION OF DESIGN	31
4.3	ANALYSIS OF THE WIDEBAND BALUN	33
4.3.1	<i>S parameter measurements of the double balun</i>	34
4.3.2	<i>TDR Measurements of the double balun</i>	36
4.3.3	<i>Simulation software validation and limitations</i>	37
4.4	SIMULATED ELEMENT AND ARRAY PERFORMANCE	38
4.4.1	<i>Single element</i>	38
4.5	INVESTIGATION OF MUTUAL COUPLING	39
4.6	ANTENNA RETURN LOSS AND TDR MEASUREMENT	39
4.6.1	<i>S11 measurement of the U of B Array</i>	39
4.6.2	<i>TDR measurement of the U of B Array</i>	40
4.7	REPRESENTATIVE RADIATION PATTERNS	41
4.8	COMPARISON OF SIMULATED AND MEASURED RADIATION PATTERNS	43
4.8.1	<i>Coordinate system for measurements</i>	44
4.9	BORESIGHT GAIN MEASUREMENT USING THE GAIN TRANSFER METHOD	45
4.9.1	<i>Gain measurement results</i>	46
4.10	RADIATION EFFICIENCY OF U OF B ARRAY (5.77MM)	47
4.11	SUMMARY OF PERFORMANCE	48
4.12	RATIONALE FOR ENHANCEMENT	49
5.	IMPROVED WIDEBAND PRINTED-DIPOLE ARRAY DESIGN	51
5.1	INTRODUCTION	51
5.2	VSWR OPTIMIZATION	51
5.3	ELEMENT SPACING	53
5.4	PHYSICAL DESCRIPTION OF THE DESIGN	55
5.5	MEASUREMENT RESULTS	57
5.5.1	<i>S11 return loss of Optimized Array-1 (6.35mm)</i>	57
5.5.2	<i>TDR measurement of Optimized Array-1 (6.35mm)</i>	57
5.6	GAIN MEASUREMENT USING THREE ANTENNA METHOD	58
5.7	RADIATION EFFICIENCY COMPARISON OF THE UNIVERSITY OF BELGRADE DESIGN AND OPTIMIZED ARRAY-1	60
5.8	REPRESENTATIVE RADIATION PATTERNS	61
5.9	FEED NETWORK ISSUES	62
5.9.1	<i>Losses</i>	62
5.10	SUMMARY OF PERFORMANCE	64
5.11	FURTHER ENHANCEMENTS	65
6.	OPTIMIZATION OF ARRAY HEIGHT OVER GROUND AND IMPROVED WIDEBAND DIPOLE MATCHING	67
6.1	INTRODUCTION	67
6.2	RATIONALE FOR IMPROVEMENT BY ELEMENT SHAPE MODIFICATION	67
6.3	COMPARISON OF RETURN LOSSES AT 8MM HEIGHT	69
6.4	COMPARISON OF BORESIGHT GAINS VS. FREQUENCY	71

6.5	COMPARISON OF RADIATION EFFICIENCIES AT 8MM GROUND-PLANE SPACING.....	72
6.6	REPRESENTATIVE RADIATION PATTERNS	73
6.7	SUMMARY OF PERFORMANCE.....	73
6.8	SOURCES OF ERROR.....	74
6.8.1	<i>Connectors</i>	74
6.8.2	<i>Accurate permittivities, loss tangents and homogeneity</i>	74
6.8.3	<i>Dimensional errors</i>	74
6.8.4	<i>Multipath</i>	75
7.	CONCLUSION AND RECOMMENDATIONS FOR FUTURE WORK	77
7.1	CONCLUDING REMARKS.....	77
7.2	ACCOMPLISHMENTS.....	77
7.3	FUTURE WORK	78
	REFERENCES	81
	APPENDIX A MATLAB® PROGRAM FOR GAIN TRANSFER CALCULATION	85
	APPENDIX B ANECHOIC CHAMBER MEASUREMENT SETUP	91
	APPENDIX C ROHACELL 31 HF™ MATERIAL DATA	93
	APPENDIX D ARLON CUCLAD 217™ MATERIAL DATA	95
	APPENDIX E U OF B ARRAY (5.77MM) E- AND H-PLANE CUTS FOR VARIOUS FREQUENCIES	97
	APPENDIX F U OF B ARRAY (5.77MM) VARIOUS PATTERN CUTS AT 10 GHZ.....	101
	APPENDIX G OPTIMIZED ARRAY-1 (6.35MM) E- AND H-PLANE CUTS FOR VARIOUS FREQUENCIES	103
	APPENDIX H OPTIMIZED ARRAY-1 (6.35MM) VARIOUS PATTERN CUTS AT 10 GHZ ...	107
	APPENDIX I U OF B ARRAY (8.0 MM) E- AND H-PLANE CUTS FOR VARIOUS FREQUENCIES	109
	APPENDIX J OPTIMIZED ARRAY-1 (8.0MM) E- AND H-PLANE CUTS FOR VARIOUS FREQUENCIES	113

LIST OF FIGURES

Table 1. Bandwidth definitions	5
Figure 1. Coplanar passive matching	9
Figure 2. Implementation of series capacitance to compensate for probe inductance	9
Figure 3. Capacitive patch	10
Figure 4. Strip Slot Foam Inverted Patch Antenna	11
Figure 5. Double Shorted Annular Patch	12
Figure 6. Varying length aperture coupled parallel dipoles used for wide bandwidth	13
Figure 7. U-Slot Element	14
Figure 8. Triangular microstrip antenna with chip resistor loading	15
Figure 9. Horizontal dipole radiation pattern and current distribution	18
Figure 10. Radiation pattern of a horizontal dipole over a ground-plane	19
Figure 11. Printed-dipole element	21
Figure 12. Evolution of microstrip line from coaxial line by unfolding	22
Figure 13. Typical Coaxial to microstrip transition	23
Figure 14. Effect of a gap between the connector flange and the antenna fixture	23
Figure 15. Cross section of Eisenhart connector	24
Figure 16. K Connector™ flange mount assembly (inches)	25
Figure 17. K Connector™ to printed antenna interface (side-view)	26
Figure 18. Microstrip connector test arrangement	26
Figure 19. Wideband balun (top-view)	28
Figure 20. Field patterns of microstrip and balanced transmission line	29
Figure 21. Microstrip patch antenna	30
Figure 22. University of Belgrade wideband printed-dipole array	32
Table 2. Dimensions of the University of Belgrade wideband array	32
Figure 23. Photo of wideband printed-dipole array	33
Figure 24. Balun test setup	34
Figure 25. Photo of double balun	34
Figure 26. Double balun S_{11} and S_{22}	35
Figure 27. Double balun S_{21}	36
Figure 28. Double balun TDR of Ports 1 and 2	37
Figure 29. Current distribution on a single wideband dipole element at 10 GHz	38
Figure 30. S_{11} of the U of B wideband array	40
Figure 31. TDR of U of B wideband printed-dipole array	41
Figure 32. Representative U of B wideband array (10 GHz) E and H-plane patterns	42

Figure 33. Photo of DDARLing anechoic chamber.....	42
Figure 34. Comparison of simulated (<i>ARPS™/IE3D™</i>) vs. measured radiation pattern.....	44
Figure 35. Relationship between the AUT and the spherical coordinate system.....	45
Figure 36. S_{21} of AUT and reference antenna.....	46
Figure 37. U of B Array(5.77mm) measured and theoretical gain	47
Figure 38. Radiation Efficiency of U of B Array (5.77mm).....	48
Table 3. Summary of U of B wideband array performance.....	49
Figure 39. Gain change due to variation of array height over the ground plane.....	52
Figure 40. Gain variation due to height over ground change.....	53
Figure 41. Current distribution at 10 GHz of 5 elements at optimized spacing.....	54
Figure 42. Mutual coupling of 5 elements of Optimized Array-1(6.35mm).....	55
Figure 43. Optimized Array-1 (6.35mm) physical layout.....	56
Table 4. Dimensions of Optimized Array-1 (6.35mm).....	56
Figure 44. S_{11} of Optimized Array-1	57
Figure 45. TDR of Optimized Array-1	58
Figure 46. S_{21} measurements for three-antennas	59
Figure 47. Optimized Array-1 gain using the 3 antenna method.....	60
Figure 48. Radiation efficiency of U of B and Optimized Array-1 designs	61
Figure 49. Representative Optimized Array-1 E and H-plane patterns	62
Figure 50. Comparison of feed network losses.....	63
Table 5. Summary of Optimized Array-1 performance	64
Figure 51. Smith chart of Original U of B wideband dipole element	68
Figure 52. Smith chart of improved wideband dipole element.....	68
Figure 53. Original and improved wideband dipole elements	69
Figure 54. S_{11} of the U of B Array at 8mm ground-plane spacing	70
Figure 55. S_{11} of Optimized Array-1 at 8mm ground-plane spacing.....	70
Figure 56. U of B Array gain at 8mm ground-plane spacing.....	71
Figure 57. Optimized Array-1 gain at 8mm ground-plane spacing	72
Figure 58. Radiation efficiency of the U of B and Optimized Array-1 at 8mm height.....	73
Table 6. Summary of U of B and Optimized Array-1 Performance	74
Table 7. Physical Properties of Rohacell 31 HF™.....	93
Table 8. Electrical Properties of Rohacell 31 HF™.....	93
Table 9. Physical and Electrical Properties of Arlon CuLad 217™.....	95

LIST OF TABLES

Table 1. Bandwidth definitions	5
Table 2. Dimensions of the University of Belgrade wideband array	32
Table 3. Summary of U of B wideband array performance.....	49
Table 4. Dimensions of Optimized Array-1 (6.35mm)	56
Table 5. Summary of Optimized Array-1 performance.....	64
Table 6. Summary of U of B and Optimized Array-1 Performance	74
Table 7. Physical Properties of Rohacell 31 HF™	93
Table 8. Electrical Properties of Rohacell 31 HF™	93
Table 9. Physical and Electrical Properties of Arlon CuLad 217™	95

ABBREVIATIONS

ϵ	Dielectric Permittivity
Ω	Ohms (Impedance)
λ	Wavelength
ARPS	Antenna Radiation Prediction Software
AUT	Antenna Under Test
CAD	Computer Aided Design
CP	Circular Polarization
CPW	Coplanar Waveguide
DDARLing	DREO DFL Antenna Research Laboratory
DFL	David Florida Laboratory
DREO	Defense Research Establishment Ottawa
EMC	Electromagnetically Coupled
ESM	Electronic Support Measures
GLONASS	Global Navigation Satellite System
GPS	Global Positioning System
HMCS	Her Majesty's Canadian Ship
LNA	Low Noise Power Amplifier
LP	Linear Polarization
MOM	Method of Moments
PEC	Perfect Electric Conductor
RMC	Royal Military College
SAR	Synthetic Aperture Radar
SSFIP	Strip Slot Foam Inverted Patch
SSPA	Solid State Power Amplifier
TDR	Time Domain Reflectometer
TE	Transverse Electric
TEM	Transverse Electromagnetic
TM	Transverse Magnetic
U of B	University of Belgrade
VSWR	Voltage Standing Wave Ratio

1. INTRODUCTION

1.1 Introduction

The present demand for increasingly high performance antennas is pushing the development of improved antenna architectures with impressive urgency. Applications as diverse as mobile and satellite communications, as well as electronic warfare and remote sensing systems, have quite similar yet critical antenna requirements. Due to the great bandwidth utilization of these modern systems, as well as the diminishing spectral resources, much research activity is being undertaken at microwave and millimeter wave frequencies. As with all commercial antenna sub-systems, the technical requirements for high performance, small, light-weight and low profile antennas, must meet the additional economic necessities of low cost manufacturing, simplicity and reliability. An antenna architecture, which can meet both the economic requirements, as well as the performance demands of advanced systems, is the microstrip antenna.

The physical and electromagnetic characteristics of microstrip antennas offer the following advantages[1]:

- a) thin profile;
- b) light weight;
- c) simple to manufacture;
- d) can be made conformal;
- e) low cost;
- f) can be integrated with circuits; and,
- g) simple arrays can be readily created.

Unfortunately, these excellent advantages are offset by several important disadvantages, including:

- a) low efficiency (at low frequencies);
- b) small bandwidth (1-3%); and,
- c) extraneous radiation from the feed network and surface waves.

As the narrow bandwidth is arguably the most critical limitation on microstrip antenna performance, considerable research has gone into the area of

increasing the operational bandwidth of these antennas. The most common techniques for bandwidth enhancement include [2]:

- a) the improvement of wideband impedance matching;
- b) the creation of multiple resonances; and,
- c) the lowering of the antenna's "Q" with the addition of

losses, at the expense of reduced efficiency.

Other less applicable possibilities include techniques which affect the radiating edge inductance or capacitance, such as the use of varactor diodes and increasing the substrate thickness or reducing its dielectric constant [3].

1.2 Thesis objectives

The primary objective of this report is to investigate the performance of a wideband printed-dipole array architecture within the 4 –20 GHz frequency range. After developing a thorough understanding of the theoretical principles of operation, a state-of-the-art wideband printed-dipole array would be fabricated and tested. Analysis of these results, together with an increased understanding of the principles of operation, would allow for the further exploitation of the architecture and production of an even more capable array. This process should also give an indication of the practical limitations of this type of printed antenna.

1.3 Organization of report

After this chapter's introduction to the report, **Chapter 2** provides a general literature survey of wideband and dual frequency printed antenna techniques. While these devices are, for the most part, based on the classical microstrip architecture, it is worthwhile to develop an understanding of these varied systems due to the several similarities they possess in comparison with printed-dipoles. The chapter also contains a brief description of **IE3D™**, the primary software simulation tool used within this study.

Chapter 3 covers wideband printed-dipole arrays in general. It begins by focusing on the basic theoretical aspects of a thin wire dipole in free space and how it evolves or relates to the horizontal dipole over a ground-plane. This theory is then expanded to a discussion of the wideband printed-dipole with comparison to a thick cylindrical dipole. The major components of the printed-dipole array will then be described with emphasis on the coax-microstrip transition, the wideband balun, the feed network and finally the printed-dipole antenna element itself.

In **Chapter 4** an array of wideband printed-dipoles, which was first reported as only a pair by the University of Belgrade (U of B) is investigated. While this device was considered to be the state of the art, no measurement results or detailed analysis of a

larger array's performance were provided. It would therefore be used as the basis or starting point for this study and will be referred to as "U of B Array (5.77mm)". Further optimization and exploitation of the architecture would be useful. Essentially, the effort would be to increase the bandwidth, as defined, of the antenna array even further. The array is simulated, analyzed, fabricated and measurements are performed.

Chapter 5 comprises the rationale for the further exploitation of the University of Belgrade design, primarily by improving the ground-plane and element spacing. This improved wideband design, referred to as the "Optimized Array-1 (6.35mm)", is described and the measured results are summarized. With this experience, a further optimization attempt is proposed.

Chapter 6 comprises the rationale and proposed design for a new broadband printed-dipole element, and its inclusion into an array with the same element spacing as "Optimized Array-1 (6.35mm)". In an effort to further study the array architecture, the U of B design and the Optimized Array-1 were measured at a new, optimized ground plane spacing. These new antennas will be referred to as the "U of B-Array (8.00mm)" and the "Optimized Array-1 (8.00mm)" respectively. Measurement results are discussed and compared with the measurements obtained from the previous work of this study.

Chapter 7 summarizes the study with a list of important accomplishments and provides possible areas for further investigation of this particular antenna architecture.

2. PRINTED WIDEBAND ANTENNAS

2.1 General

As has been stated in the previous chapter, microstrip antenna elements have an inherently narrow bandwidth of just a few percent. This limitation is a result of the thin substrate between the patch and the ground plane producing a high Q resonance. While some improvement can be obtained by using a thicker substrate, one then has to contend with the possible excitation of surface waves and also increasing the probe or feed inductance. Due to the bandwidth limitation being the most significant negative characteristic of microstrip antennas, a tremendous research effort continues, in an attempt to improve their wideband performance. These efforts are complicated by the fact that wideband antennas are generally insensitive to parameter changes of geometry or electrical qualities.

2.2 Bandwidth definitions

It is of some importance to acknowledge that the subject of antenna bandwidth is clouded with various "selective" definitions of bandwidth. In general, the bandwidth of an antenna has been defined as: "the range of frequencies within which the performance of the antenna, with respect to some characteristic, conforms to a specified standard." [31] The bandwidth descriptors used within this study are summarized within the following table.

Bandwidth Definitions		
Bandwidth Quality	Limit for bandwidth	Alternative Description
VSWR	<2	$S_{11} < 9.6\text{dB}$
Radiation Efficiency	>50%	Measured Gain < 3dB below Maximum 100% Efficient Antenna Gain
Pattern	Sidelobes and grating lobes > 10dB down from the maximum (boresight)	

Table 1. Bandwidth definitions

While these are the bandwidth qualities used, other combinations of measurement parameters such as polarization or axial ratio can also be utilized. Additionally, while the bandwidth of narrowband antennas is often expressed as a

percentage of the centre frequency, that of wideband antennas is often described as a ratio of the upper to lower frequency (i.e. 2:1 or an octave). In this study, bandwidth will be expressed as a ratio, or explicitly as a frequency range.

2.3 Applications for wideband antennas

The applications requiring antennas, which possess wideband antenna performance, are quite diverse. The following three sections are purely a sampling of the many systems that use or could use wide bandwidth antennas. While some of the systems are obviously dual or perhaps multi-band, they are mentioned as they could benefit from a single wider bandwidth antenna if the frequencies in question could be encompassed by the wideband antenna element or array.

2.3.1 GPS and GLONASS

Two satellite based navigation systems, the American Global Positioning System(GPS) and GLONASS, the Russian equivalent, are similar in that they are multifrequency systems in the 1 to 2 GHz range. GPS uses two frequencies (L_1 at 1575.42 MHz and L_2 at 1227.6 MHz) to provide ranging and navigational data using CDMA (Code Division Multiple Access). GLONASS on the other hand, also uses an L_1 and L_2 frequency, however the pair of frequencies are different on each satellite and fall within the 1.5 to 2.2 GHz range[4]. Obviously, it would be desirable to develop antenna systems that could operate over the entire range of each, or even over that of both navigation systems. This last capability is especially important with regards to the development of dual capability receivers required by the aviation industry.

2.3.2 SAR

Synthetic-Aperture-Radar (SAR), is a novel method of improving the resolution of a radar through the "synthesis" of a larger aperture by movement of the radar antenna. Detailed imagery can then be recreated with the aid of signal processing. While traditionally developed for usage on air or space-borne platforms, the technology is now also being turned towards the terrestrial based detection of land-mines[5]. Wide bandwidth for these systems is essential as it allows for better target discrimination. As a result, the bandwidth of the published landmine detection system is 50-1200 MHz.

Radarsat I, an example of spaceborne SAR, on the other hand operates with a bandwidth of up to 30 MHz. Obviously, the wideband antenna will be an increasingly critical component for the follow-on system's function. It is also important to realize the challenges of developing spaceborne antennas. Besides having to perform under extreme environmental conditions, they must also be lightweight and very small in size (at least at launch).

2.3.3 Satellite Communications – Direct Broadcast Satellite

(DBS)

The use of satellites to provide television broadcast signals to consumers has grown dramatically in recent years. While the actual frequency band usage varies, they are generally in the C or Ku band. An example of these are dual-band systems, which operate at 14/12 GHz and 6/4 GHz simultaneously[6]. Due to the mass market potential of these systems and the possibility of multiple satellite usage, there will be great demand for low cost, wide bandwidth antennas. A similar argument can be made for the multi-system reception requirement, which some consumers may require. Having a single antenna, which can support communications via several satellite systems over a wide bandwidth, is a distinct advantage for reasons of simplicity and cost. However, one should not exclude the wideband antenna from narrow band usage. Often a wideband antenna can perform adequately without the “factory tuning” often required by narrow band systems.

2.3.4 Electronic Support Measures (ESM)

ESM is a broad field of detection and classification of signals throughout the radio frequency spectrum, generally for military purposes. As such, there is an ongoing requirement for wideband antennas with omni-directional performance to provide for the detection of signals from all directions and frequencies of interest. Measurement of phase difference between two antennas can allow for the calculation of signal direction. This can also be done using a mechanically or phased steered array. A bank of wideband printed-dipoles could easily cover the entire frequency spectrum, especially above 1 GHz.

2.4 Various wideband enhancement techniques

From the previous discussion of wideband antenna applications, it is apparent that there will only be an increasing requirement for antennas, which can meet these demanding specifications. Besides providing functionality for systems requiring continuous operation over a range of frequencies, wideband antennas may also meet the needs of dual band systems if the 2 frequencies are close enough to provide continuous performance. If the wideband antenna can replace several narrowband antennas, it is inherently cost effective and can save precious real estate on mobile or space-borne vehicles.

As stated in the previous chapter, the bandwidth of microstrip antennas can be increased by one of the following three basic methods for bandwidth enhancement [2]:

- a) The improvement of wideband impedance matching;
- b) The creation of multiple resonances; and,
- c) The lowering of the antenna's "Q" with the addition of losses, at the expense of reduced efficiency.

The following sections summarize these methods for improving the inherently narrow bandwidth of printed or microstrip antennas, and also provide an example of each bandwidth enhancement technique.

2.4.1 Impedance matching

The addition of a lossless matching network to an antenna element can improve its impedance bandwidth and much work has gone into this aspect of the basic microstrip antenna element. While this can be either on or off board, the simplest implementations generally involve microstrip structures that are coplanar with the antenna. Of course, this can only be implemented if there is adequate room on the substrate. These methods tend to have a realistic bandwidth limitation of 10-30%. An example of a straightforward passive coplanar matching network follows in Section 2.4.2.

Another method involves the addition of a series capacitor, which can be used to compensate for the inductance associated with the coax probe or microstripline feed. This unavoidable inductive input impedance is especially problematic for thicker substrates, where the coax probe is even longer. The compensation for this effect, is generally implemented by capacitively coupling the feed to the antenna element.

2.4.2 Coplanar matching networks

Using a passive coplanar network, Pues and Van de Chapelle were able to attain bandwidths of up to 12% [7]. Upon considering the input impedance of the microstrip antenna element as a series or parallel resonant circuit, the objective would be to devise a matching network which would cause the frequency dependent complex impedance to be completely real over as wide a bandwidth as possible. A basic example of such matching, depicting the microstrip outline on the substrate, is seen in Figure 1.

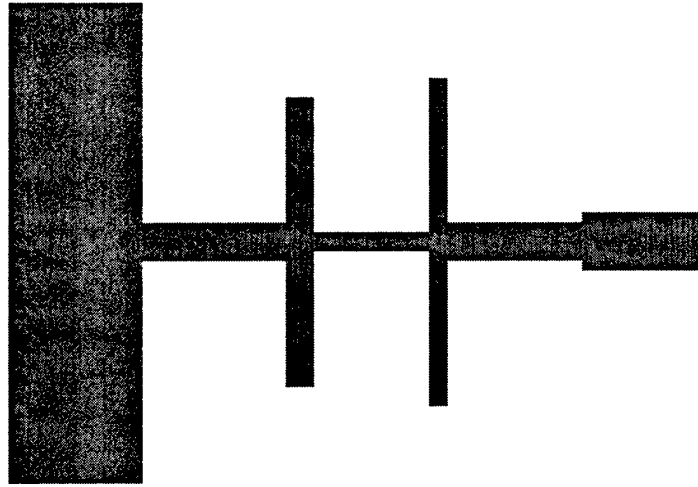


Figure 1. Coplanar passive matching

2.4.3 Series capacitance

There have been numerous methods for introducing the compensating series capacitance into the microstrip system. An early method for coax-fed microstrips, has the probe terminated to a tab (as depicted in Figure 2), with no direct contact with the microstrip element [8]. While sensitive to fabrication tolerances, the design has achieved bandwidths of 30%.

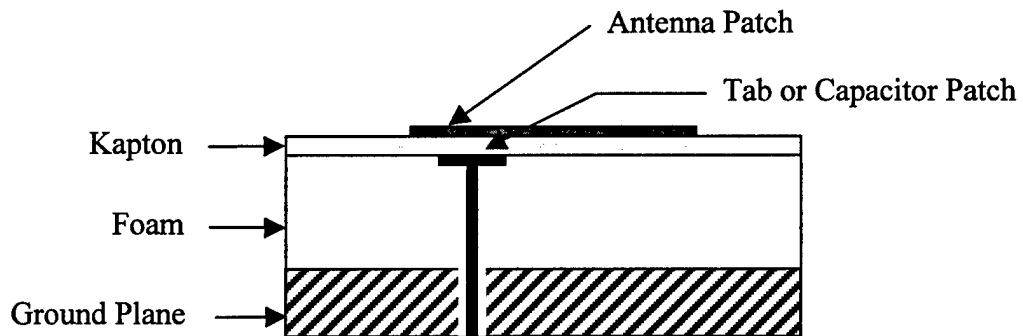


Figure 2. Implementation of series capacitance to compensate for probe inductance

A more recent adaptation of this design by Roy [9], consists of modifying the probe's tab to form a capacitive patch, which is slightly smaller than the radiating antenna patch. The capacitive patch utilized in this technique is depicted in Figure 3. For a given patch separation there is a particular capacitive patch size, which will reduce the

resonant reactance to zero. While the literature indicates broadband enhancement, exact improvements were not yet available from the author.

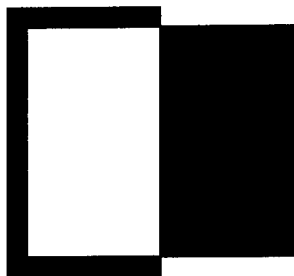


Figure 3. Capacitive patch

2.4.4 Multiple resonances

The technique of implementing additional elements which resonate close to the main element, in order to provide wider bandwidth, is seen in many applications. Stacked patches are often implemented, which can provide bandwidths of 10-20%. While this architecture is normally used in dual frequency applications, if the resonances are sufficiently close, the antenna can be considered as wideband. For wideband performance the stacked elements are close in size, whereas for dual band performance this constraint can be relaxed. A major advantage of the stacked patch is that the improved bandwidth doesn't come at the expense of footprint size, which is critical for implementation in arrays. Other advantages include; the tight coupling to the fed element and the symmetrical radiation patterns over the bandwidth.

In a similar fashion, the "extra" resonators can be coplanar elements, which are also parasitically coupled. While bandwidths of 25% have been realized, the design suffers from the fact that each element will radiate in a slightly different way, thus producing variations in the pattern over the bandwidth. As well, the growth in the element footprint complicates the integration of coplanar structures such as feed lines.

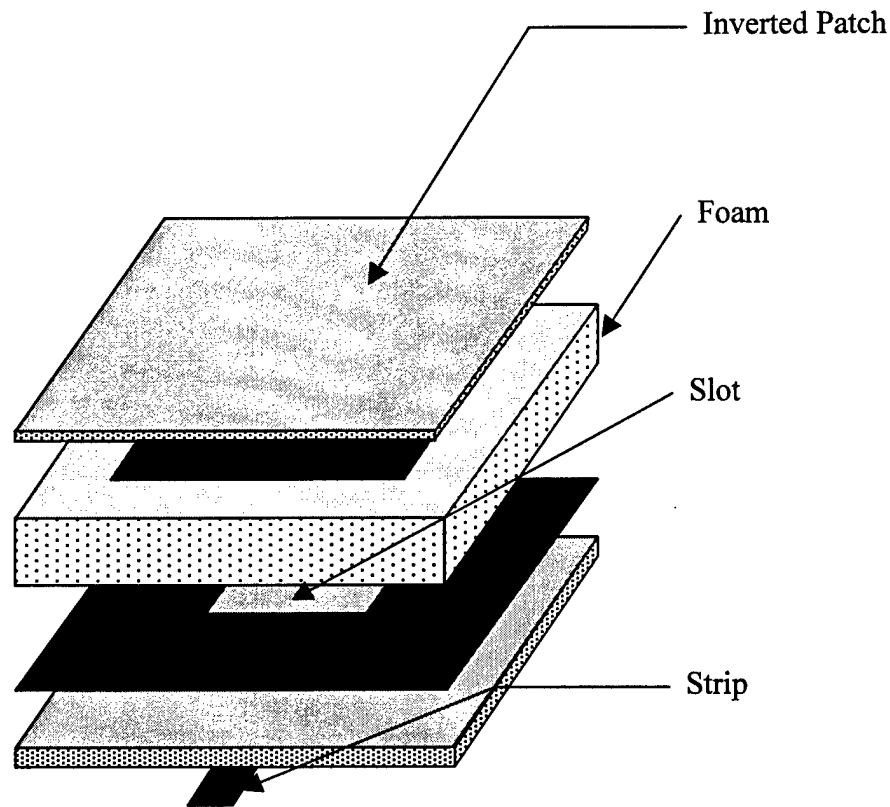


Figure 4. Strip Slot Foam Inverted Patch Antenna

2.4.5 Strip-Slot-Foam-Inverted-Patch (SSFIP) Antenna

An architecture, which exploits the fact that patches with thicker substrates can have thicker bandwidths, is the Strip-Slot-Foam-Inverted-Patch (SSFIP) antenna[10]. As depicted in Figure 4, the antenna comprises a non-resonant slot coupled to an inverted patch. The metallic patch is deposited on the underside of the thin plastic radome due to the fact that the foam's surface roughness is inappropriate for metal deposition. Also, since surface waves could result from the use of standard thick substrates, low permittivity foam is employed to mitigate the negative effects of surface waves. Surface waves must be avoided as they can induce scan blindness in phased arrays due to undesirable coupling between elements [11]. As well, since surface wave energy represents energy, which is not radiated in the intended direction, it effectively reduces the antenna's efficiency. Eventually surface waves will radiate when they diffract from a discontinuity, thereby causing further degradation of the antenna's radiation patterns. The device has attained a bandwidth of 11.7% for a 2:1 SWR. Further increases in the bandwidth, to upwards of 33%, are possible with the addition of a stacked second element.

2.4.6 Annular rings

Recently, a short-circuited ring, with an outer annular ring, was developed with a bandwidth up to 30% [12]. Careful tuning of the outer ring was performed so as to excite 2 higher modes (TM_{41} and TM_{51}) near the lower and upper limits of the band of the central ring.

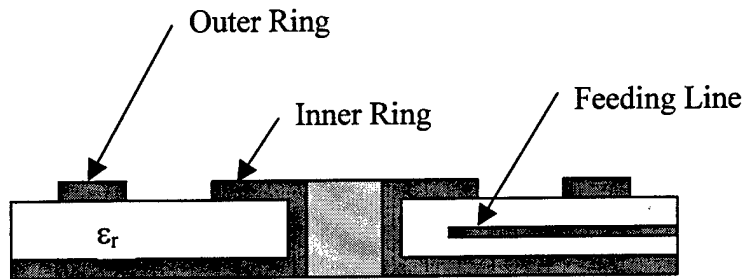


Figure 5. Double Shorted Annular Patch

2.4.7 Aperture coupled parallel resonators

As stated previously, wideband performance can be gleaned from multi-frequency systems in which the resonating elements are close enough to provide continuous frequency coverage. An architecture, which exploits this principal, was proposed by Croq and Pozar [13]. Their design was based on parallel dipoles of varying lengths being fed by the aperture coupling of a microstrip line, as depicted in Figure 6. Pozar has stated that due to the design's compactness and inherent symmetry, its patterns are more stable than parasitically coupled coplanar patches.

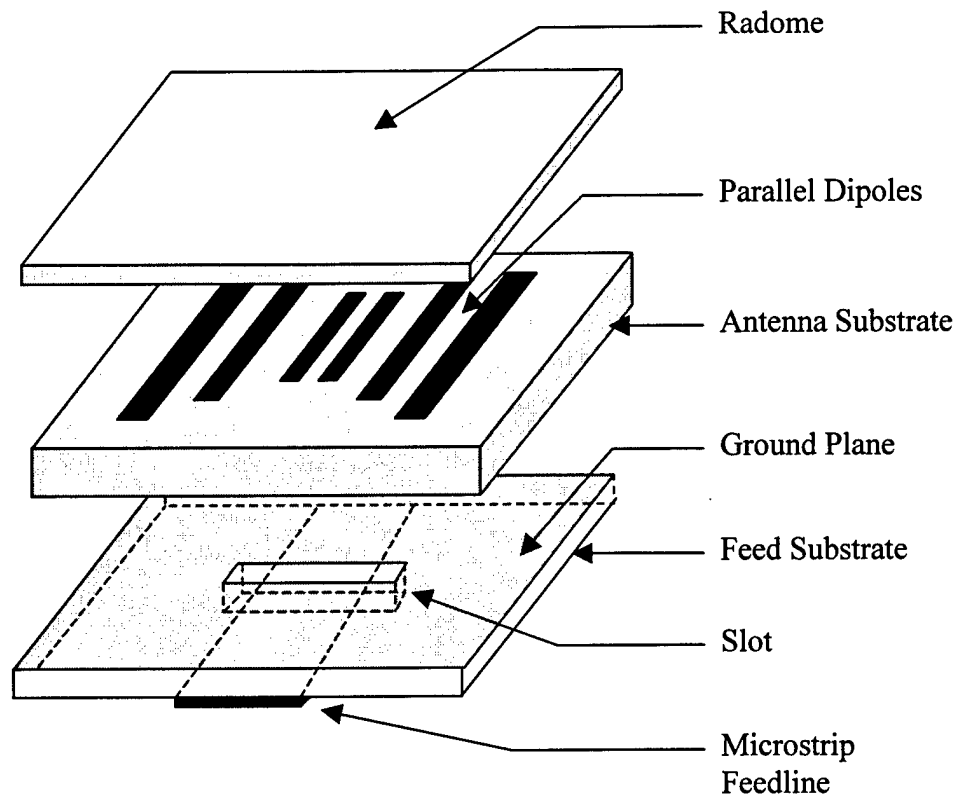


Figure 6. Varying length aperture coupled parallel dipoles used for wide bandwidth

2.4.8 U-slot rectangular patch

Recent work by Lee et al [14] achieved a 30% bandwidth using a coaxially fed rectangular patch with a U-shaped slot on a foam substrate. Besides having very good bandwidth, the element possessed good pattern characteristics and a thin profile, these types of elements appear to provide better wideband performance than simple rectangular slots. Dual band operation is also possible by modifying one of the dimensional parameters such as patch width. An additional benefit is that the U-shaped slot appeared to have a capacitive component, which tended to counteract the inductance due to the probe feed.

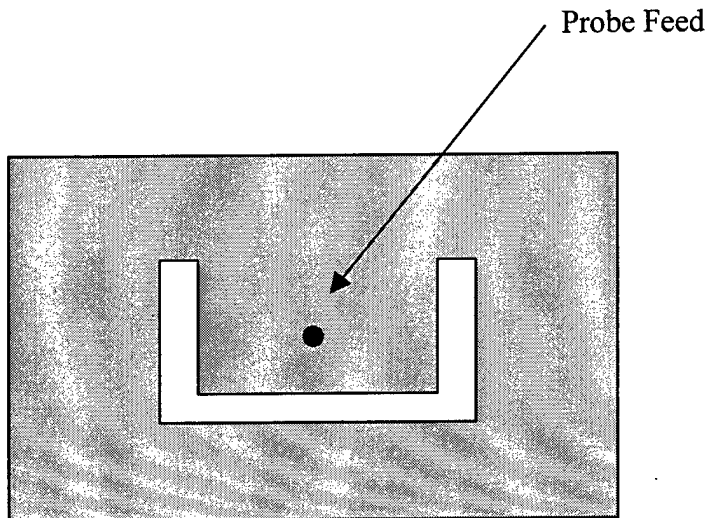


Figure 7. U-Slot Element

2.4.9 Loading and losses

As with any resonant circuit, the introduction of loss or loading can increase the bandwidth while reducing the Q of the element. Unfortunately, the price to be paid for this solution to narrow bandwidth, is reduced radiation efficiency. This technique of introducing loss can be implemented with the use of lossy substrates or films, while chip resistors can be used as physical loads applied to the elements themselves.

2.4.10 End loading

A novel compact broadband triangular microstrip antenna, with an inset microstrip-line feed and end loading chip resistor, has been recently developed by Lin and Wong [15]. Essentially, the design consists of a chip resistor loaded triangular patch antenna, which is matched with an inset 50Ω microstrip line, as seen in Figure 8. Besides reducing the size to 8% of that of a conventional microstrip, the design provided a bandwidth as wide as 19%. The end loading of this reduced size design was found to be more effective at bandwidth enhancement than the use of shorting pins. While possessing the qualities of a small wideband element, it suffers from some asymmetry in the radiation patterns and 2 dB of gain loss when compared to the use of shorting pins. Accurate fabrication of the chip resistor would also pose a challenge.

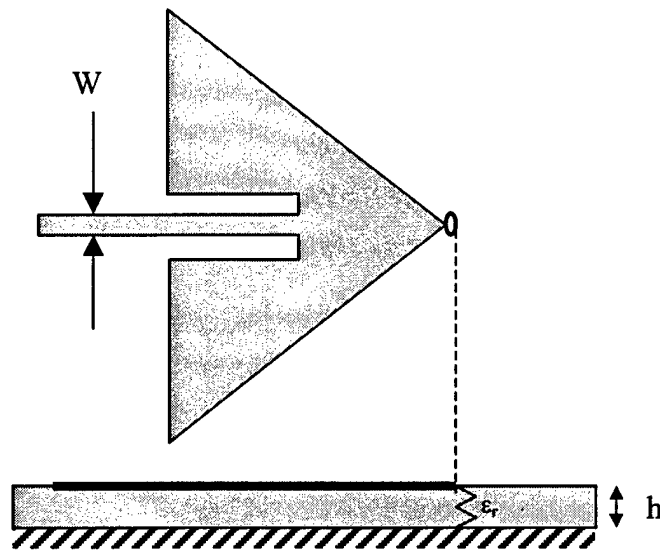


Figure 8. Triangular microstrip antenna with chip resistor loading

2.4.11 Other structures

The intent of the previous discussion was simply to provide a brief overview of some of the wideband techniques, which have shown promise for significantly enhancing the bandwidth of printed antenna elements. There are numerous other techniques, generally used for dual-band systems, which don't provide sufficient wideband operation. These architectures include the technique of reactively loading the microstrip patch with; shorting pins, stubs, slots, notches, air gaps and spur lines [16].

2.5 Design and fabrication issues

Having reviewed several of the most common methods of improving the bandwidth of microstrip elements, it is important to consider the practical aspects of implementing these low gain printed antenna elements into arrays. An important criterion for the practical comparison of different antennas is the complexity of their fabrication procedures. While narrow band antennas must function to a stringent frequency tolerance, a general advantage of most all wideband designs is that they have greater dimensional and material tolerances. While fabrication quality remains very important to any antenna's final operation, the wideband antenna will normally be designed so that the antenna actually has "guard" room outside the utilized bandwidth. This differs from single or dual band designs where the antenna usually has to operate within narrow frequency bands. For these reasons, the previous techniques have potential for numerous applications, but are not universally applicable. While each is useful for certain functions, they are all restricted to varying degrees, in their usefulness as components of very wideband arrays.

Wideband impedance matching has limited potential for very wideband systems, additionally, the matching network will present a real estate challenge. Multi-resonators, as expected from their very definition, have tight design requirements for each resonator's size and location. Additionally, they generally require an increase in volume from the standard patch. For stacked elements this is a vertical increase, while for coplanar, a horizontal increase. This growth in element size can make incorporation into arrays rather difficult. Whether stacked or coplanar, these architectures also represent challenging design problems and intricate fabrication procedures.

Finally, any architecture, which uses a vertical probe feed, suffers from additional probe inductance as well as an extra fabrication step.

In summary, there is a pressing requirement for the development of inexpensive wideband antennas. For the frequency range in question, printed microstrip designs show great promise. However, within this category, many wideband elements are inappropriate for implementation into arrays, as they are simply too large or difficult to feed. For this reason, further investigation needs to be done in the area of wideband printed antenna elements. As the gain of the single wideband element is low, they would be most likely employed in arrays to achieve greater gain. This research effort must therefore not lose sight of each element's appropriateness for use in wideband arrays.

2.6 Discussion of *IE3D* software

The various antenna architectures currently being researched, whose radiation patterns can be described by closed form expressions, are rare indeed. While some problems may be solved with approximate expressions, more accuracy and design flexibility may be required. Fortunately the advancement of the desktop PC has brought the capability of CAD and powerful numerical methods into common usage. The numerical methods software tool used in this report was *IE3D*TM produced by Zeland Software Inc[®].

2.6.1 Theory of operation

*IE3D*TM is an electromagnetic simulator, which uses the "method of moments" (MoM). Essentially, this technique solves an integral equation, which includes the boundary conditions, for the current distribution over the meshed structure. This allows for the solution of S-Parameters, radiation patterns, RLC equivalent circuits, etc[17]. The process for finding a solution by MoM, can be generalized into four steps [18]:

- 1) the unknown (current) is expanded into a series of basis functions;
- 2) suitable inner product and weighting or testing functions are defined;
- 3) inner products are taken and the matrix equation is formed; and,
- 4) the matrix is solved for the unknown coefficient's.

3. WIDEBAND PRINTED-DIPOLE ARRAYS

3.1 General

Perhaps the simplest and most widely known antenna is the thin wire dipole. Although this antenna is covered rigorously in various texts and literature, the basic principles of a horizontal dipole over a ground-plane will be briefly covered in the following sections, as they form the foundation for the operation of the wideband printed-dipole array under study. This discussion will progress from that of a single dipole in free space, to that of a horizontal dipole over a ground-plane. Its implementation into arrays will be addressed, as will the bandwidth enhancement principle of thick dipoles.

3.2 Basic dipole theory

Essentially, a dipole, like any antenna, "is a transition device, or transducer, between a guided wave and a free-space wave, or vice versa" [19]. As current on the conductor is ultimately the source of the radiation, it is useful to realize that the current distribution of a centre-fed dipole disappears at the ends of the dipole. In the far-field, E_θ can be described by:

$$E_\theta \cong j\eta \frac{I_0 e^{-jkr}}{2\pi r} \left[\frac{\cos\left(\frac{kl}{2} \cos\theta\right) - \cos\left(\frac{kl}{2}\right)}{\sin\theta} \right] \quad (3.1)$$

Where:

η = intrinsic impedance of free space, 377Ω

l = length of antenna

$$k = \frac{2\pi}{\lambda}$$

r = distance from antenna

θ = direction (as shown in Figure 9)

While increasing the length of the dipole antenna makes it more directive up to a length of one wavelength, lengths greater than about a wavelength increase the number of lobes due to more complex current distributions on the wire and thus reduce the directivity. The half wavelength dipole is popular due to its good directivity of 1.643 and its inherent radiation resistance of 73Ω , which is close to the characteristic

impedance of many transmission lines, thus simplifying matching. A representative example of a half-wavelength, thin dipole in free-space was simulated in *IE3D™*. The well known doughnut pattern was produced as seen in Figure 9. It is of interest that although the dipole was oriented horizontally, a co-ordinate transformation, within the simulation was necessary to place the dipole's longitudinal axis at $\theta=0$. This yielded a better simulation result, given that a null occurs in this direction.

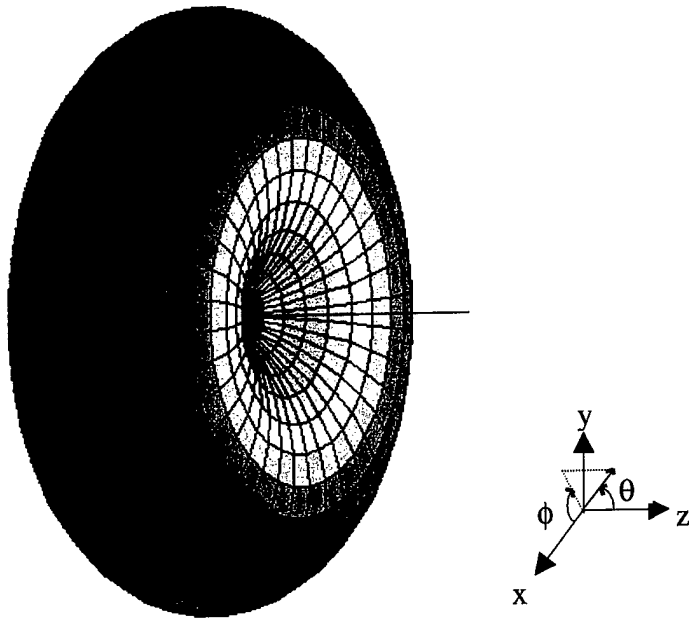


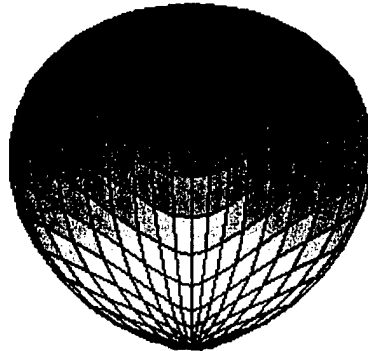
Figure 9. Horizontal dipole radiation pattern and current distribution

3.3 Horizontal dipole over a ground-plane

As we are fundamentally interested in radiation into a defined beam within a hemisphere, it is logical to align the dipole horizontally over a ground plane, as in Figure 10. This will put the dipole's null at the horizon and project the maximum radiation in a direction normal to the ground-plane. Vertical orientation of the dipole would have the negative effect of producing a null at boresight. The concept of image theory can be applied to the horizontal dipole, which from another perspective is simply the pattern multiplication of the array factor (2 elements) and the element factor. As the height of the dipole above the ground-plane is increased to greater than $\lambda/4$, a null begins to form at boresight (normal to the ground plane) and the pattern breaks into two lobes. As the height of the dipole increases, the number of lobes continues to increase by the following approximate relationship:

$$\text{number_of_lobes} \approx 2 \left(\frac{h}{\lambda} \right) \quad (3.2)$$

The directivity is a maximum of 7.5 for small heights over the ground plane and a maximum of 6 when $h \approx (0.725 + n/2)\lambda$, $n=0,1,2,3$



● View Along The Dipole

Figure 10. Radiation pattern of a horizontal dipole over a ground-plane

3.4 Array considerations

In order to make the antenna even more directive, its electrical size must be increased. For the purposes of this study, the best method of improving directivity is to create an array of elements. As stated by Balanis, there are five general methods of modifying the radiation patterns of arrays. These methods include the modification of:

- 1) the geometrical shape of the array;
- 2) the element spacing;
- 3) the amplitude of the signal at each element;
- 4) the phase of the signal at each element; and,
- 5) the radiation pattern of each element.

Given that this study will involve a 32 element rectangular array of printed-dipoles and a corporate feed network, the only degrees of freedom for design modification would initially be the element spacing followed by a possible element shape modification. Since it is desirable to have the maximum directivity in the broadside direction, each array element should have equal phase and amplitude excitation.

3.5 Thick dipole theory

Historically, the biconical and cylindrical architectures have been used to enhance the bandwidth of dipoles, most notably in the VHF and UHF bands. Essentially, the improved bandwidth performance is a result of the input impedance not varying much with frequency, as is the case with thin dipoles. Since the physical volume of such designs is a significant encumbrance, they evolved into analogous two-dimensional shapes, such as wire frames. These lower profile antennas, tended to retain most of the bandwidth qualities of their three-dimensional counterparts, yet were not as bulky.

In general, where a thin wire ($l/d \approx 5000$) may have a bandwidth of 3%, a thick wire ($l/d = 260$) can possess a bandwidth of 30% [19].

3.6 The wideband printed-dipole

While considerable research has focused on the classical microstrip dipole, there has been a smaller, though sustained, interest in the implementation of the double-sided printed-dipole. This particular architecture, as seen in Figure 11, consists of a dipole with each arm printed on opposite sides of the substrate. The dipole is then fed by a balanced transmission line. Because the substrate supporting the balanced transmission line is very thin, the dipole arms are only slightly out of plane, hence there is insignificant effect on their radiation patterns. The dipole is spaced approximately a quarter wavelength above the ground plane so radiation is uni-directional, with the single lobe having a maximum normal to the ground plane.

Originally developed for use in a "tactical, battlefield, man-pack type, two-pound radar" by Wilkinson in 1974 [20], more recent research has shown impressive bandwidth performance [21, 35]. The application has also been implemented as a uniplanar CPW fed bow-tie slot antenna, which attained a 36% bandwidth using a 20 degree extended angle [22]. Most work has tended to optimize the impedance characteristics of the element by implementing the familiar flared or bow tie configuration in which the dipole arms are gradually spread [23]. However Mikavica et al [21] have proposed the use of wide rectangular dipoles, based on the analogy with cylindrical dipole antennas having more uniform input impedance (reactance and resistance) when thicker. While use of the normal bow-tie configuration has attained bandwidths of 33%, the rectangular dipole has achieved one octave bandwidths. A similar implementation using pentagonal shaped dipoles achieved a 30% bandwidth, though at the much higher 60 GHz range [24]. Such impressive performance is worthy of further research.

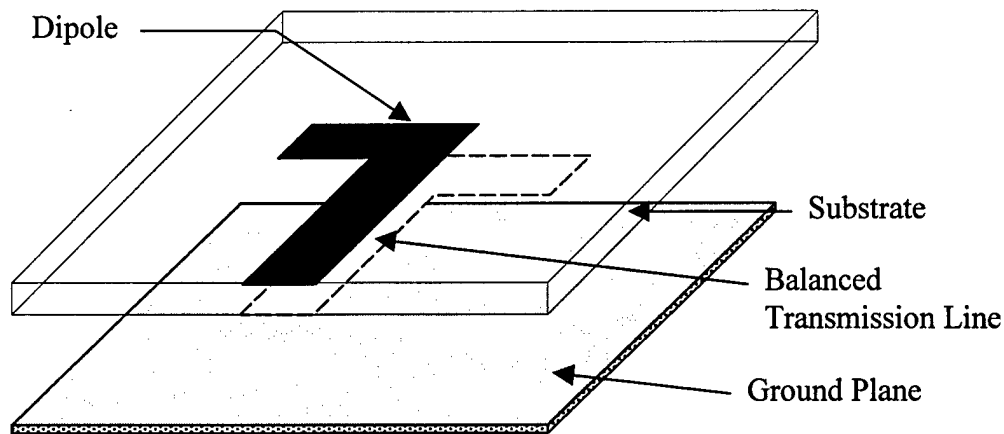


Figure 11. Printed-dipole element

3.7 Components of the wideband printed-dipole array

Despite the rapid advancements in computing power and the concurrent developments in electromagnetic(em) simulation software, it is still impossible to fully simulate large arrays with their feed networks. While the use of periodic walls¹ allows the exploitation of symmetry, this is not always possible. Array patterns can be created by first modeling single elements and then applying an array factor, however, this ignores the impact of mutual coupling. Elements can be simulated separately from their feed networks, however, even this is of limited value in reducing the simulation size for large arrays. As well, this method ignores mutual coupling between the elements and the feed network. Generally, array design still involves the deconstruction of the antenna into its component parts, some of which can be easily simulated, others which defy the capabilities of currently available off the shelf software and desktop PCs.

The printed-dipole array possesses a distinct architecture with several components providing critical capabilities for its overall operation. A number are unique to the design, while others share similar features with familiar microstrip structures. As the performance of the array requires the matched operation of all components, each one is worthy of further discussion.

3.7.1 Microstrip to coax transition

At some point every antenna has to be connected to the real world, usually a receiver or transmitter system. In the laboratory, and often in the real world as well, this

¹ IE3D™ can exploit array symmetry through the use of electric or magnetic periodic walls. With two parallel, appropriately spaced “walls”, a number of images can be selected, which allows for an equivalent solution to that of a simulation which models each array element.

transition is via a 50Ω coaxial connection. The technical challenge for this component of the antenna system is that the unbalanced coaxial transmission line must efficiently couple its electromagnetic energy to a printed microstrip line. If this transition is not performed well, the resulting errors may overshadow the measurement of the antenna's properties.

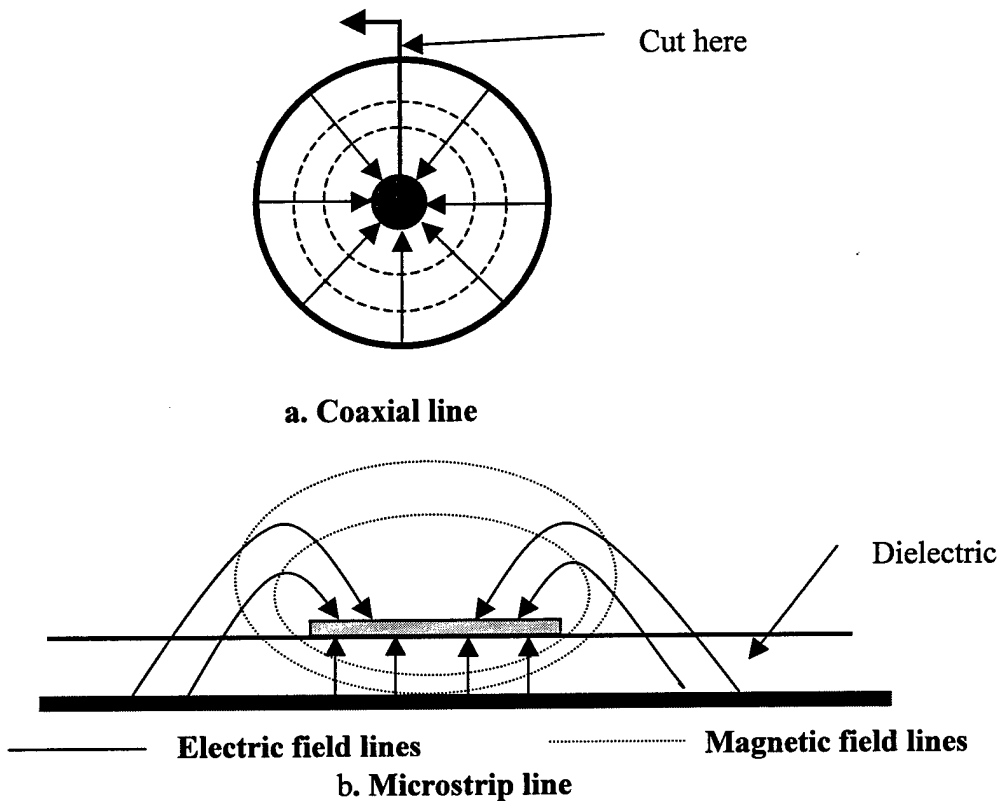


Figure 12. Evolution of microstrip line from coaxial line by unfolding

While it is critical that the impedance values of each medium are equivalent in order to minimize reflections, it is equally as important that the field transition from one medium to the other be as gradual as possible. Throughout the transition, the boundary conditions for a perfect electric conductor (PEC) remain; particularly that the tangential electric field disappears at each surface. In going from coax to microstrip, one can best understand the transition which must occur by depicting the field structure in each case, as seen in Figure 12 [25]. The most common form of “in line” or coplanar coax – microstrip transition [26] is as shown in Figure 13. In this implementation, the coax cable is in the same plane as the substrate and the centre pin is soldered to the microstrip, while the coax's outer conductor is connected to the ground plane.

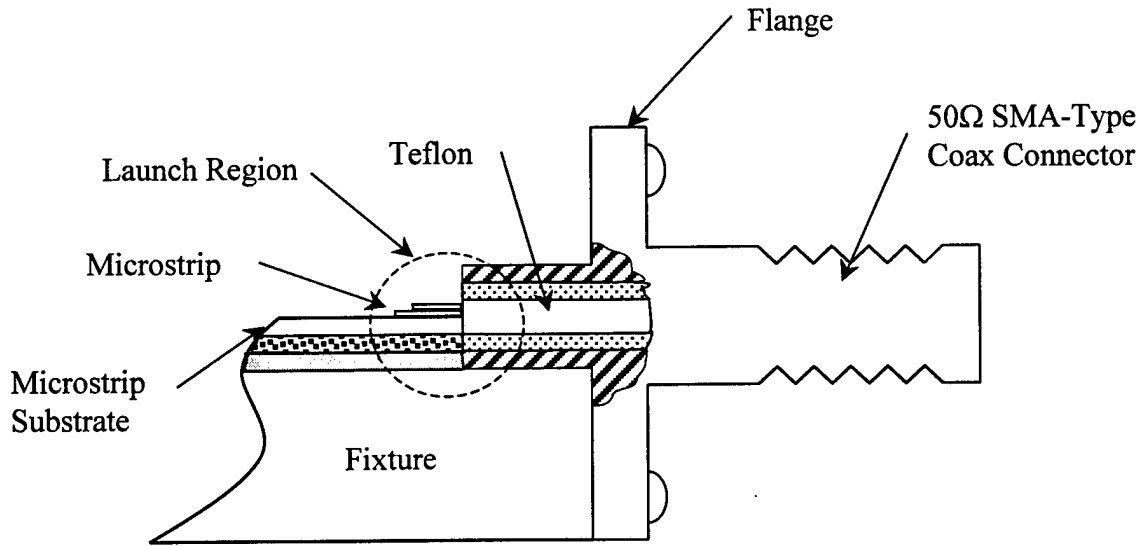


Figure 13. Typical Coaxial to microstrip transition

The other popular arrangement is the vertical feed probe in which the centre pin of the coax is fed through a via and soldered to the transmission line on the top layer (microstrip), while the coax's outer conductor becomes the ground-plane. Unfortunately this approach results in a more difficult fabrication step, as well as undesirable probe inductance. An important design and fabrication aspect of the horizontal feed design is that there should be no air gap between the coax's outer conductor and the microstrip's ground plane. This air gap would result in both a path length difference between the current on the ground plane and that of the centre conductor, as well as a possible capacitive effect. This variation would result in a phase imbalance and undesirable radiation [27]. The following figure provides a graphical representation of this potential problem.

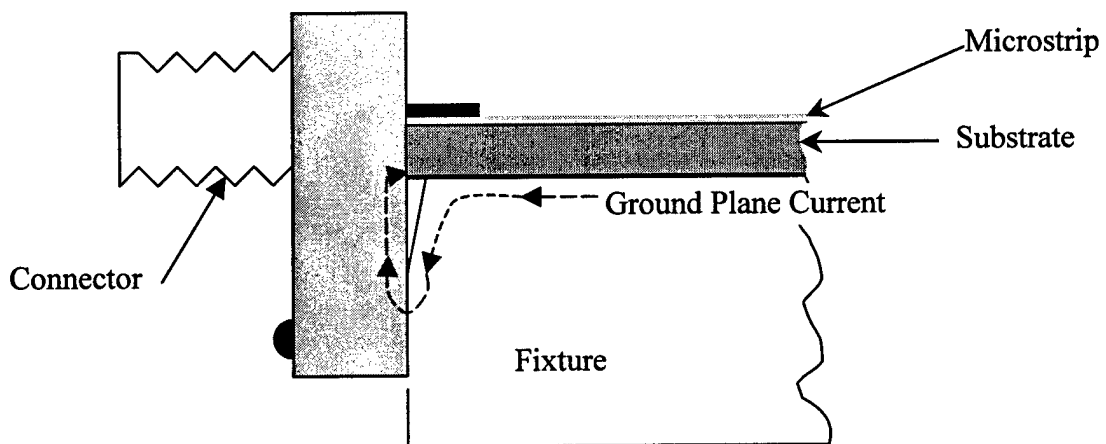


Figure 14. Effect of a gap between the connector flange and the antenna fixture

Having stated that a gradual field transition is critical to the connector system's performance, the only connector design found in the literature, which actually matches the fields at the interface, is the "Eisenhart" connector depicted in Figure 15 [28]. By using a tapered, off-centered inner conductor, a smooth transition from coax to microstrip is attained. The 50Ω impedance is thus maintained throughout the connector. This design has attained an impressive VSWR of approximately 1.1 below 18 GHz. While the elegance of this architecture is obvious, this type of connector was not readily available so an acceptable commercial alternative was utilized.

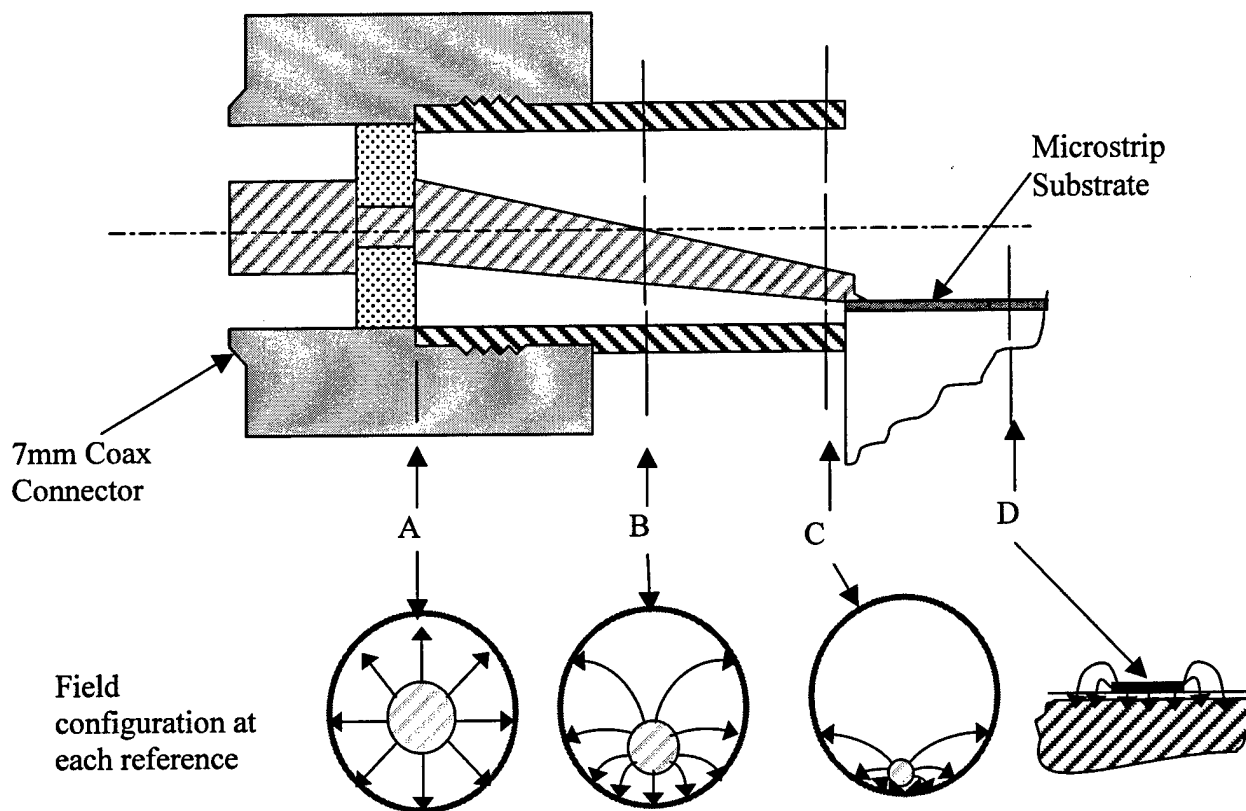


Figure 15. Cross section of Eisenhart connector

3.7.2 The K Connector™

The connector used throughout this study was the *K Connector™* manufactured by Anritsu Inc®. Chosen for its superiority over the SMA connector, the principal component of the *K Connector™* is a glass bead in the launcher assembly. This .012 inch Corning 7070 bead has a gold plated centre conductor, as well as a gold plated Kovar collar[29].

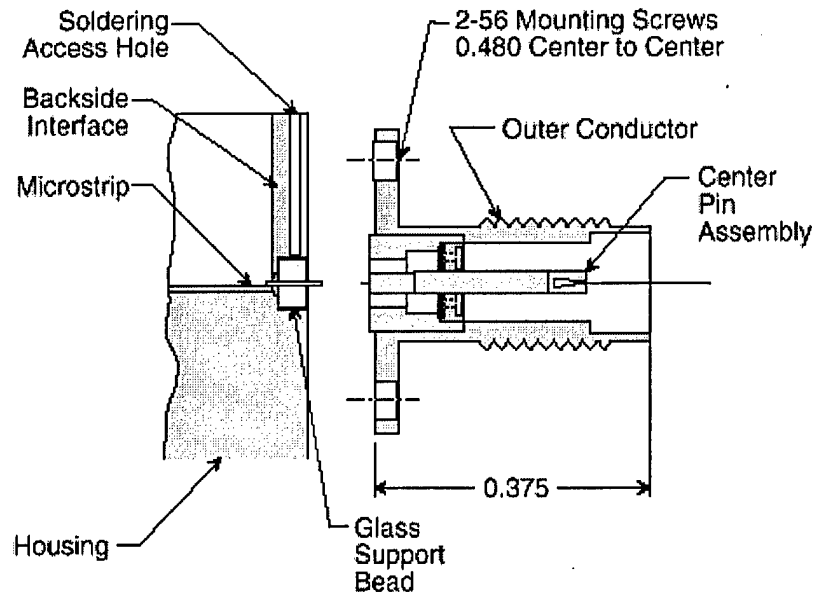


Figure 16. *K Connector*[™] flange mount assembly (inches)

As this design results in minimal discontinuity along the transition, its specified return loss is better than -25dB below 18 GHz. A complication for experimental work, however, is that the manufacturer generally intends for the user to install the glass bead directly in the outer wall of the microwave circuit's housing, with the connector attached to the housing's outer surface, as depicted in Figure 16.

3.7.3 Connector to antenna interface

A more flexible adapter was required for the testing of the printed-dipole antenna and its associated balun, which would allow for a simpler circuit support structure, yet still maintain the benefits of the *K Connector*[™]. It was considered that the best approach would be to construct an adapter flange, which would contain the glass bead and also act as an interface between the male *K connector*[™] and the printed antenna. This approach, depicted in Figure 17, would allow for quicker connector changeouts and less complication, when minor support structure modifications were required. For example, if the array height over the ground plane required modification, only the aluminum spacer block and foam thickness need be changed. The alternative would have been to build a completely new antenna support structure each time a change of ground-plane separation was desired.

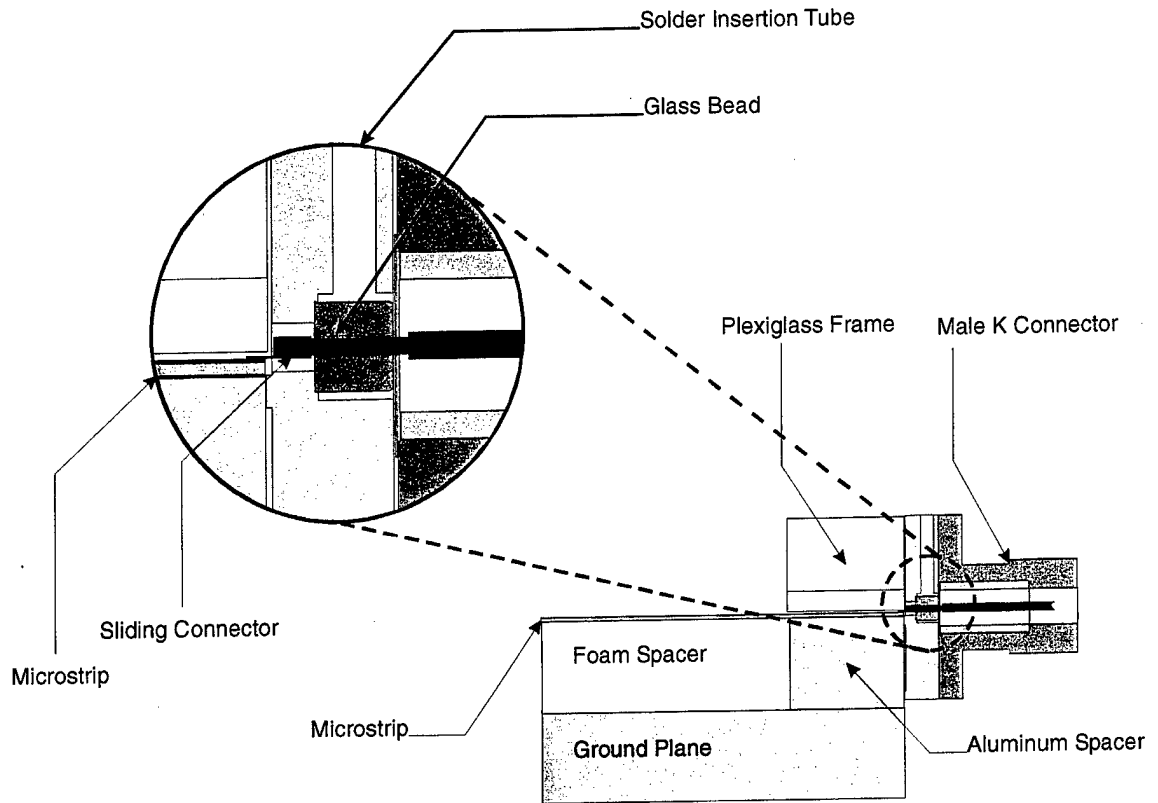


Figure 17. *K Connector™* to printed antenna interface (side-view)

The connector was not without its difficulties, however, as mounting the sliding connector and soldering the glass bead in place were often problematic and difficult to fabricate to a consistent standard. While the manufacturer suggests that the VSWR can be optimized by adjustment of the sliding connector, this was not done as the connector was extremely fragile and the necessary micro-positioning equipment was not available. Some minor “tuning” was however obtained by delicate adjustment of the substrate position prior to the final securing of the plexiglass frame.

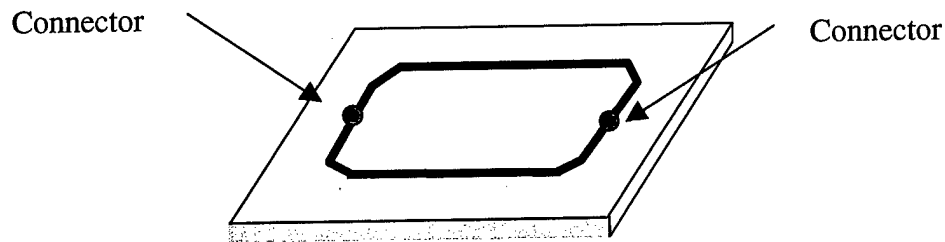


Figure 18. Microstrip connector test arrangement

As it was important to characterize the coax to balanced microstrip transition, several techniques were considered. A very good method for measuring the performance of a coax to microstrip line connection involved two, vertically mounted coax connections on opposite sides of a microstrip loop [30], as depicted in Figure 18. Because the connections are identical, the technique is very sensitive, as there is coherent summation of the connector reflections. By taking measurements with one connection open and then terminated, the performance of a single connection can be accurately derived. However, due to the fact that the balanced transmission line used in this study required a coplanar coax feed, this established testing technique was not appropriate. Instead, two baluns were placed end to end so that a straight through measurement could be performed, as described in the following section. A major benefit of pursuing this approach was that it allowed the simultaneous testing of both the connector and the balun.

3.7.4 Wideband balun

While the feed network for the printed-dipole array is based on balanced twin lead transmission line, the overall antenna is fed from a 50Ω coax cable. If the inner and outer conductor of the coax cable were connected directly to each of the transmission lines, one would find that each pair of connections would not couple in the same way[31]. This would result in undesirable current flow on the outside of the coax cable. Besides representing obvious inefficiency, this situation could also severely degrade the intended radiation patterns of the antenna.

Devices, which effectively make this transition from balanced to unbalanced systems, are known as "baluns". In many modern systems, these devices must meet the added demand of performance over a wide bandwidth. Duncan and Minerva [32] developed such a wideband balun which essentially peeled away the outer conductor of the coax in a gradual fashion until a balanced twin line remained. This transition was done in such a way that the S_{11} had a Chebycheff response in the pass band [33]. The length of the balun was determined to be a function of the lowest operating frequency. The idea of gradually peeling away the outer conductor of the coax was simplified and made more practical by Gans et al [34], who devised an architecture whereby the outer conductor of a vertically fed patch becomes a circular finite ground plane, with the centre pin becoming the top transmission line. The ground plane is then gradually reduced in size to become the bottom line of the balanced pair.

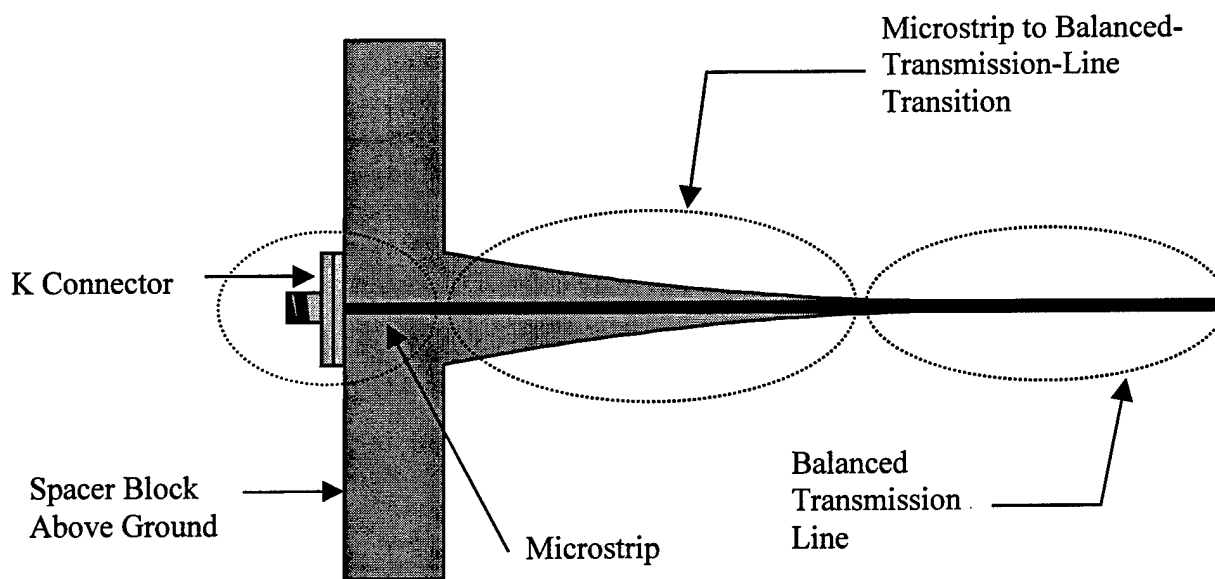


Figure 19. Wideband balun (top-view)

A further simplification of the balun design was introduced in which the balun was fed horizontally by the coax, thus negating the requirement for any vias. The transition could now be viewed as comprising three distinct zones; unbalanced-coax to unbalanced-microstrip (the connector), unbalanced-microstrip to balanced transmission line (the balun) and finally the balanced transmission line itself, which is the fundamental structure for the rest of the feed network. While empirical design data for optimum balun taper and length was not available, it was decided to use a generally accepted balun length of greater than 1λ and an opening angle of less than 6 degrees in order to produce acceptable VSWR performance. As the balun used in the U of B Array fell within these guidelines and since measurements detailed in the following chapter indicated that it performed adequately, the previously used U of B balun would not be modified as part of this research.

3.7.5 Balanced transmission line

As previously stated, printed-dipoles are fairly common in the form of EMC and aperture coupled dipoles. These and various other microstrip antenna systems are similar in their use of an unbalanced microstrip feed network. The use of a balanced twin line feed network is perhaps one of the most unique aspects of the doubled-sided printed-dipole array currently being studied. Since the transmission line utilizes both sides of the same substrate that each arm of the printed-dipole resides upon, the architecture exploits all of the well-known advantages of the planar microstrip system. This type of twin line feed is particularly advantageous, as the radiation losses can be exceptionally low due to the fact that the substrate can be very thin ($.01 \lambda$)[35]. As seen in Figure 20, the microstrip and balanced transmission lines have quite similar field structures. However if

the fields are to remain the same as the microstrip thickness is halved, the voltage and conversely the impedance of the balanced transmission line is doubled.

$$Z_c (\text{twin line}) = 2Z_c (\text{microstrip}) \quad (h \rightarrow d/2) \quad (3.3)$$

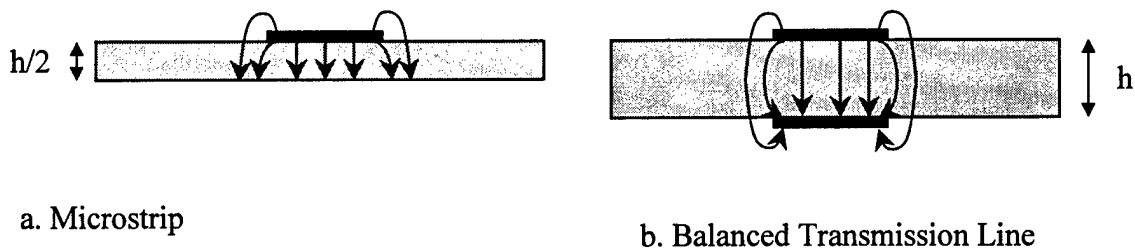


Figure 20. Field patterns of microstrip and balanced transmission line

While the definitive work on balanced transmission lines by Wheeler [36] covers the issue rigorously, the relationship from equation 3.3 was used in conjunction with the standard formulae for microstrip impedance in order to provide for the calculation of 50 and 100Ω balanced transmission line widths.

3.7.6 Feed network

Besides the uniqueness of using balanced transmission lines in a printed antenna array, the remainder of the system, with the exception of the double-sided dipoles, is a standard corporate feed system. Though a relatively simple feed architecture, resistive losses and radiation can lead to problems in gain and radiation patterns [37]. As well, susceptibility to surface waves and mutual coupling may cause further problems. In order to be able to conduct array performance comparisons, the dimensions were kept at the 4 x 8 elements used in the University of Belgrade design. As the feed network had to operate effectively over an unusually large bandwidth, linear tapers were used to make the impedance transformations from 50 to 100Ω.

3.8 Printed-dipoles – difference from classical microstrip

While the wideband printed-dipole has been studied within the context of printed antennas, it is important to differentiate its architecture and mode of operation from the more widespread classical microstrip antenna. The simplest microstrip patch antenna usually comprises a thin copper patch, which is photo etched to the top surface of a substrate. This substrate, which generally has a relative permittivity of between 1 and 4, situates the patch a few fractions of a wavelength above a perfectly conducting ground plane. The permittivity of the substrate enhances the fringing fields, which are the source

of the desired radiation. The patch can be fed via various mechanisms including; microstrip line, coaxial feed, and aperture coupling [38].

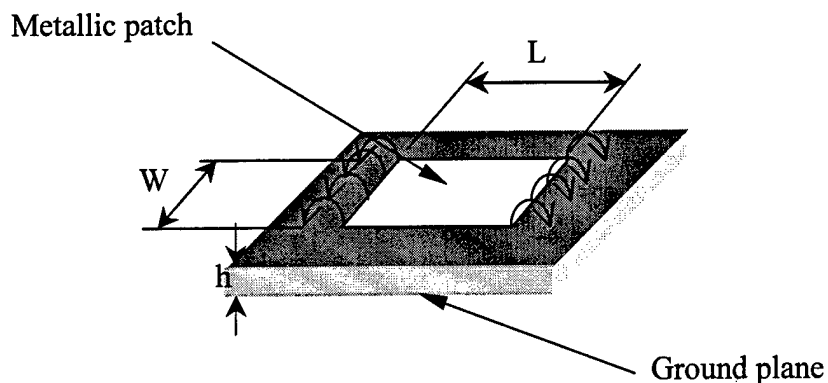


Figure 21. Microstrip patch antenna

Whereas the height for the classical microstrip is an important parameter, as it refers to the thickness of the substrate, height in the case of the double-sided printed-dipole is also a critical dimension, but for a different reason. In this case, height refers to the separation between the dipole element and the ground-plane (see Figure 11). The dipole element is usually kept at its desired height by a foam spacer which has an ϵ_{eff} of close to 1 and thus has negligible effect.

With regards to the substrate, the double-sided printed-dipole only requires the substrate structure to act as the dielectric between the balanced feed lines. The substrate has almost no discernable effect on the operation of the dipole itself. Its effect is only seen in very slight asymmetry in the radiation patterns, a result of the fact that each arm “sees” the dielectric differently, since one arm is below and the other above the substrate.

4. ANALYSIS OF U OF B PRINTED-DIPOLE ARRAY

4.1 Introduction

As stated in the previous chapter, the initial stage of this study would involve an in depth analysis of what was considered to be a promising wideband printed-dipole array architecture developed by Mikavica et al [21]. Since no measurement or performance data was available for this 32 element design, this analysis would increase the understanding of both the theoretical and practical aspects of this array architecture, thereby facilitating further development and exploitation.

The chapter will begin with a general physical description of the design and then proceed to describe the technique that was used to characterize the wideband balun. After assessing the results of the balun study, a review of the simulation results of single and multiple dipole elements, including mutual coupling will be presented. After comparing the simulated and measured radiation patterns of the array, more detailed measurement results of the array are provided

4.2 Physical description of design

The design consisted of a 32-element array of wideband printed dipoles, as described in section 3.6. Essentially each dipole can be considered as centre-fed by a balanced transmission line. As the conductors of the transmission line are on opposite sides of the substrate, so to is each dipole arm. The printed array was etched onto a 7 x 7", 0.254 mm thick piece of *Arlon, Cu Clad 217TM* substrate. It was then positioned 5.77mm above a ¼" thick aluminum ground plane using a *Rohacell 31 HFTM* foam spacer, which was milled to the required dimension. This ¼ λ height was selected based on the desired performance at 13 GHz. The ¼ λ height over ground is a function of the highest frequency of operation. All components were held in place by the use of a square plexiglass ring. The connector arrangement was as described in section 3.7.1. The actual etched antenna, with top and bottom layers shown, is portrayed in Figure 22 and 23, with detailed dimensions listed in Table 2. Figure 22 also shows a representation of the effective aperture, which is later used in the calculation of theoretical gain. In order to simplify experimentation as much as possible, none of the components were bonded together. This did not present a problem, as the 20 perimeter screws around the plexiglass ring were adequate for ensuring that there were no appreciable air gaps and that the array surface remained flat. Electrical and other properties of the foam and substrate material may be found at APPENDIX A and C respectively.

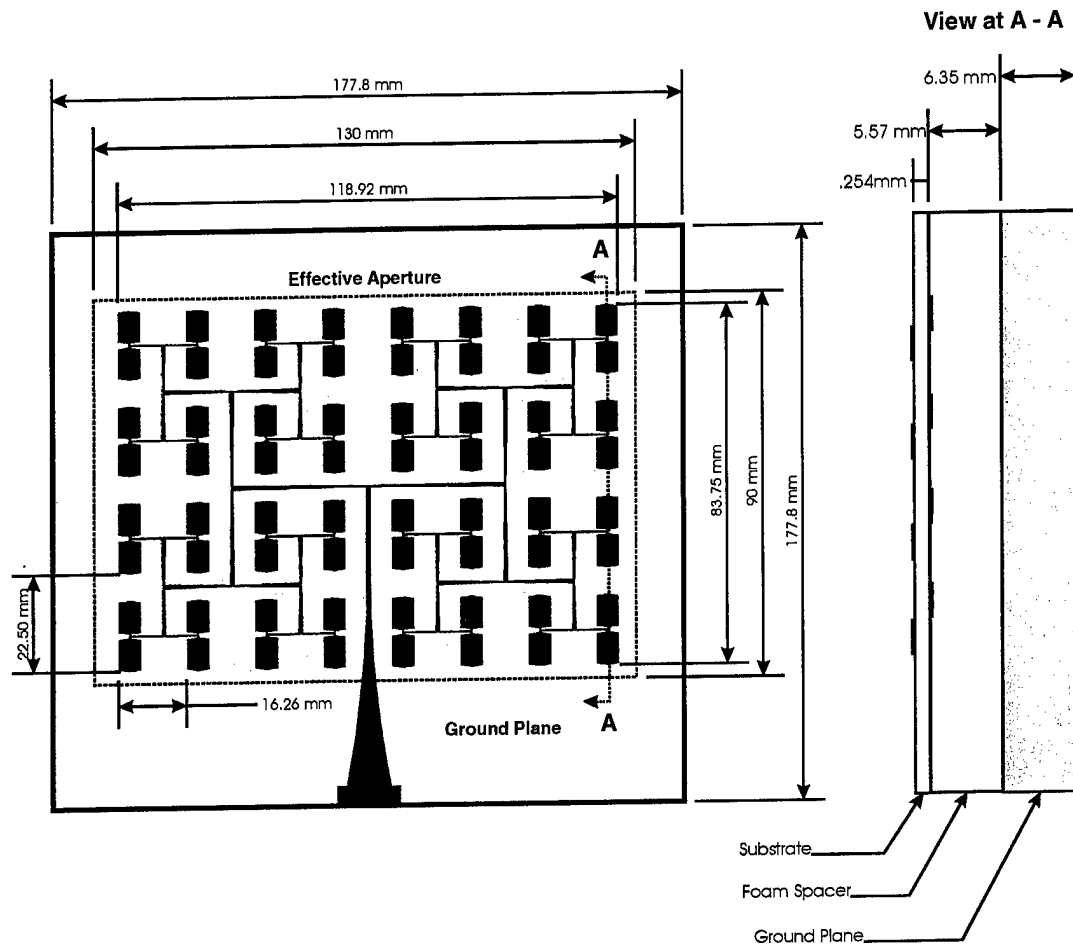
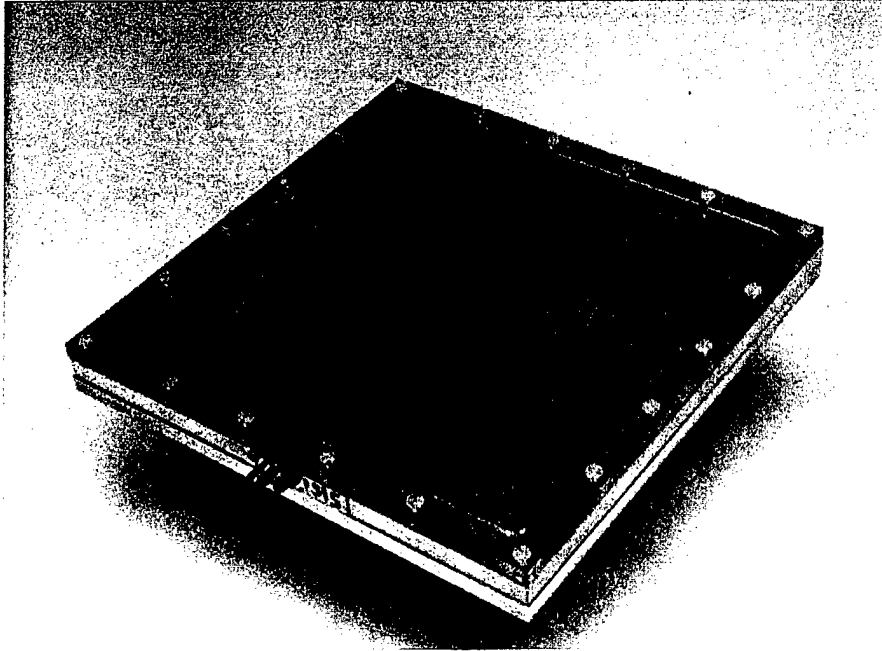


Figure 22. University of Belgrade wideband printed-dipole array

Parameter	Dimension (mm)	Parameter	Dimension (mm)
Dipole Length	16.26	Element Colinear (y)-Spacing	22.50
Dipole Width	5.21	Element Broadside (x)-Spacing	16.26
Array Length (x)	118.92	Aperture Length (x)	130
Array Width (y)	83.74	Aperture Width (y)	90
Height Over Ground	5.77		

Table 2. Dimensions of the University of Belgrade wideband array



© DREO 99-1111

Figure 23. Photo of wideband printed-dipole array

4.3 Analysis of the wideband balun

As the balun was constructed with microstrip at one end and balanced transmission line at the other, a back to back testing arrangement was necessary so that coax *K Connectors*[™] could be used throughout, as depicted in Figures 24 and 25. This setup provided for good S parameter measurements, which indicated not only the wideband match to the balun, but also the reproducibility of the *K Connection*[™]. A TDR measurement was also conducted in an effort to analyze discontinuities within the balun structure. All measurements were conducted using a *Wiltron 360*[™] vector network analyzer (VNA).

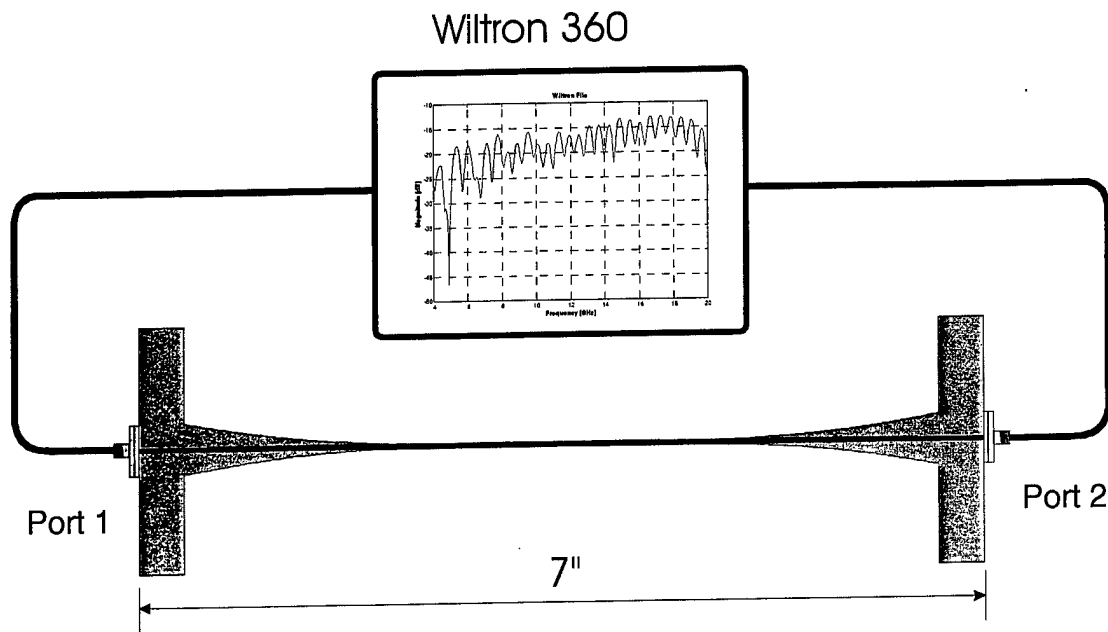


Figure 24. Balun test setup

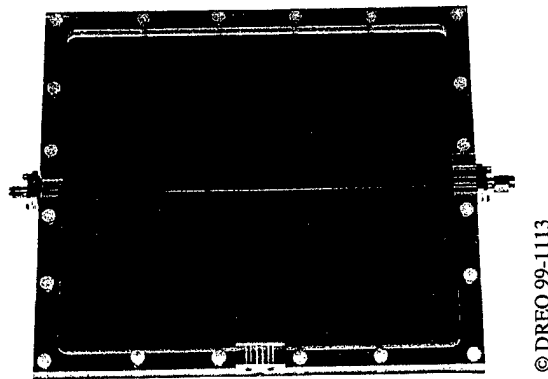


Figure 25. Photo of double balun

4.3.1 S parameter measurements of the double balun

S_{11} and S_{22} were measured using the *Wiltron 360*TM from 4 to 20 GHz. The S_{11} port utilized a male while the S_{22} port used a female *K Connector*TM. As can be seen in Figure 26, S_{11} was found to be less than -15 dB below 16 GHz and S_{22} somewhat worse, but never more than -13 dB. A 600 MHz ripple was observed which was most likely due to reflections back and forth between the two connectors. S_{22} is plotted on the same graph and shows identical ripple, though with much shallower nulls than S_{11} .

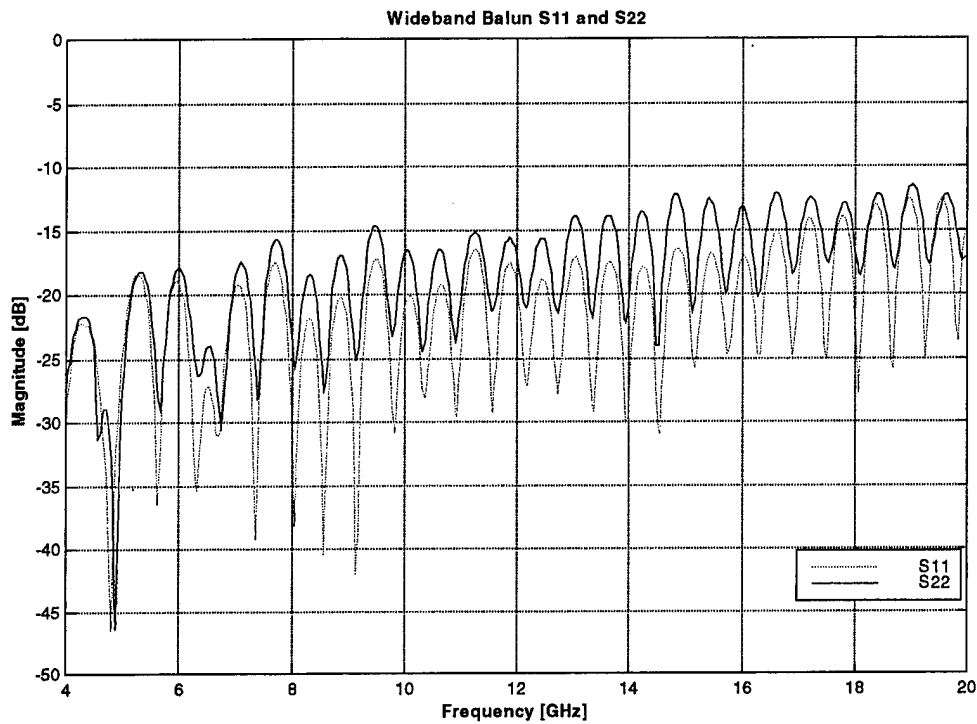


Figure 26. Double balun S_{11} and S_{22}

S_{21} was also measured, with results as shown in Figure 27. The increasing loss with frequency is due to conductive loss in the baluns and transmission line. It varied from -1.2 dB at 4 GHz to -4.7 dB at 20 GHz. A practical check of the balun's effectiveness, in ensuring that no current traveled on the outer surface of the coax, was performed by simply measuring S_{21} with and without one's hand on the connector. As no change was observed due to this possible perturbation, it could be inferred that there was no current on the outer surface to radiate. Thus, the balun was doing its job in this capacity. Again a 600 MHz ripple was observed, which was associated with interconnector reflections. These results are also important as they give an indication of how the losses will vary with frequency, in the complete array.

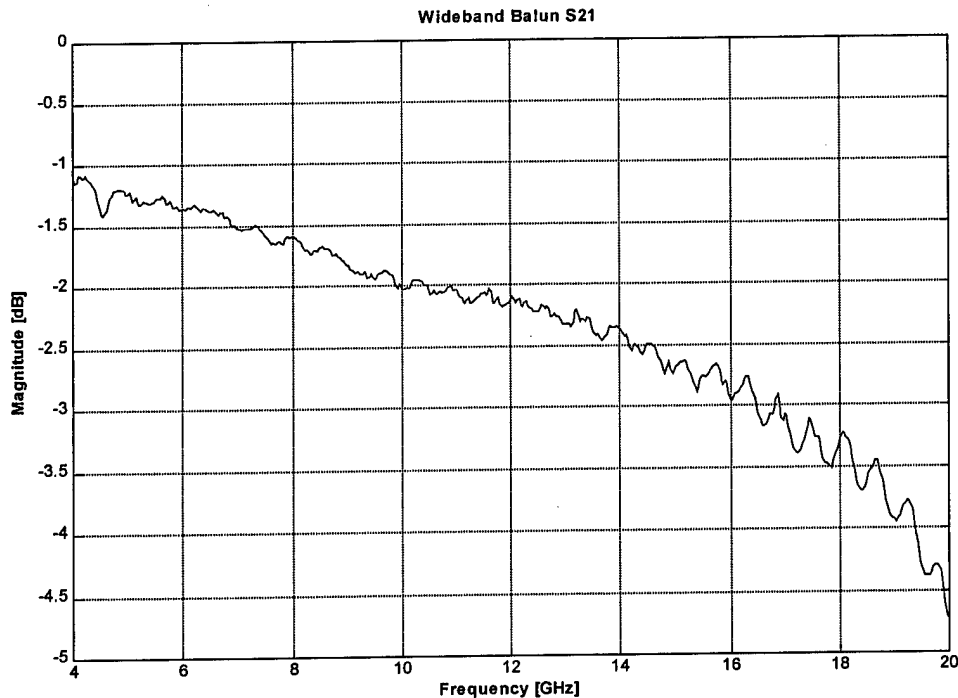


Figure 27. Double balun S_{21}

4.3.2 TDR Measurements of the double balun

TDR measurements were conducted from both ports of the double balun. This proved to be very useful, as it indicated the major sources of reflection (mismatch) and the asymmetrical nature of the setup. As is clearly visible from inspection of Figure 28, the two major reflections or mismatches were as expected, the launchers or sliding connectors. The Port-1 connector measured -21.8 dB and Port-2 was found to be -25.1 dB. As the manufacturer's specification was -25 dB, the results indicate the difficulty in reproducing these high tolerance connections. Variations in the magnitude of the measured reflections of the same location measured from the two ports is due to the fact that only the mid-point is equidistant from the two ports. Thus reflections from all other points suffer different losses, depending from which port the measurement was conducted. Other noticeable features include the middle two peaks of -40 dB which are the balun/transmission line transition. The transmission line itself was less than -50 dB.

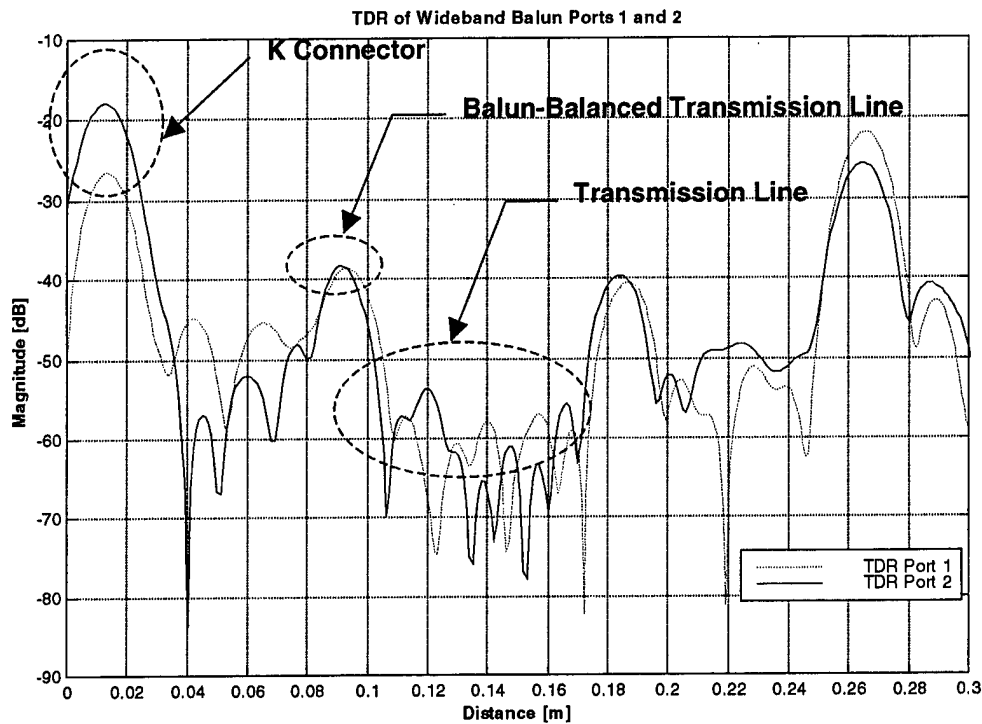


Figure 28. Double balun TDR of Ports 1 and 2

4.3.3 Simulation software validation and limitations

In an effort to gain confidence in the accuracy of the simulations, as well as skill in using the software tool, several simple devices were simulated and the results compared to theory. These devices included a microstrip patch, a thin dipole, a transmission line and a T-splitter.

This activity proved very useful as it highlighted several useful features of the software as well as a number of its limitations. By understanding these limitations, their effect on the accuracy of the simulations was minimized. Some key variables impacting the accuracy of the simulations included the number of cells per guided wavelength (discretization), the de-embedding scheme and number of de-embedding cells used, and whether edge cells were used or not. While *IE3D*TM used efficient non-uniform meshing optimization, the user still had to make a judicious tradeoff between cell size (which drives the number of cells) and simulation time. A rather important restriction is that for many of *IE3D*'sTM features, the default port impedance of 50Ω must be used. This tended to complicate the development of simulations, as the dipole elements being used in this study were always around 100Ω. Thus linear tapered impedance transformers had to be added to several simulations solely to exploit some of *IE3D*'sTM features, which require 50Ω port impedance's.

4.4 Simulated element and array performance

As with most modern antenna investigations, simulations can provide an effective method of understanding the architecture's operation. This study was no exception, with single and multiple elements being looked at.

4.4.1 Single element

Single wideband dipole elements, of various geometries, were simulated throughout the study. In order to negate any complications introduced by the balanced feed line, the simulated dipoles were centre fed using *IE3D*TM's 'vertical localized' feed mechanism. Simulations using dipoles fed by balanced feed line were virtually identical to those using the "vertical localized" scheme. Although the balanced feed was more representative of the actual dipole's feed mechanism, they required more cells and took longer to simulate, for no appreciable difference in accuracy. Thus, the vertical localized feed would be used throughout this study.

Figure 29 is representative of the current distribution of all the wideband dipole elements used in this study. It is apparent that the majority of the current is concentrated on the sides of the dipole. It was also noted, by viewing the current vector display in *IE3D*TM, that over the bandwidth of operation, only a single mode existed.

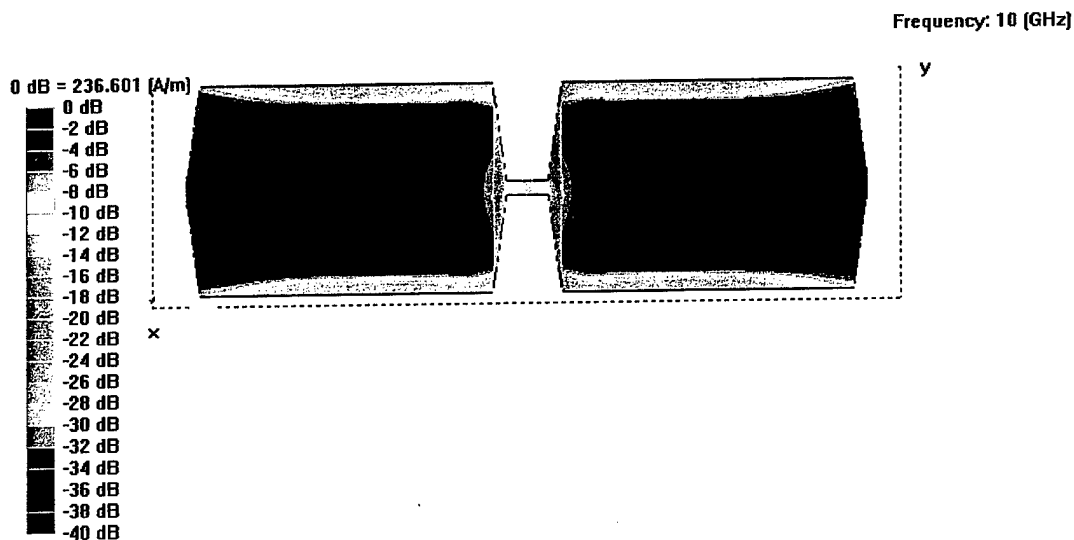


Figure 29. Current distribution on a single wideband dipole element at 10 GHz

4.5 Investigation of mutual coupling

It is known that if mutual coupling were nonexistent, the input impedance of an element in an array would be the same as that of an isolated element, and the input impedance of any particular element in an array would not be a function of the excitations of the other elements[39]. While this study is focused on a broadside beam and thin substrate architecture, which is normally considered to be somewhat less sensitive to mutual coupling problems, it is nonetheless important to investigate the issue. Mutual coupling, as it applies to dipole arrays, has been thoroughly investigated [40, 41, 42]. As highlighted in a study by Alexopoulos and Rana [43], for a single mode, most of the coupling in the broadside orientation is due to direct, higher order and leaky waves, while TM mode surface waves tended to be the main source of coupling in the colinear direction. If two modes were present, broadside coupling was primarily due to TE surface waves, with colinear coupling due mostly to the TM mode. Mutual coupling can increase the main beamwidth and sidelobe levels of an array, hence reduce its gain. While this is a considerable problem if aperture tapering functions are to be used, recent research has successfully developed “mutual coupling compensation techniques”[44]. A physical study of mutual coupling (ie. simulations, then fabrication and testing of dipole elements at various spacings) would entail a significant investment in time and material. Therefore, only the simulation of several elements was performed to determine their interaction, and provide an indication of whether mutual coupling would be an issue detrimental to array performance or not. In large arrays, most elements are surrounded by 8 immediate neighbours, which are the most significant contributors to mutual coupling. The minority of elements at the edges do not suffer the same effects. Therefore, a generalized worst case would be the centre element in a square group of nine. Further minimization of the simulation could be done by ignoring the effect of echelon elements, which generally have a minor mutual coupling effect. The results of such a simulation are depicted in Figure 41.

4.6 Antenna return loss and TDR measurement

Again using the *Wiltron™360* VNA, the return loss was measured and a TDR performed, for the U of B Array (5.77mm).

4.6.1 S₁₁ measurement of the U of B Array

The S₁₁ of the U of B array, as seen in Figure 30, was less than -10 dB over the 6 – 18 GHz bandwidth. At lower frequencies it increased substantially, most likely due to the proximity of the ground plane. The ripple was again caused by internal reflections between the dipoles and the launcher.

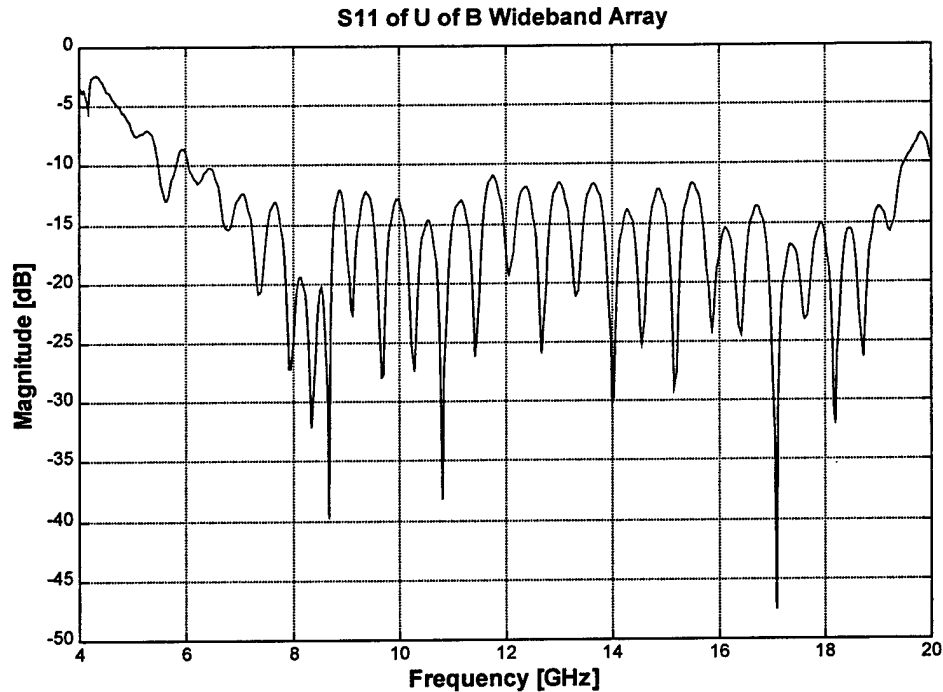


Figure 30. S₁₁ of the U of B wideband array

There was concern about the planarity of the array face, as it was not bonded to the foam spacer. In an effort to assess the impact of any ripples in the surface of the array, artificial distortions were introduced and the effect on S_{11} was observed. It was found that S_{11} was very tolerant to minor distortions or warping. Severe warps (7 mm elevation at the array midpoint) did however produce localized (2 GHz affected region) 10 dB deviations when compared with the original S_{11} . This indicated that while array planarity was important, experimentation without bonding the substrate material to the foam, would not detract from accurate measurements. Since the effects of planarity on radiation pattern consistency would be more serious, every effort was made to ensure that the printed array remained flat and parallel to the ground plane.

4.6.2 TDR measurement of the U of B Array

In an effort to further characterize the antenna, a TDR measurement was performed, the results as depicted in Figure 31. The 2 major -20 dB peaks were near the start point (launcher) and the 25 cm locations (dipole elements). Due to the symmetry of the array, similar physical discontinuities would occur at several places, which were all the same distance from the launcher. Since these reflections were equidistant from the measurement point, they would add in the time domain, thus making the isolation and identification of each mismatch a realistic endeavour. The reflections were artificially enhanced by facing the antenna upwards and placing metal screws, on their heads, at all

similar discontinuities (ie. all T splitters). The resulting changes in the TDR were then observed. By this method all major peaks were identified as seen in Figure 31. While the launcher and dipoles themselves produced reflections of -20 dB, all other internal discontinuities were less than -25 dB. Therefore any improvements in the match of the launcher and the match of the individual dipole elements themselves, would improve the overall efficiency of the antenna. The match of the dipoles is probably worse than indicated, as the TDR measurement doesn't account for the conductive losses, which the round trip reflections from the dipoles would suffer. Since the remaining reflections are below -33 dB, it is unlikely that any further improvement in the feed network could be easily obtained, without first improving the match at the dipole elements.

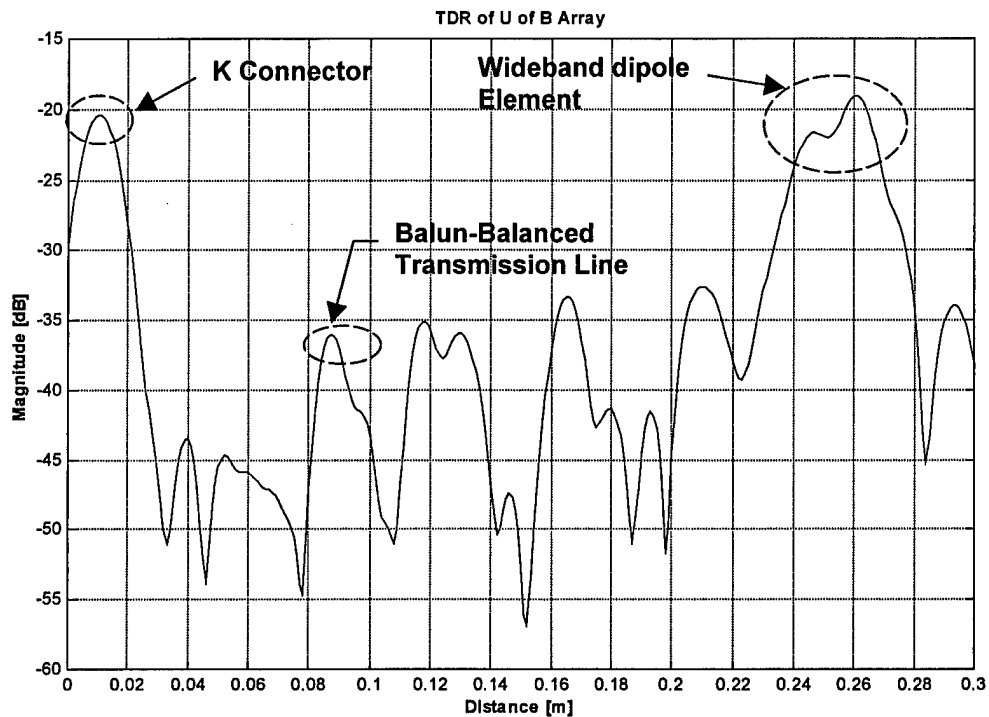


Figure 31. TDR of U of B wideband printed-dipole array

4.7 Representative radiation patterns

Radiation patterns were measured in the DDARLing anechoic chamber (Figure 33), using the setup depicted at APPENDIX B. From 4 – 20 GHz, in 2 GHz increments, co and cross-polarization patterns were taken every 15 degrees (ϕ cuts), from -100 to 100 degrees. The co-ordinate system is described in section 4.8.1. While representative E and H-plane cuts are shown at Figure 32, a complete set of measurements is available at APPENDIX E. In general, sidelobes remained below -12 dB from 4 – 18 GHz in the H-plane and 6-14 GHz in the E-plane. The difference in the

patterns of the 2 planes is due to the fact that the array is rectangular and has only four elements in the E-plane. As well, the elements are spaced 22.5mm in the E-plane and 16.26mm in the H-plane.

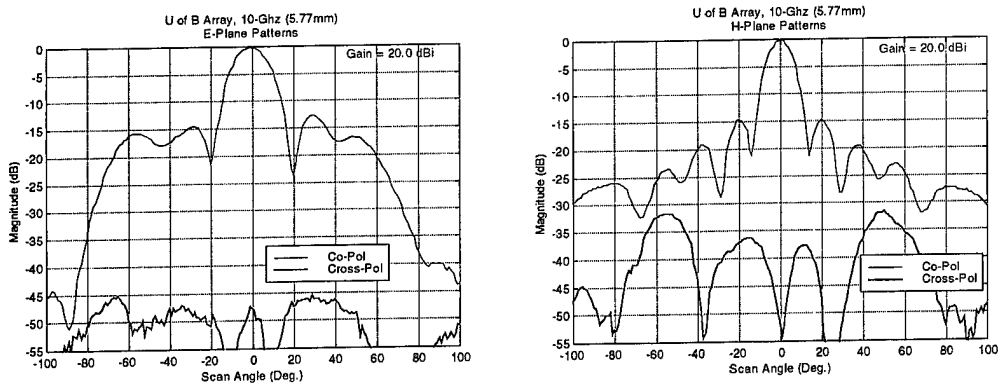
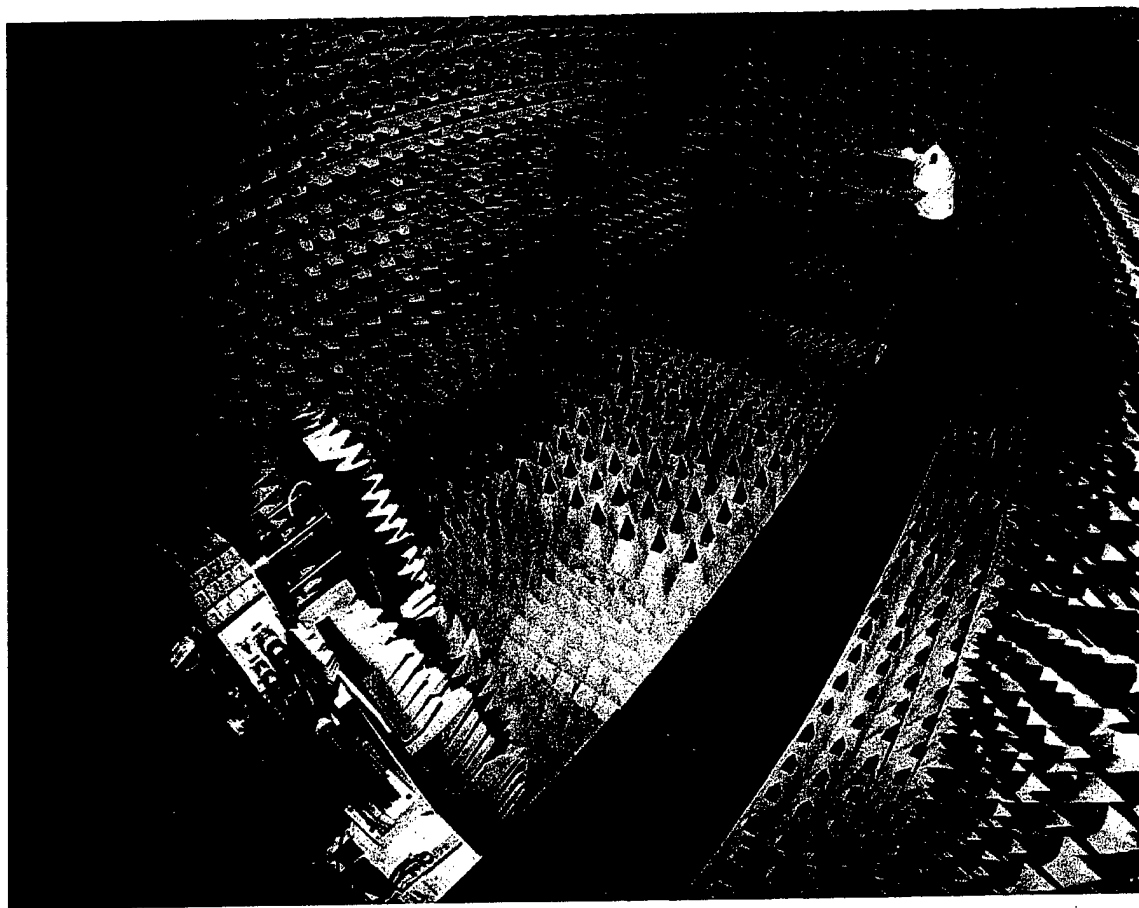


Figure 32. Representative U of B wideband array (10 GHz) E and H-plane patterns



© DREO 99-1040

Figure 33. Photo of DDARLing anechoic chamber

Examination of the patterns at different frequencies showed the expected results. However, there were some unexpected results such as the 40 degree beamwidth observed in the E-plane at 4 GHz. This was most likely due to mutual coupling effects. As well, some distortion is noted in the $\phi=90^\circ$ cut, which is associated with the balun and feed point. However, this is the only frequency at which this effect was observed. Grating lobes became unacceptable at 16 GHz in the E-plane and 20 GHz in the H-plane.

Inspection of sequential cuts at APPENDIX F, reveals an excellent cross-polarization ratio of at least -40 dB. Symmetry about the geometric diagonals of the array were noted as appropriate for a rectangular array.

4.8 Comparison of simulated and measured radiation patterns

In an effort to determine the validity of various simulation packages, measured radiation patterns were compared to normalized patterns simulated in *ARPS*TM and *IE3D*TM. The objective of this effort was to ensure that these packages would be appropriate for further use in optimizing the array's element spacing. At Figure 34, one can see a representative example of the good correlation between the measured and simulated radiation patterns. It is significant that for the 10 GHz pattern, *ARPS*TM and *IE3D*TM produced patterns very similar to the measured data, even though they produced their patterns from single element patterns and an array factor and did not consider mutual coupling as part of the simulations. This indicates that at this frequency mutual coupling is not a serious concern. The greatest variation between simulation and measurement was observed near the horizon (the plane of the array). This may indicate the effect of the finite ground plane on the physical antenna, whereas the simulations assumed an infinite ground plane. The finite ground plane and edge effects may also account for the slight variation in the location of the nulls and side lobes.

U of Belgrade Array Normalized H-Plane Patterns (Cut-Angle 0 deg)

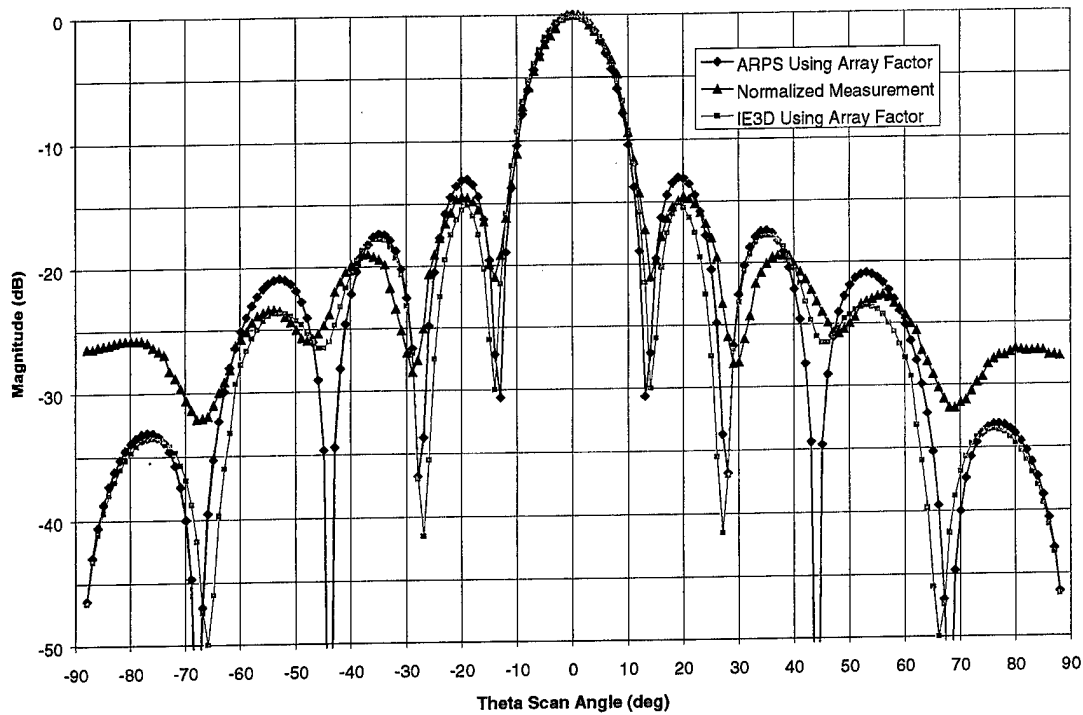


Figure 34. Comparison of simulated (*ARPS*TM/*IE3D*TM) vs. measured radiation pattern

4.8.1 Coordinate system for measurements

In order to facilitate the inspection of radiation patterns, Figure 35 is provided as a depiction of the relationship between the physical mounting of the AUT in the chamber and the far field spherical co-ordinate system. Ludwig's 3rd definition of polarization was used throughout the measurements[45].

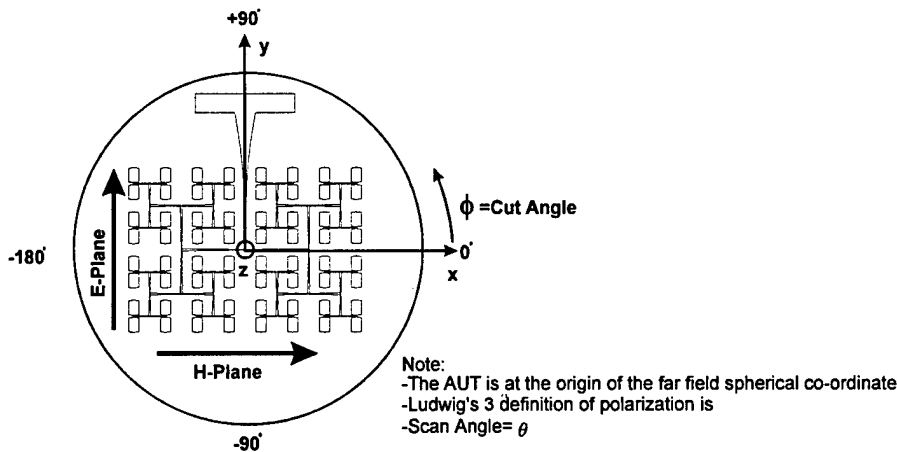


Figure 35. Relationship between the AUT and the spherical coordinate system

4.9 Boresight gain measurement using the gain transfer method

While the measurement of gain can be an absolute measurement, with an accurately calibrated probe and sensitive test facility, it is more often derived via the gain comparison or transfer method [46]. The basis of this method involves a standard gain antenna, normally a horn, for which the gain has been previously accurately determined. Then with the AUT measured, its absolute gain can be derived by comparison with the gain standard. A *Matlab*[®] program (the program listing may be found at APPENDIX A) was written which would manipulate the “Gain standard” file with the AUT measurement. Correction factors are applied to account for any difference in the distances between the gain standard and the test probe, compared to the distance between the AUT and the test probe. Additionally, the effective aperture size is entered so that the maximum theoretical gain can be displayed concurrently with the actual derived gain. For the purposes of this study, it was assumed that the array was a “uniform distribution aperture on a ground plane”. The maximum theoretical directivity (boresight) of such an aperture is given by the following formula [47].

$$directivity = \frac{4\pi}{\lambda^2} (area) = 4\pi \left(\frac{ab}{\lambda^2} \right) \quad (4.1)$$

The DDARling chamber was utilized for the gain measurement. The probe and the gain standard horn were both 6 – 18, GHz *Tecom*[™] quad-ridged horns. The measurement was repeated, to produce the final results, with the insertion of a 6 dB pad (attenuator). This had the positive effect of reducing the effect of any mismatch between the AUT and the rest of the system.

4.9.1 Gain measurement results

With what is basically an S_{21} measurement of the AUT (U of B Array) and the reference gain standard (Figure 36), the absolute gain of the reference antenna was applied to the AUT's S_{21} , to convert it to an absolute gain (dBi). As the data file for the archived gain standard was not produced at the same frequency increments of the current S_{21} measurements, interpolation was performed within the gain transfer program, so that appropriate S_{21} "corrections" could be applied to the AUT measurement.

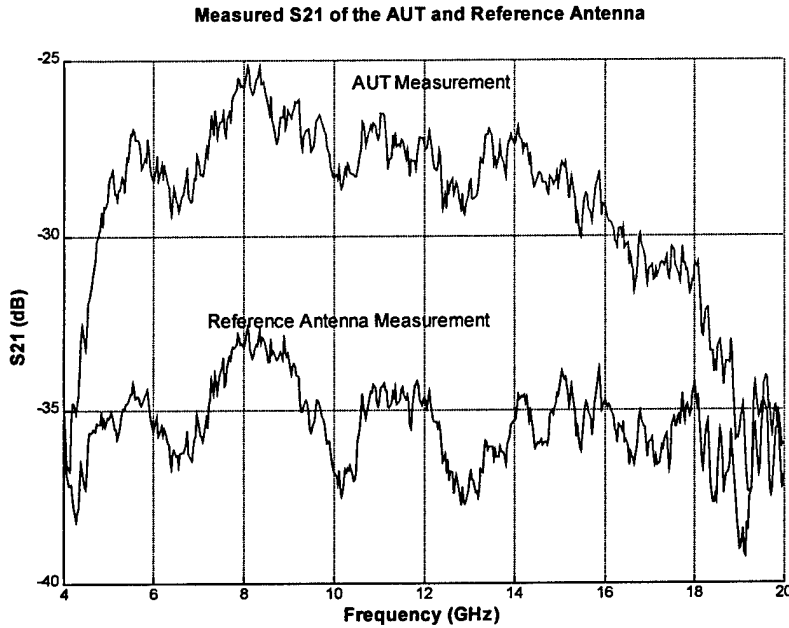


Figure 36. S_{21} of AUT and reference antenna

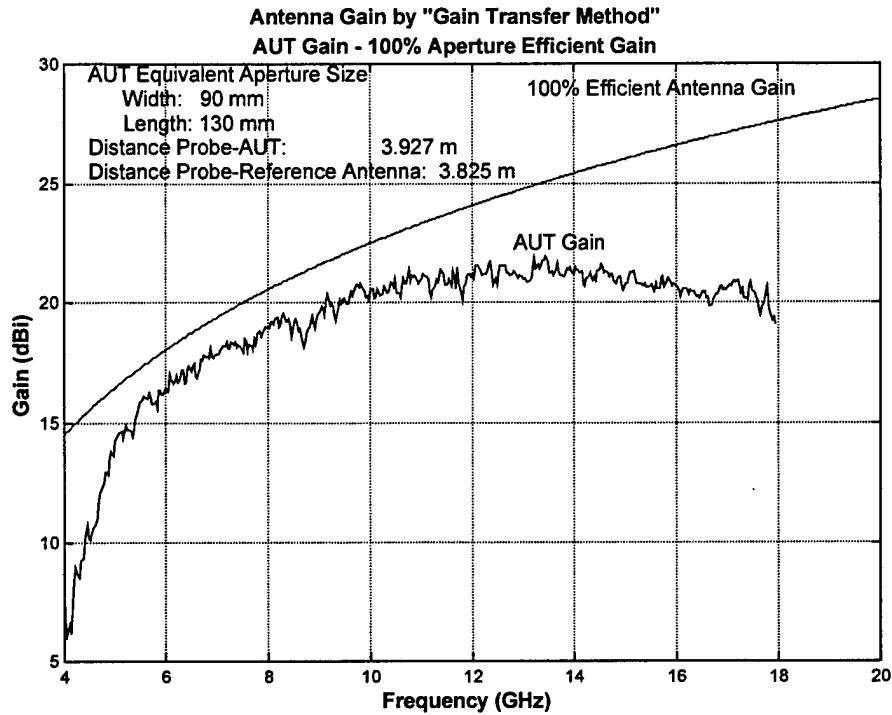


Figure 37. U of B Array(5.77mm) measured and theoretical gain

The boresight gain is found to track the theoretical maximum to within 3 dB from 6 to 12 GHz and then falls off to 8 dB below the theoretical maximum at 18 GHz.. The overall gain, within the bandwidth of interest, ranged from 16 dB to 22 dB. The minor deviation in gain at 8.875 GHz was verified by using a *Flann*[™] horn as the gain standard. It was most likely the result of a standing wave existing within the AUT.

4.10 Radiation efficiency of U of B Array (5.77mm)

Although it is useful to observe how the gain varies with frequency, the information is better represented in a practical fashion, as radiation efficiency. Arguably, one of the most constructive definitions of bandwidth is the bandwidth over which the radiation efficiency is above a certain value. This aspect of the U of B Array is provided in the following figure for a threshold of 50%.

Using the measured boresight and theoretical gains, the following relationship was applied to find efficiency:

$$Efficiency = \left[10^{\left(\frac{AUT_{gain(dbi)} - Theoretical_{gain(dbi)}}{10} \right)} \right] \times 100\% \quad (4.1).$$

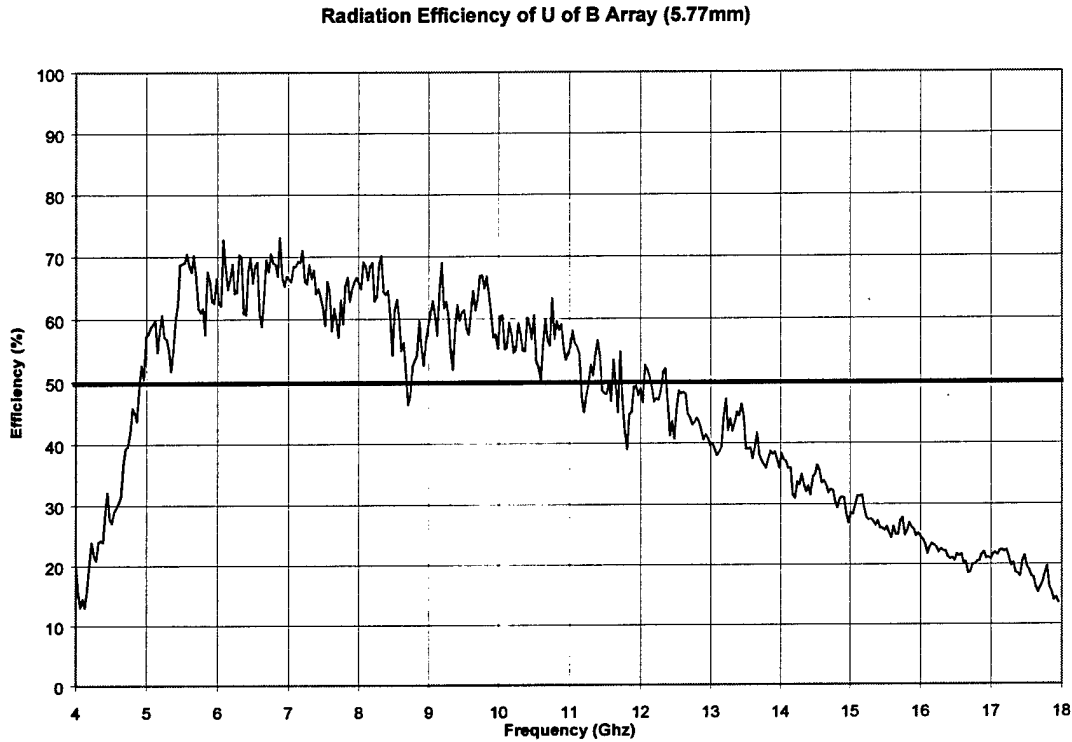


Figure 38. Radiation Efficiency of U of B Array (5.77mm)

As can be seen the 50% efficient bandwidth is from 4.9 to 11.2 GHz with one minor deviation at 8.75 GHz. The efficiency has a general maximum of 65% towards the low end of the bandwidth.

4.11 Summary of performance

In general, the wideband printed-dipole array design provided by the University of Belgrade proved to be an excellent starting point and further bandwidth enhancement would prove challenging. The measured performance is summarized in the following table:

Bandwidth Definition	Bandwidth (GHz)
Gain Bandwidth (Efficiency > 50%)	5-11.2 GHz

VSWR Bandwidth	6-20 GHz
Pattern Bandwidth	6-14 GHz (E-plane) 4-18 GHz (H-plane)

Table 3. Summary of U of B wideband array performance

4.12 Rationale for enhancement

Given the above performance, it was decided that the upper portion of the bandwidth would be a promising area for further exploitation, primarily due to the fact that the gain, hence efficiency, tapered off gradually with increasing frequency. Additionally, it was hoped that some improvement could be achieved at the lower end of the bandwidth. These enhancement efforts would involve:

better selection of the array's height over the ground-plane with the objective of improved VSWR, at the low frequencies especially; and,

further optimization of the element spacing with the objective of reducing grating lobes at 16 GHz (E-plane especially) to an acceptable level.

The process of addressing these objectives will be covered in the following chapter.

5. IMPROVED WIDEBAND PRINTED-DIPOLE ARRAY DESIGN

5.1 Introduction

The optimization of any antenna element can be a complex undertaking. Often, as in the case of this study, the objective is to increase the bandwidth of the antenna element. However, as was pointed out previously, there are several definitions of bandwidth. The complication is that for each type of bandwidth, whether VSWR, pattern, gain or efficiency, there are conflicting optimization parameters. For example, what may be an optimal modification parameter for the improvement of VSWR may actually have a negative effect on gain. Thus, in the end, optimization becomes an iterative series of performance tradeoffs. At the present time, this global optimization process must be performed manually as the scope of parameters is beyond the capacity of current desktop work-stations and commercially available software. Hopefully a logical, yet manual, approach will allow the best balance between the competing definitions of bandwidth and the parameters, which affect each.

As highlighted in the previous chapter, the objective of improving the array bandwidth, would primarily consist of finding a better height over the ground-plane and improved element spacing. Due to what would be a significant research effort for marginal gain, further improvement of the balun would not be undertaken. This initial optimization attempt would be referred to as the "Optimized Array-1", throughout the remainder of this study.

5.2 VSWR optimization

The optimum height over the ground plane was investigated by simulating single wideband dipole elements at various heights using *IE3D™*. The results of these simulations (Figure 39) would indicate that a height of 10.35mm would provide the best compromise between VSWR and bandwidth.

VSWR Change vs Height Over Ground

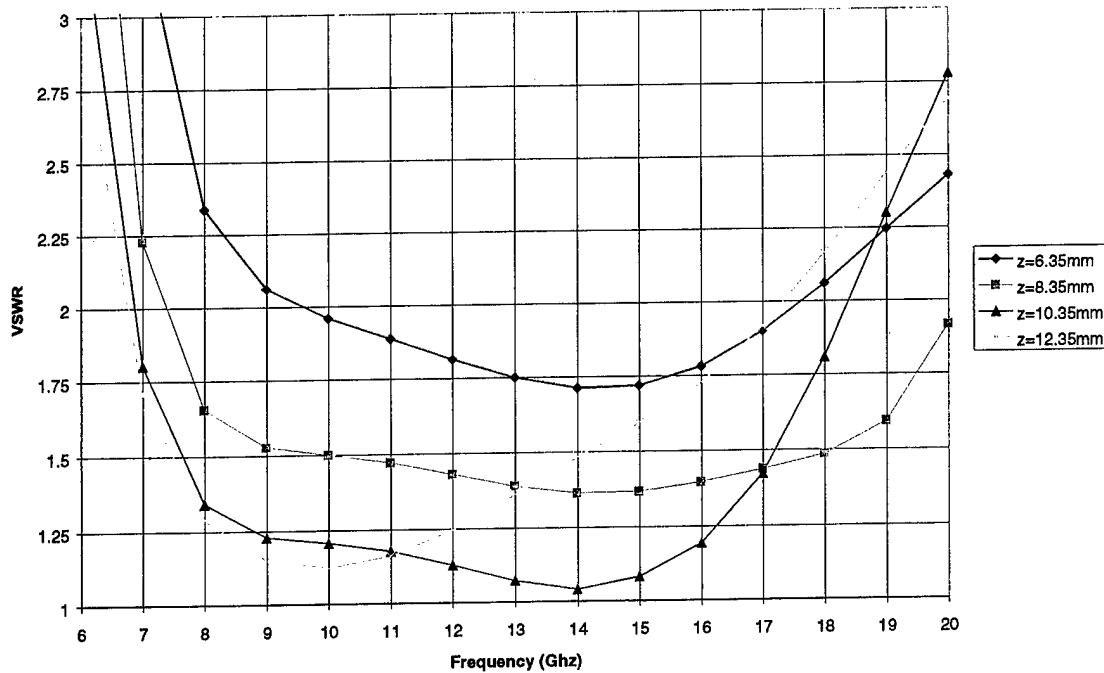


Figure 39. Gain change due to variation of array height over the ground plane

Unfortunately for the antenna designer, one also has to consider how a height variation will affect the radiation patterns and boresight gain. Due to this concern, further simulations were conducted on single elements in order to assess how boresight gain, hence efficiency, varied with frequency. Four simulations were conducted covering the original height and three others. As can be seen in Figure 40, since a large null appears in the $z=8.35\text{mm}$ gain curve at 17 GHz, no greater ground-plane spacings were simulated. Thus, although we would have originally chosen a height of 8.35mm, we acknowledge that this height would suffer severe degradation in the gain due to the formation of a null at boresight. For this reason, the compromise height of 6.35mm was chosen based on balancing the simulated element VSWR and radiation efficiency. It was acknowledged that the effect on a complete array may be somewhat different.

Gain vs Frequency for Various Heights Over Ground

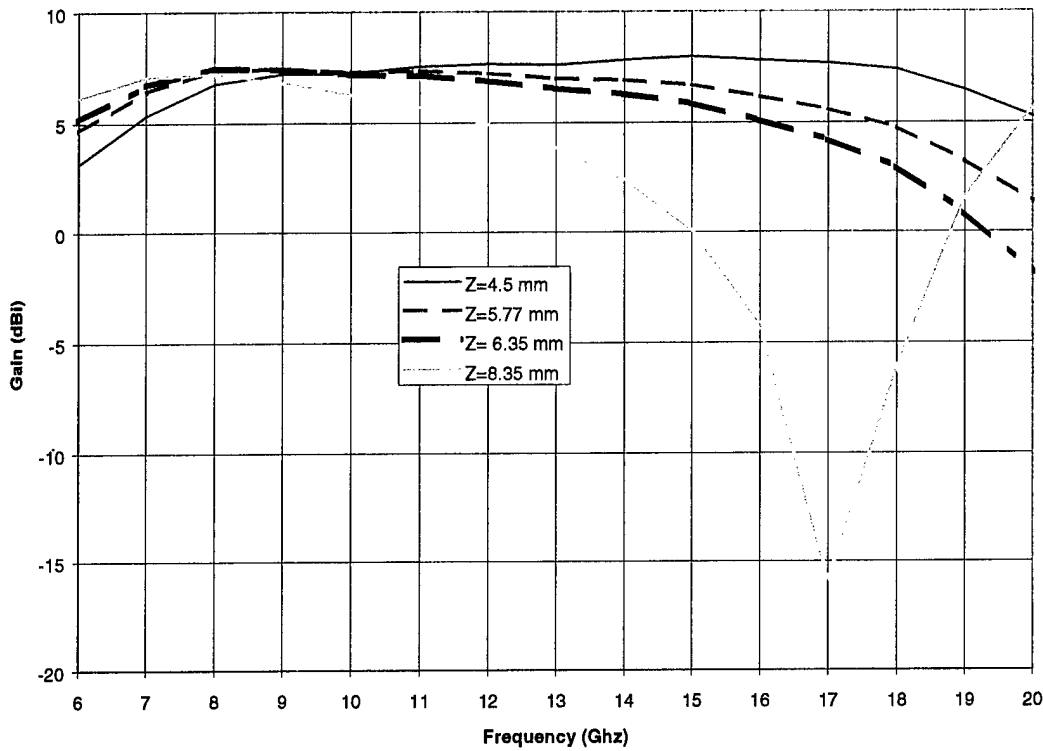


Figure 40. Gain variation due to height over ground change

5.3 Element spacing

As stated in the previous chapter, it was also an objective to reduce the grating lobes at 16 GHz. If this could be done, it would represent a 25% improvement in the pattern bandwidth. With considerable confidence in the correlation between measured and simulated radiation patterns, simulations for various element spacings were conducted in *ARPS™*. These simulations were sequenced in an effort to determine the maximum element spacing, which would still produce acceptable radiation patterns in the E and H-planes. It was found that the elements would have to be moved 2.26 mm closer in the broadside dimension (x) and 3.50 mm closer in the colinear dimension (y).

As with all arrays, dipoles in particular, there is a physical limitation on how small the element spacing can be. While it is generally desirable to have a symmetric beam shape, this may not be possible, as the elements are rectangular. If a minimum broadside dimension was found, there would be overlapping of elements in the colinear direction. An additional issue, not to lose sight of, is that room must be protected for the coplanar feed network. As well, it should be considered that before physical contact of

the elements and the feed network becomes a problem, mutual coupling amongst the various tightly packed structures will arise. To account for this, once the optimal spacing was determined in *ARPS*TM, five elements at that spacing would be simulated in *IE3D*TM to determine if mutual coupling between elements was a concern or not. Five elements in a cross configuration was considered adequate as the effect of mutual coupling between echelon elements was previously determined to be minimal. Although not investigated rigorously it was accepted that the inherent shrinkage in the feed network, due to closer element spacing, would mean that the linear taper transformers would be shorter and thus would cause a small increase in reflections. Previous simulations had indicated that as long as the tapered sections were approximately a wavelength long, losses would be minimal.

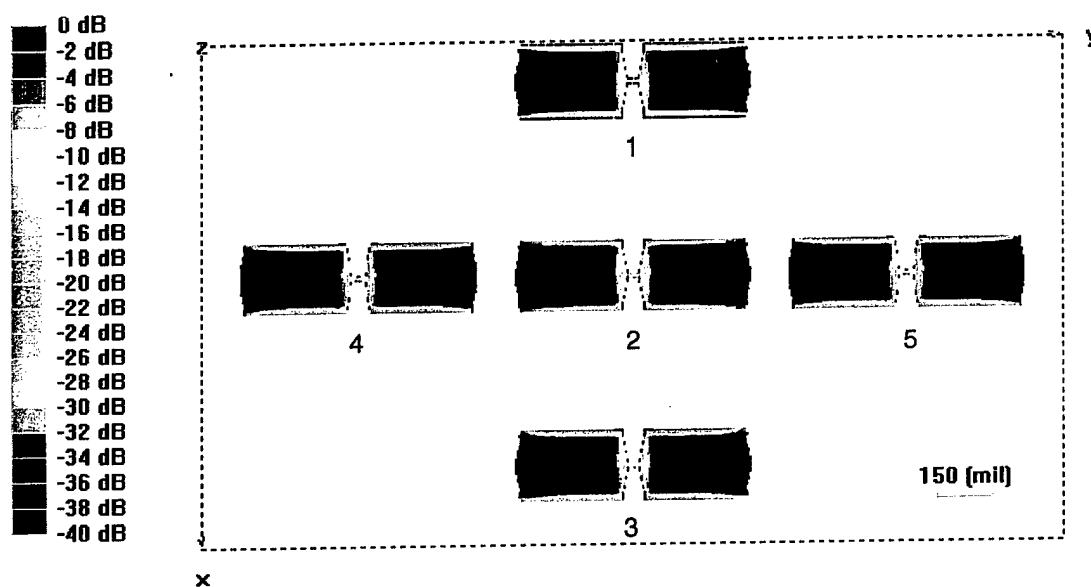


Figure 41. Current distribution at 10 GHz of 5 elements at optimized spacing

Mutual Coupling of 5 Elements of Optimized Array-1

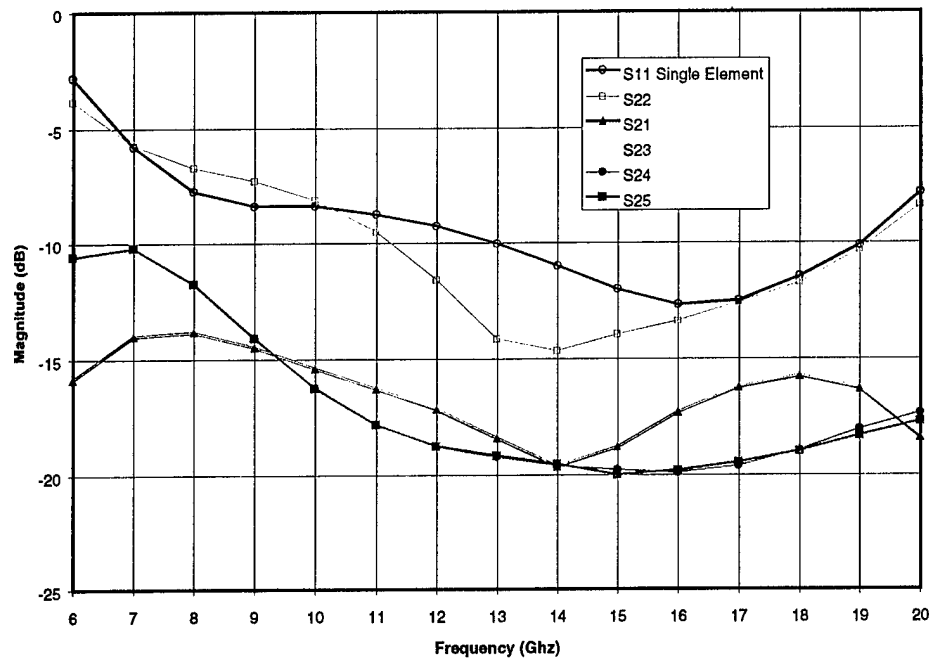


Figure 42. Mutual coupling of 5 elements of Optimized Array-1(6.35mm)

While Figure 41 provides a visual indication that the current distribution on each element is not significantly affected by mutual coupling with its neighbours, Figure 42 gives more quantitative information. Mutual coupling remains at least below -10 dB over the entire bandwidth. Self-impedance has not changed very much over the single isolated element case, though a slightly better match may be possible. While these simulations may indicate that the elements could be moved even closer together, it was decided that this was the smallest possible spacing which would still reasonably contain the feed network.

5.4 Physical description of the design

In addition to the printing of a new antenna, the fabrication of this array structure involved the construction of new foam and aluminum spacers. The important dimensions are as depicted in the following figure.

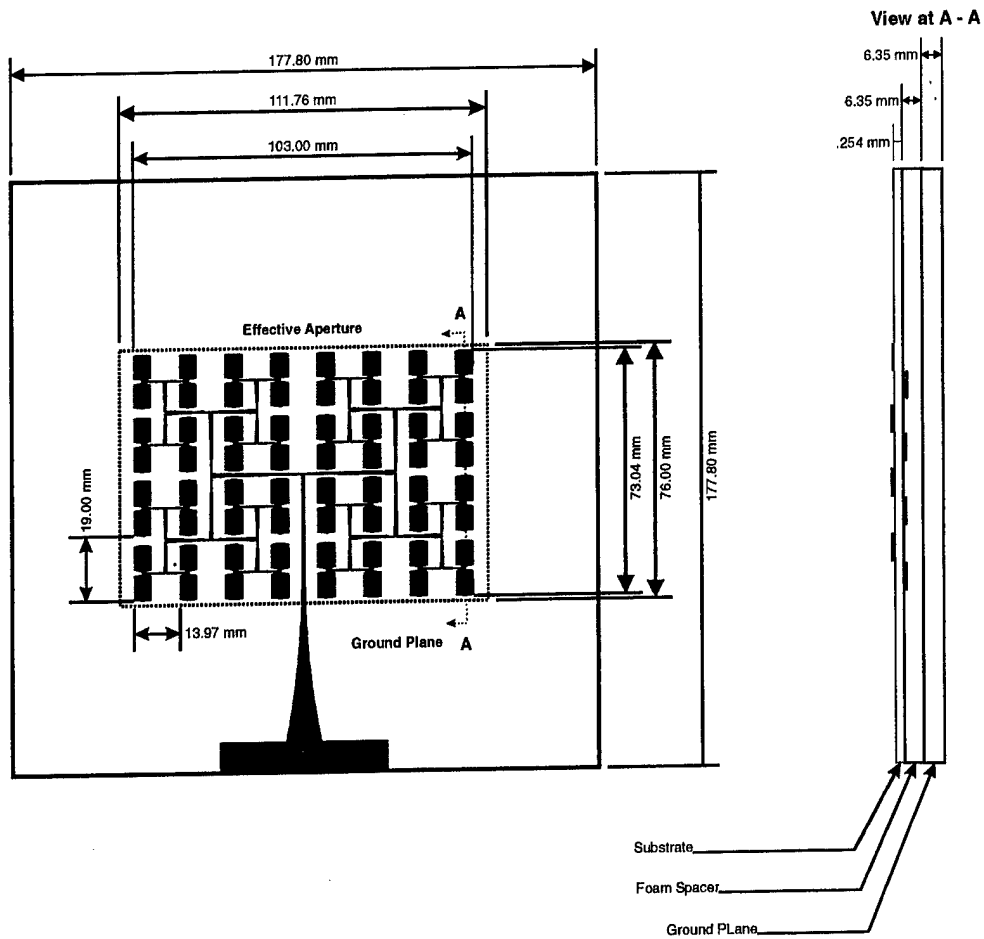


Figure 43. Optimized Array-1 (6.35mm) physical layout

Parameter	Dimension (mm)	Parameter	Dimension (mm)
Dipole Length	16.26	Element Colinear Spacing (y)	19.00
Dipole Width	5.21	Element Broadside Spacing (x)	13.97
Array Length (x)	103.00	Aperture Length (x)	111.76
Array Width (w)	73.04	Aperture Width (y)	76.00
Height Over Ground	6.35		

Table 4. Dimensions of Optimized Array-1 (6.35mm)

5.5 Measurement results

As it was intended to compare the performance of the U of B Array and the Optimized Array-1, similar antenna measurements were conducted in the DDARLing lab.

5.5.1 S11 return loss of Optimized Array-1 (6.35mm)

The return loss of the Optimized Array-1 (Figure 44) shows marginal improvement over the U of B Array. Between 5 and 7 GHz, S_{11} is 5 dB lower. This is most likely a result of the increased height over ground-plane, which as would be expected, has a greater effect at the lower frequencies.

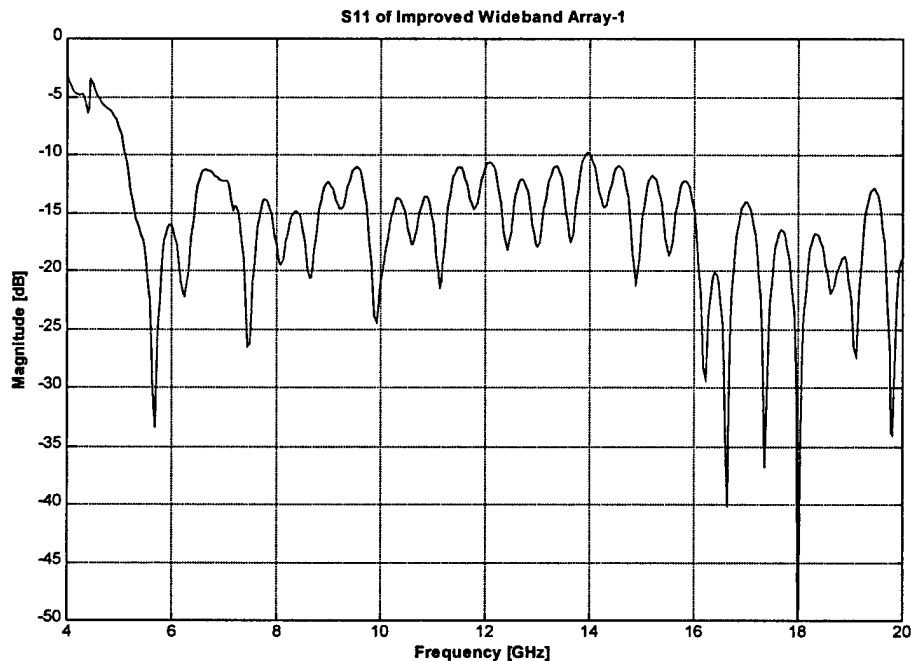


Figure 44. S11 of Optimized Array-1

5.5.2 TDR measurement of Optimized Array-1 (6.35mm)

The TDR measurement at Figure 45 was very similar to that of the U of B Array, possessing all of the same attributes, with only slight variations. The most notable difference being a 3 dB improvement in the connector/launcher performance (fabrication tolerance). While some of the nulls were deeper, the graph scale was maintained to facilitate comparison with the measurements of the U of B Array (figure 31).

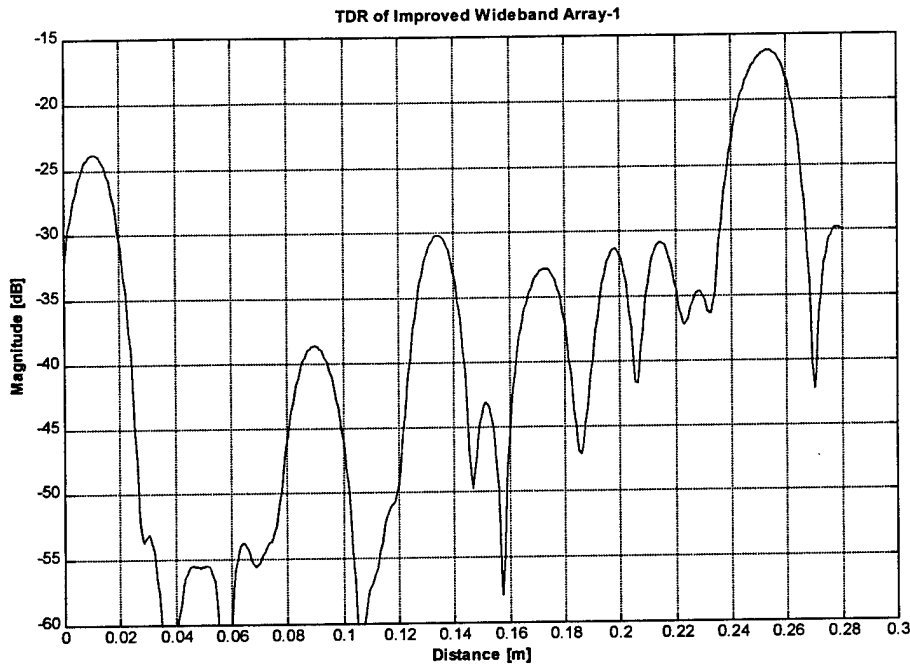


Figure 45. TDR of Optimized Array-1

5.6 Gain measurement using three antenna method

The boresight gain of the Optimized Array-1 was measured using the “three antenna method”, which is an absolute gain measurement method. Although a somewhat more complex measurement method than “gain transfer”, it should provide for a more accurate gain measurement [48]. Essential to the methodology is the Friis Transmission formula:

$$P_r = P_t G_A G_B \left(\frac{\lambda}{4\pi R_{AB}} \right)^2 \quad (5.1)$$

which for this application, is more conveniently written in logarithmic form:

$$G_{A-dB} + G_{B-dB} = 20 \text{Log}_{10} \left(\frac{4\pi R_{AB}}{\lambda} \right) + 10 \text{Log}_{10} \left(\frac{P_r}{P_t} \right) \quad (5.2)$$

Where:

$$G_{A-dB} = \text{maximum gain of antenna A in dB} = 10 \text{Log}_{10} G_A$$

- G_{B-dB} = maximum gain of antenna B in dB = $10\text{Log}_{10}G_B$
- R_{AB} = separation distance in meters between antennas
- λ = wavelength of the transmitted signal in meters
- P_t = signal level at the input of the transmitting antenna
- P_r = signal level at the output of the receiving antenna

Figure 46 portrays what are in fact S_{21} measurements, which were completed between antennas A and B, A and C, and between B and C. As these S_{21} measurements are actually a power ratio between ports 1 and 2 of the VNA, a correction term must be obtained to account for the amplifiers, as well as the losses between the antennas and their respective VNA ports. This “cable-thru” measurement was performed by directly connecting the transmitting and receiving circuitry. (see test arrangement at APPENDIX B) With this correction factor applied for each of the resulting three measurements at equation 5.2, the 3 unknowns, the absolute gains, can be derived.

Inspection of the S_{21} graphs at Figure 46 reveals a steep null at 18.5 GHz. As this is outside the specified bandwidth of the probe, it could be due to a higher order mode or standing waves within the *Tecom*[™] horns.

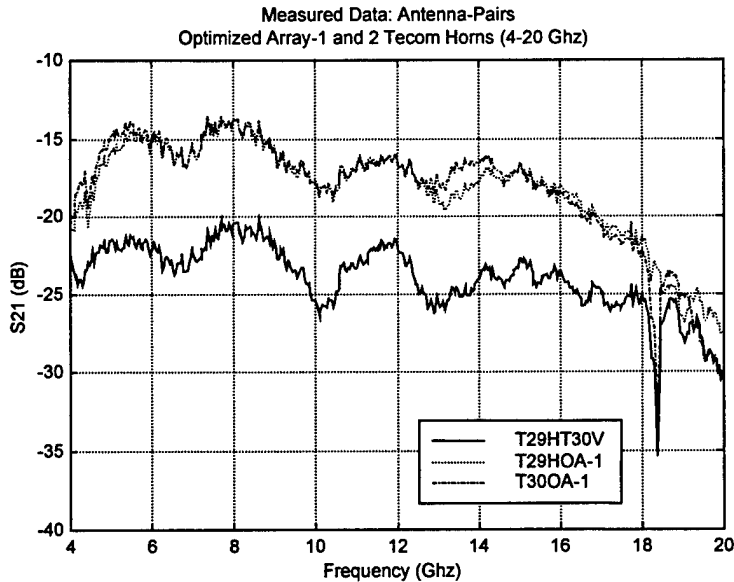


Figure 46. S21 measurements for three-antennas

Comparison of the calculated gains of the U of B Array, at Figure 37, and the Optimized Array-1 gain below at Figure 47, indicates that the 3-antenna method has realized approximately a 50% improvement in the “measurement noise” (+/- .2 dBi to +/-

.1 dBi) Thus, though a more complicated measurement, the 3-antenna method does yield a more accurate result.

Again, since the direct comparison of antenna gains is somewhat artificial when each antenna possesses a different aperture size, comparison of their radiation efficiencies is considered to be a more worthwhile endeavour. This approach was described in the previous chapter.

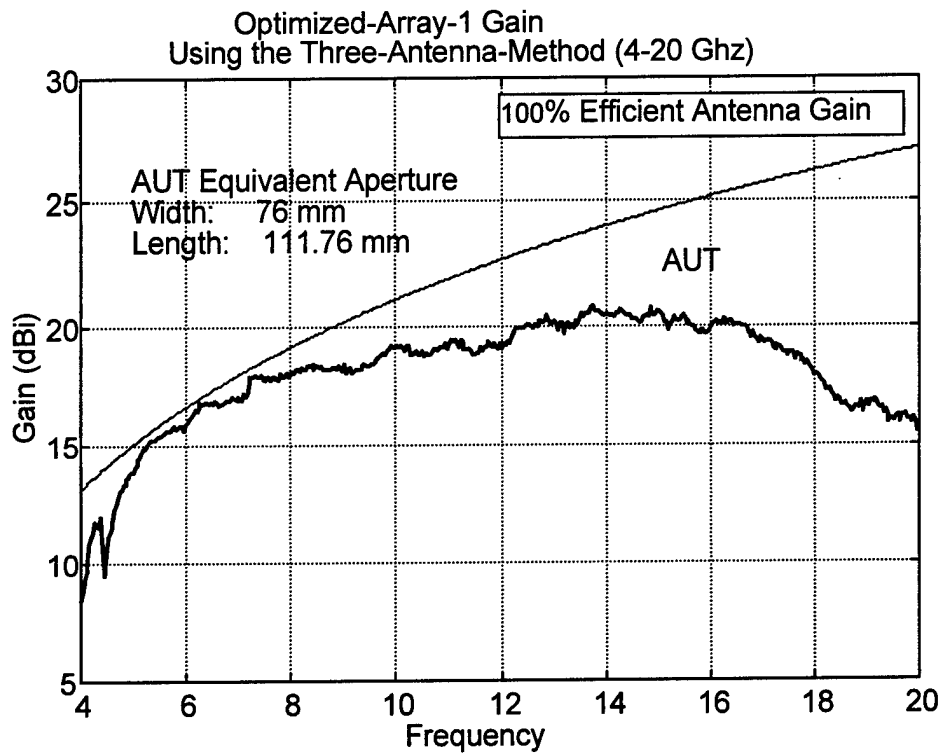


Figure 47. Optimized Array-1 gain using the 3 antenna method

5.7 Radiation efficiency comparison of the University of Belgrade design and Optimized Array-1

An excellent attribute for comparing antennas is their radiation efficiency over a certain bandwidth. As described in the previous chapter, the boresight gains are compared with the theoretical gain over the bandwidth of 4 to 20 GHz to produce their radiation efficiencies over the same bandwidth.

Radiation Efficiency of U of Belgrade and Optimized Array-1

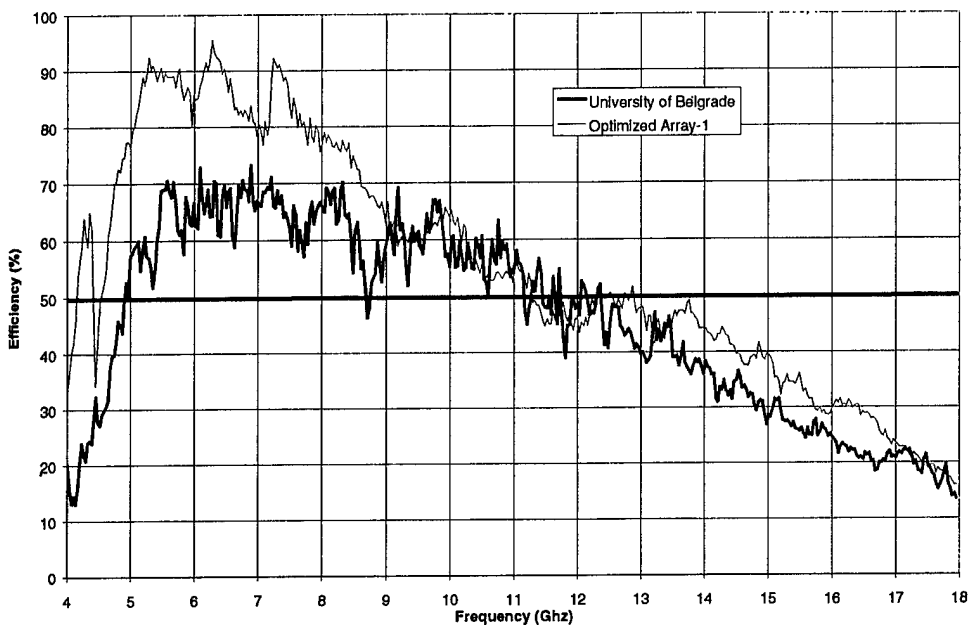


Figure 48. Radiation efficiency of U of B and Optimized Array-1 designs

These results indicate a 10 – 20% improvement in the boresight gain, between 4.5 and 8 GHz, and a 5% improvement from 13.5 – 16.6 GHz. While the upper frequency improvement in radiation efficiency may be attributable to the closer element spacing, that at the low frequencies is possibly due to better directivity and improved VSWR.

5.8 Representative radiation patterns

The improvement in side lobe “roll-off” due to the closer element spacing within the array, can be seen in the E and H-plane patterns at APPENDIX G. A pair of representative patterns at 16 GHz, are shown in the following figure.

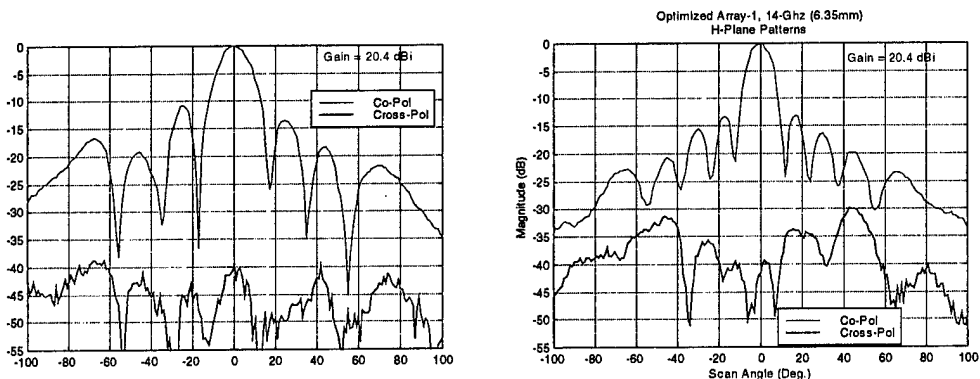


Figure 49. Representative Optimized Array-1 E and H-plane patterns

5.9 Feed network issues

The corporate feed networks used by the arrays in this study possess the well known advantage of simplicity, especially with regards to the creation of a broadside beam. As well, the general architecture is suited to the rectangular element layout used in these arrays. However, as with all corporately fed arrays, as the number of elements increase, so does the size of the feed system. This is of particular concern, as the transmission line length is a major source of loss and is in fact a limiting factor for array size.

5.9.1 Losses

The loss suffered by a signal travelling through the feed network can be attributed to conductor loss, α_c , and dielectric loss, α_d [49]. Thus the total attenuation can be represented as:

$$\alpha_T = \alpha_c + \alpha_d \quad (5.4)$$

where:

$$\alpha_c = 1.38A \frac{R_s}{hZ_0} \frac{\left(32 - \frac{W_e}{h}\right)^2}{\left(32 + \frac{W_e}{h}\right)^2} \quad \text{for } W/h \leq 1 \quad (5.5)$$

$$\alpha_c = 6.1 \times 10^{-5} A \frac{R_s Z_0 \epsilon_{re}}{h} \left[\frac{W_e}{h} + \frac{0.667 \frac{W_e}{h}}{\frac{W_e}{h} + 1.444} \right] \quad \text{for } W/h \geq 1 \quad (5.6)$$

and

$$\alpha_d = 27.3 \frac{\epsilon_r}{\epsilon_r - 1} \frac{\epsilon_{re} - 1}{\sqrt{\epsilon_{re}}} \frac{\tan \delta}{\lambda_0} \quad (5.7)$$

where

$$A = 1 + \frac{h}{W_e} \left[1 + \frac{1.25}{\pi} \ln \left(\frac{2\pi W}{t} \right) \right] \quad \text{for } W/h \leq 1/2\pi \quad (5.8)$$

$$A = 1 + \frac{h}{W_c} \left[1 + \frac{1.25}{\pi} \ln \left(\frac{2h}{t} \right) \right] \quad \text{for } W/h \geq 1/2\pi \quad (5.9)$$

$$R_s = \sqrt{\frac{\pi f \mu_0}{\sigma}} \quad (5.10)$$

where:

W_e	= equivalent width
h	= height of substrate
Z_0	= characteristic impedance
R_s	= resistivity
t	= strip thickness
σ	= conductivity of substrate

While the dielectric loss is negligible when compared to the conductor loss [27], it remains a part of the software program MICRO [49], which was used to estimate the losses in the feed network. As the feed network is comprised of 100Ω and 50Ω transmission lines, as well as tapered transformers and a balun, it was generalized as a length of 50Ω transmission line, to facilitate an estimation of loss.

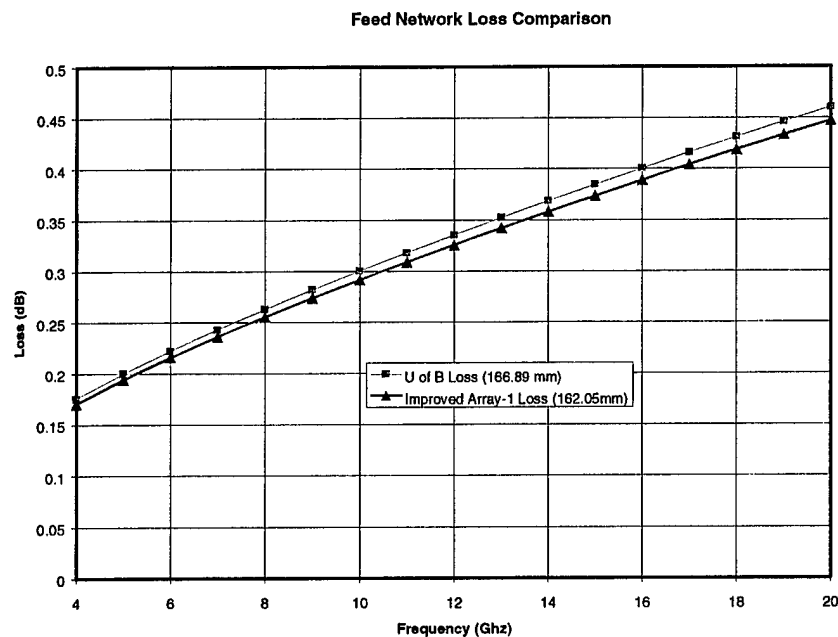


Figure 50. Comparison of feed network losses

Although the “Optimized Array-1” array had tighter element spacing it was better centered in the mounting frame which resulted in the lengths of transmission lines

having a difference of only 5mm. It is apparent from Figure 50 that there is no significant difference in the transmission line losses between the two arrays. In fact over the measured bandwidth, there is only a 0.25 dB increase in the losses from 4 to 20 GHz. This appears low, especially in comparison to the losses observed in the measured S_{21} of the double balun, at Figure 27. The double balun test arrangement was within 15mm of the length of the feed networks, yet it depicted losses increasing to 3 dB at 16 GHz. Most likely there are additional losses in the array and feed system which have not yet been characterized, such as splitter losses. As well, if the losses due to the balun are significant, then the measured losses of the double balun may approach twice that of the single balun used in the array designs.

As the array element spacing is compressed, the linear tapered transformers must carry out their impedance transformations over a shorter length. The price for this is increased return loss. However, this effect is negligible given the relatively small shrinkage in array size. Additionally, as the elements get closer together, the dipoles, especially their ends, get closer to the feed lines. This will eventually create undesirable coupling between the dipole elements and the feed network.

The array was not square, but rather 4 by 8. Initially this was simply due to the desire for commonality for comparison with the University of Belgrade design. However, as the support structure was made 7" by 7" for these designs, arrays of larger size were not possible.

5.10 Summary of performance

In general, the Optimized Array-1 showed some marginal improvement over the University of Belgrade implementation. Although the efficiency bandwidth was approximately the same, the actual efficiency within this low frequency region of the improved design was close to 10% better. Unfortunately, the efficiency improvement of only 5% around the 16 GHz region was not adequate for meeting the efficiency objective of 50%. The VSWR bandwidth showed slight improvement, especially at the lower end of the bandwidth, most likely due to the greater ground-plane spacing. The pattern bandwidth showed expected improvement in the E-plane, almost attaining the 16 GHz design objective.

Bandwidth Definition	Bandwidth (GHz)
Gain Bandwidth (Efficiency > 50%)	4.5 - 11.3GHz
VSWR Bandwidth	4.5 - 20 ⁺ GHz
Pattern Bandwidth	6 - ~16 GHz (E-plane) 4 - 18 ⁺ GHz (H-plane)

Table 5. Summary of Optimized Array-1 performance

5.11

Further enhancements

As it appears that efficiency improvement at the higher frequencies was difficult to obtain, compared to the lower end of the band, it is felt that relaxing the bandwidth objective to 14 GHz would allow a further height increase and even better performance in the lower part of the bandwidth. Since the simulation of a single wideband dipole element was used to select the height for Optimized Array-1, the impact of the array factor in improving the slight boresight null was not considered. As the array factor has this positive effect, the height criteria could be relaxed to $\frac{3}{8} \lambda$ vice the previous $\frac{1}{4} \lambda$. Thus for acceptable operation at 14 GHz, the array height over the ground-plane could be increased to 8.0 mm. Correct operation (i.e. no unacceptable reduction in the boresight gain of the simulated array) of a dipole at this height was verified using *ARPS™*.

6. OPTIMIZATION OF ARRAY HEIGHT OVER GROUND AND IMPROVED WIDEBAND DIPOLE MATCHING

6.1 Introduction

Having made an initial attempt at optimizing the wideband printed-dipole array, a further attempt at enhancing the bandwidth would be undertaken. This effort, which basically entailed an investigation of improved element shape and an additional attempt at better ground-plane spacing, will be described in the following chapter.

6.2 Rationale for improvement by element shape modification

Once the height and element spacing of the array has been optimized, the only remaining improvements to be had are the reduction of losses and the improvement of the broadband match of the basic wideband printed-dipole element. Since losses are difficult to reduce, an effort was undertaken to increase the broadband match of the dipole elements. This optimization was performed by modifying the dipole shape and then simulating the structure in **IE3D™**. Again, the vertically localized port definition was used in the simulations. Inspection of the resulting return loss and Smith charts provided an indication of which geometric parameters could improve the wideband match of the dipole elements. Numerous parameters were studied including length, width, end-shape and opening angle. Generally, improvement at the low end of the operating bandwidth could only be obtained by increasing the dipole length. This was not desirable due to element spacing constraints within the array. Additionally, this effort was abandoned as the array already performed reasonably well at these frequencies.

The element's broadband match seemed to be relatively insensitive to all but the most radical of shape changes. As most of the current was observed on the sides of the dipole, a simulation was performed which involved modifying the dipole arms into "U" shapes (ie. removing the centre area of the dipole arms, which possessed little or no current). Even this did not significantly impact the element's operation, further indicating the insensitivity of the wideband match to certain geometric modifications. The parameter, which seemed to improve the wideband match of the element most effectively, was the opening angle of the dipole arms. As indicated by the following two Smith charts, one can see that with a slight increase in the opening angle, a better match

can be obtained, as long as appropriate adjustments are also made to the input impedance of the dipole element.

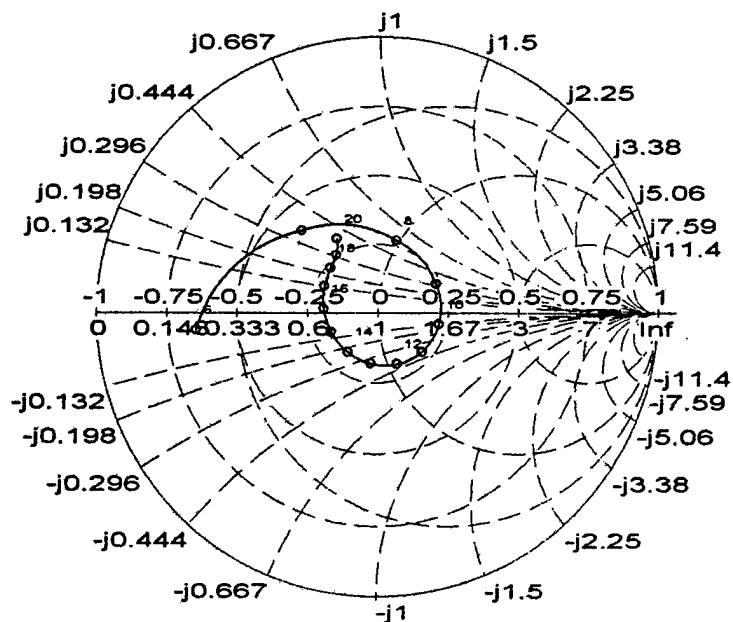


Figure 51. Smith chart of Original U of B wideband dipole element

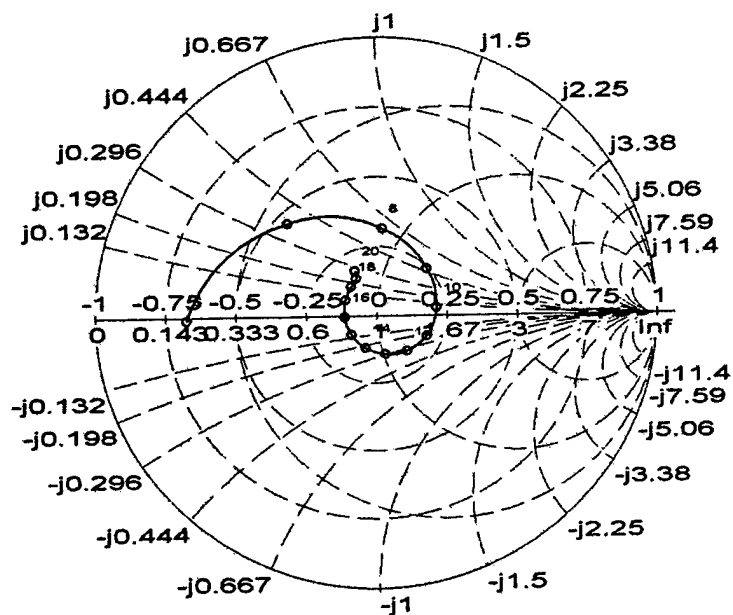


Figure 52. Smith chart of improved wideband dipole element

The relative shape modification can be seen in Figure 53. While representing a small improvement in wideband match, the enhancement becomes relatively insignificant when the losses within the feed network are considered. For this reason it was decided that construction of an array with these elements would not be worthwhile.

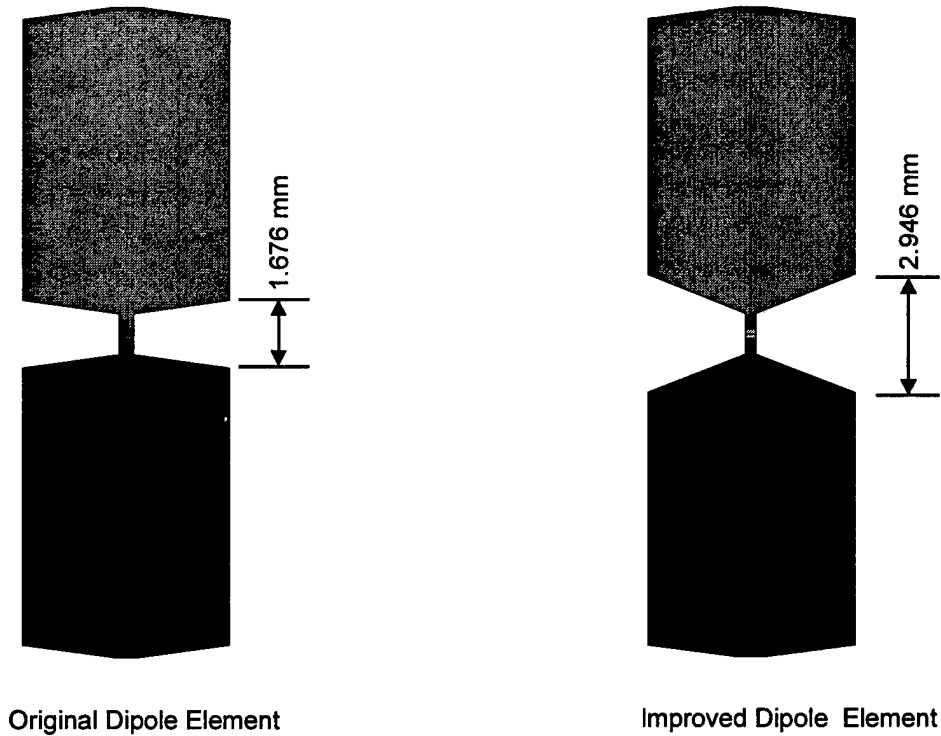


Figure 53. Original and improved wideband dipole elements

6.3 Comparison of return losses at 8mm height

Due to the decision that the fabrication of a new array, which implemented the improved wideband dipole elements, would not be worthwhile, the rationale for a further increase in the ground-plane spacing, proposed in the previous chapter, was undertaken. Both the University of Belgrade design and the Optimized Array-1 were remeasured with each at the same ground-plane spacing of 8.0 mm. This approach would not only improve the performance of both arrays, but also assist in isolating ground-plane and other effects within the arrays.

As seen in the following return loss measurements, the increase in array heights over the ground-plane has improved the performance at the lower frequencies. While the nulls in the ripple had shifted, their period remained, confirming that this effect was due to internal array reflections and not other effects.

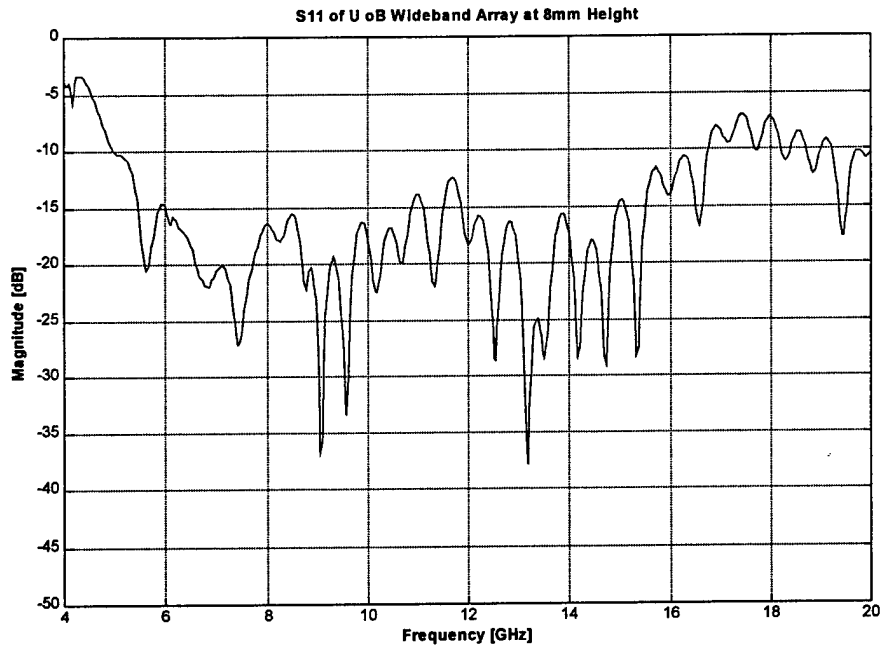


Figure 54. S11 of the U of B Array at 8mm ground-plane spacing

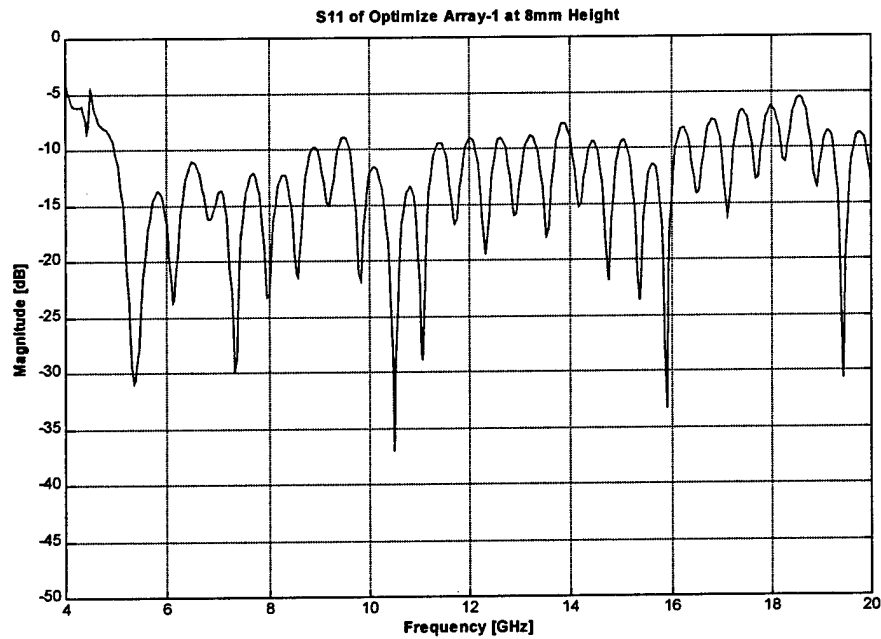


Figure 55. S11 of Optimized Array-1 at 8mm ground-plane spacing

6.4 Comparison of boresight gains vs. frequency

As expected, the increase in ground plane spacing brought the $\lambda/2$ null into the measurement bandwidth, similar to the *IE3D*TM simulation at Figure 40. The negative effects of this (ie. a 2 dB drop in gain at 14 GHz from the previous ground-plane spacing) were observed down to 13 GHz. The positive effect was a 2 dB increase in gain at 4.5 GHz.

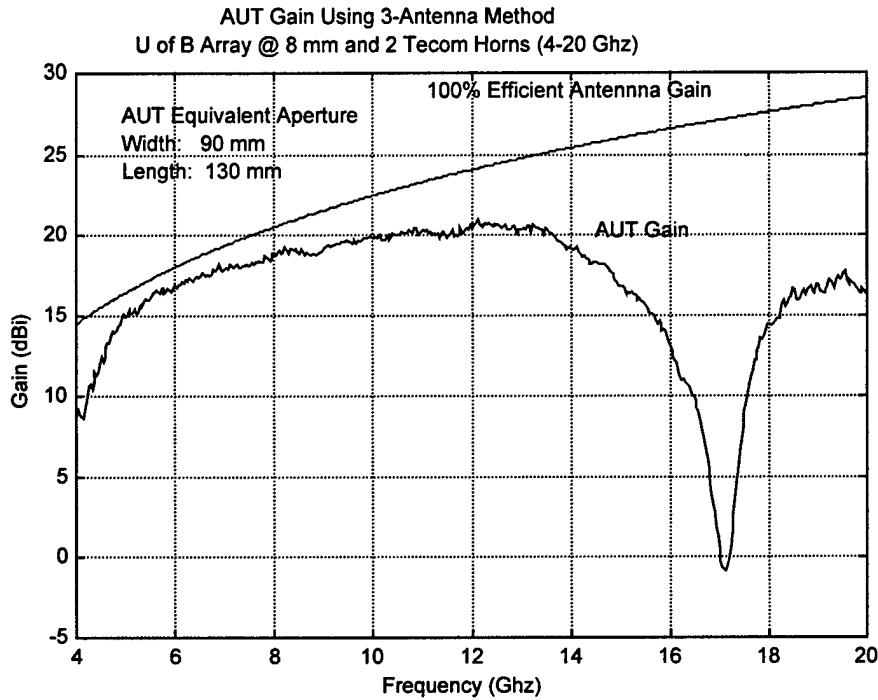


Figure 56. U of B Array gain at 8mm ground-plane spacing

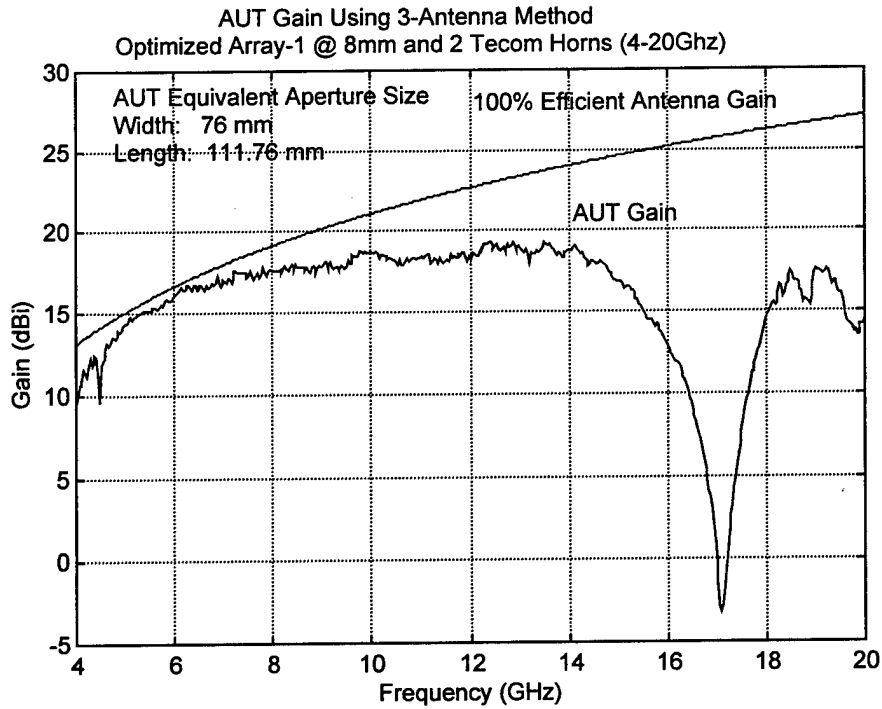


Figure 57. Optimized Array-1 gain at 8mm ground-plane spacing

6.5 Comparison of radiation efficiencies at 8mm ground-plane spacing

Comparison of the radiation efficiencies of the 2 arrays at the same height provided the advantage of a more straightforward comparison of the 2 antenna designs. Again due to the different aperture sizes, the comparison between the antennas must be done via radiation efficiencies rather than gain. For the Optimized Array-1, the height change from 6.35 to 8.00mm resulted in a loss of 1 GHz of bandwidth at the upper frequencies, with marginal effect at the lower frequencies. The U of B Array height change from 5.77mm to 8.00mm, on the other hand, resulted in 400 MHz being added to the low end of the bandwidth for a sacrifice of 500 MHz at the high end.

These results are strong indication that the boresight null entering the bandwidth, due to the array height over the ground-plane, is the predominant consideration for the upper frequency of operation. The sacrifice for some improvement in the radiation efficiency at the low end of the bandwidth seems to be in the order of 2:1.

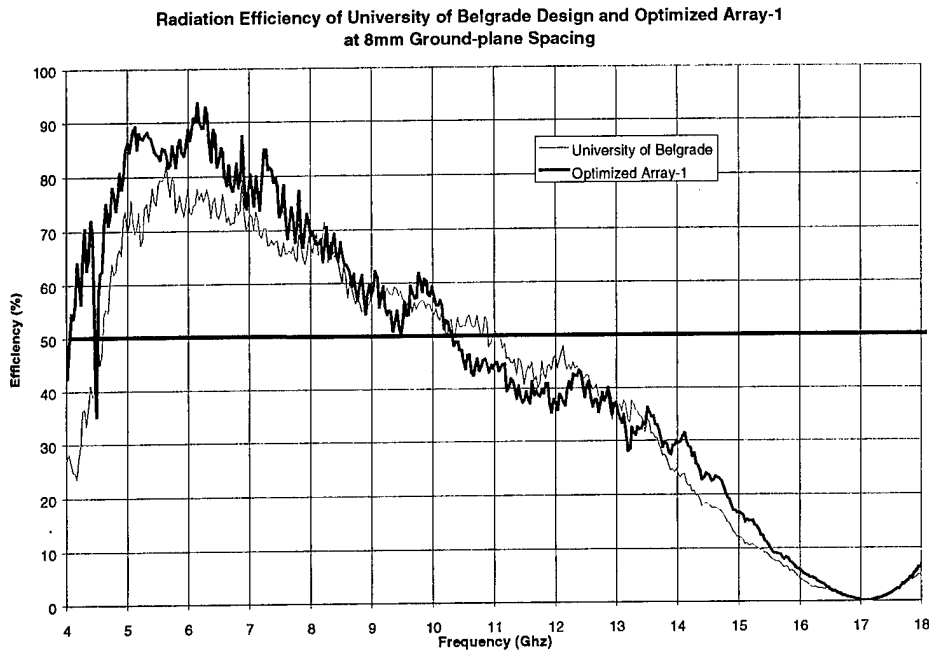


Figure 58. Radiation efficiency of the U of B and Optimized Array-1 at 8mm height

6.6 Representative radiation patterns

For the Optimized Array-1, the change of ground plane height did not significantly affect the radiation patterns. The cross polarization ratio remained better than 30 dB. The detrimental effect of the boresight null is clearly distinguished by pattern distortions at 16 and 18 GHz (either side of the null frequency). Similar effects due to the height change were observed for the U of B design as well.

These results indicate that for arrays of this type, the radiation patterns are more a function of element spacing than ground plane separation. The relevant radiation patterns are available at Appendices I and J².

6.7 Summary of performance

Having measured the U of B Array and Optimized Array-1 at the same height over the ground-plane of 8.00 mm, the results are summarized in the following table.

² The reader should be aware when comparing this set of measurements with previous ones, that an LNA (low noise amplifier) was used in these measurements. This 20 dB of gain is not observable in the measurements due to normalization.

Bandwidth Definition	Bandwidth (GHz)	
	U of B Array (8.0mm)	Optimized Array-1 (8.0mm)
Gain Bandwidth (Efficiency <50%)	4.6 – 10.3	4.5 – 10.3
VSWR Bandwidth	4.5 – 16.4	4.5 - ≈16
Pattern Bandwidth	4 - 14	4 - 14

Table 6. Summary of U of B and Optimized Array-1 Performance

As can be seen, the overall effect of this greater ground-plane spacing was negative. Due to the large null entering the bandwidth, gain, pattern and VSWR performance deteriorated. While this result was somewhat unfortunate, in that it didn't produce the hoped for bandwidth improvement, it provides strong evidence of the high frequency limitations of this particular architecture.

6.8 Sources of error

The potential sources of error within this study are similar to those of any investigation involving microstrip antennas. They include those associated with design (simulation), fabrication and measurement.

6.8.1 Connectors

Every effort was made to minimize losses in the connector. Unfortunately it was impossible to guarantee reproducible connectors. This problem could be alleviated with the use of micro-positioning and soldering equipment.

6.8.2 Accurate permittivities, loss tangents and homogeneity

Any variation of these electrical constants would impact the simulations, optimization and design, resulting in a deviation from the expected antenna performance.

6.8.3 Dimensional errors

Given the wideband nature of the antennas being studied, their performance was generally insensitive to small dimensional errors in fabrication, one of the hidden values in wideband designs. Planarity of the array was acceptable even without bonding between the layers.

6.8.4 Multipath

Multipath was assessed in the chamber and found to be negligible for the purposes of this study. Several gain measurements were repeated with different combinations of probes to ensure that the probe-AUT reflections were insignificant.

7. CONCLUSION AND RECOMMENDATIONS FOR FUTURE WORK

7.1 Concluding remarks

As the current demand for wideband arrays requires the complementary development of appropriate wideband antenna elements, it is logical to initiate such efforts with the optimization of these elements and consideration of their implementation into arrays. The double-sided wideband printed-dipole element and its functionality within a 32-element array has demonstrated success in meeting the wide bandwidth demands of modern antenna systems.

7.2 Accomplishments

The design, fabrication, test, analysis and optimization of wideband printed-dipole arrays was carried out as part of this report. Since the array design originally produced by the University of Belgrade possessed no measurement data with which to characterize its performance, it was considered as a useful starting point. Comprehensive investigations to successfully determine the optimum array height over ground, element spacing and element shape were performed. Several important aspects of the architecture were characterized with a view to further optimization. The overall effort of this study has resulted in several significant accomplishments, which are particularly relevant to the further investigation of this antenna architecture. These achievements include:

Demonstration of Bandwidth Potential – Perhaps the most significant contribution of this study was the demonstration of the excellent bandwidth characteristics of the wideband printed dipole architecture. The characterization of the how radiation efficiency varies with frequency may give an indication of what future enhancement efforts would most quickly produce positive results.

Insensitivity of Basic Wideband Element – Through simulation, it was determined that the performance change of the basic element, due to all but the most drastic dimensional modifications, was very insensitive. Minor improvements in broadband match were obtained by varying the opening angle of the dipole arms from the feed point to the final width. While this indicates an element of simplification for large scale fabrication of this design (ie. the performance of the basic element was tolerant of

dimensional errors), it also means that further exploitation of the basic model will be challenging.

K Connector™ Utilization - An easily reconfigurable adapter arrangement was designed and fabricated. This apparatus allowed the high quality **K Connector™** to be used in the antenna test arrangement. It was particularly useful for facilitating the modification of ground-plane spacing or substrate thickness. The adapter would have utility for many experimentation situations.

Importance of Ground-Plane Spacing on Array Performance - With two different arrays having been constructed, generalizations on the effects of variations in ground-plane spacing were obtained. It appeared that once an array was fabricated using the desired elements, the final performance was primarily a function of the ground-plane spacing. The upper bandwidth limitation is clearly driven by the boresight null, which begins to enter the array's bandwidth as the height is increased. The lower bandwidth limitation is much less sensitive to array height variations, however as the array was lowered to improve performance at high frequency, some gain (due to VSWR increase) was sacrificed. Optimal ground-plane spacing should be determined first by simulation then verified by 'tuning'.

Balun Test Arrangement – As baluns are a critical component of many antenna systems, it is important to assess their performance through experimentation. In order to evaluate the microstrip to balanced transmission line transition, a double wideband balun test arrangement was constructed as a two port device. It was found to be a very good method for characterizing this component of the wideband printed-dipole array and return losses of less than 15 dB were achieved over a very wide bandwidth. This approach would be suitable for the assessment of any such balun structures.

Validation of Simulation Software – Excellent correlation was achieved between radiation patterns simulated using **IE3D™** and **ARPS™** and actual measured patterns. As the simulations ignored mutual coupling and finite ground plane effects, it could be inferred that these concerns were not of great importance for this study. While **ARPS™** and **IE3D™** are excellent tools for predicting the performance of the arrays and assisting in the selection of ground-plane spacing, **IE3D's™** ability to plot radiation efficiencies for various array heights, was the preferred tool. **ARPS™** was however very useful for quickly determining the radiation patterns, which would result from single elements and arrays.

7.3 Future work

As with any "time limited" study of an antenna architecture, there are numerous issues which, if investigated further, could add important information to the overall understanding of the wideband printed-dipole array. The ultimate objective of such a comprehensive volume of knowledge, is the development of simplified design

guidelines. These would hopefully allow the designer to produce an optimally-shaped element, which could then be implemented into an array. The following topics are offered as possibilities for further investigation into the wideband printed-dipole array:

Essentially, two attempts were made at optimizing the array height over the ground plane. This process was performed in steps by first simulating, then fabricating and measuring the antenna. Future "tuning" of the antenna, could be facilitated by constructing a mounting arrangement, which would allow for continuous variation of the antenna height, even when mounted on the measurement system.

Losses in the balanced feed system could be better characterized. Perhaps the best focus for such a study would be on the wideband balun itself. An initial objective would be the identification of a suitable simulation package for such a problem.

Once it was understood that the previous wideband dipole element was indeed a very good wideband architecture, time constraints pushed the investigation towards the implementation of the wideband printed-dipole elements into arrays. While an improved element was designed for implementation into an array, there is a requirement for the development of design curves, which could guide the designer towards an optimum element shape to attain a desired bandwidth performance.

While the literature had suggested that bandwidth was enhanced due to mutual coupling in the colinear direction, this was not observed in any significant results. As well, most mutual coupling studies have concentrated upon electromagnetically coupled EMC fed dipoles. A comprehensive study of the mutual coupling phenomenon between double-sided printed-dipole elements would be very useful.

Further efficiencies could be attained through the use of even thinner substrates and possibly the removal of the substrate material over the lower dipole arm. The practicality of such an effort should be considered.

The use of the wideband printed-dipole element with other types of feed networks could be investigated. This study could include series feed systems as well as variations of element placement to improve the symmetry in radiation patterns.

REFERENCES

-
- [1] J. James and P. Hall, "HandBook of Microstrip Antennas," London, U.K., Peter Peregrinus Ltd, 1989, p. 6.
- [2] D. Pozar, "A review of bandwidth enhancement techniques for microstrip antennas," Microstrip Antennas – the analysis and design of microstrip antennas and arrays, IEEE Press, Piscataway, NJ, 1995, p.159.
- [3] P. Bhartia, K. Rao and R. Tomar, "Millimeter-Wave and Printed Circuit Antennas," Artech House, Boston, 1991, p. 183.
- [4] E.D. Kaplan, "Understanding GPS Principles and Applications," Artech House, Boston, 1996.
- [5] L. Cairn, N. Geng, M. McClure, J. Sichana, and L. Nguyen, "Ultra-wide-band synthetic aperture radar for mine field detection," *IEEE Antennas and Propagation Magazine*, vol. 41, no. 1, pp. 18-33, Feb. 1999.
- [6] D. Roddy, "Satellite Communications," Mc Graw Hill, Toronto, 1996, p. 400.
- [7] H.F. Pues and A.R. Van de Chapelle, "An impedance matching technique for increasing the bandwidth of microstrip antennas," *IEEE Transactions on Antennas and Propagation*, vol. AP-37, pp. 1345-1354, Nov. 1989.
- [8] F.S. Fong, H.F. Pues and M.J. Withers, "Wideband multilayer coaxial-fed microstrip antenna element," *Electronic Letters*, vol. 21, pp. 497-499, 1985.
- [9] J.S. Roy, "A Broadband microstrip antenna," *Microwave and Optical Letters*, vol. 19, no. 4, pp. 307-308, Nov 1998.
- [10] J. Zurcher and F Gardiol, "Broadband Patch Antennas," Artech House, Norwood, MA, 1995.
- [11] D. Pozar and D. Schaubert, "Scan blindness in infinite phased arrays of printed-dipoles," *IEEE Transactions on Antennas and Propagation*, pp. 602-610, vol. 32, 1984.
- [12] G. Amendola and G. Di Massa, "Double-Ring wideband patch antennas," *Microwave and Optical Technology Letters*, vol. 19, no. 4, Nov 1998.
- [13] F. Croq and D.M. Pozar, "Multifrequency operation of antennas using aperture coupled parallel resonators," *IEEE Transactions on Antennas and Propagation*, vol. 40, pp.1367-1374, Nov. 1992.

-
- [14] K.F. Lee, K.M. Luk, K.F. Tong, S.M. Shum, T. Huynh and R.Q. Lee, "Experimental and simulation studies of the coaxially fed U-slot rectangular patch antenna," *IEE Proceedings - Microwaves Antennas Propagation*, vol. 144, no. 5, pp. 354-358, Oct 1997.
- [15] Y. Lin and K. Wong, "Compact Broadband Triangular microstrip antenna with an inset microstrip-line feed," *Microwave and Optical Technology Letters*, vol. 17, no. 3, Feb 1998.
- [16] H.F. Hammand, "Dual and broad band antennas using spur-line filters for communication systems," MSc Thesis, Queen's University, Kingston, ON., 1997.
- [17] IE3D™ Users Manual Release 5.01, Zeland Software Inc., Fremont, CA., 1999.
- [18] R. Mittra, "Computer Techniques for Electromagnetics," Hemisphere Publishing Corp, New York, p. 16, 1987.
- [19] J. D. Kraus, "Antennas," Mc Graw Hill, 2nd Edition, Toronto, ON, 1988
- [20] W. Wilkinson, "A class of printed circuit antennas," *IEE AP-S Int Ant and Prop Symp. Dig*, 1974, pp. 270-274.
- [21] M. Mikavica, B. Kolundzija, A. Nestic and M. Marjanovic, "Wideband properties of two mutually coupled printed-dipole elements," *Proc ANTEM 98*, Ottawa, ON, pp. 615-618.
- [22] J.F. Huang and C.W. Kuo, "CPW-fed bow tie slot antenna," *Microwave and Optical Technology Letters*, vol. 19, no. 5, pp. 358-360, Dec 1998.
- [23] A. Agrawall and W. Powell, "A printed circuit cylindrical array antenna," *IEEE Transactions on Antennas and Propagation*, vol. AP-34, no. 11, Nov 1986.
- [24] A. Nestic, I. Radnovic, and V. Brankovic, "Ultrawideband Printed Antenna array for 60 GHz frequency range," *IEEE Proc APS*, 1997, pp. 1272-1275.
- [25] J. Izadian and S. Izadian, "Microwave Transition Design," Artech House, Norwood, MA, 1988,
- [26] M. Majewski, J. Scott, "Modeling and Characterization of Microstrip-to-Coaxial Transitions," *IEEE Transactions on Microwave Theory and Techniques*, vol. MTT-29, no. 8, pp. 799-805, Aug 1981.
- [27] K.C. Gupta, R. Garg, I. Bahl, P. Bhartia. "Microstrip Lines and Slotlines," Artech House, Norwood, MA, 1996.

-
- [28] R. Eisenhart, "A Better microstrip connector," *MTT-S International Microwave Symposium Digest*, pp.318-320, 1978
- [29] *Anritsu Product Catalogue* 1997.
- [30] E. Levine, D. Treves, "Test technique improves coax-to-microstrip transitions," *Microwaves and RF*, pp. 99-102, Jul. 1986.
- [31] C. Balanis, "Antenna Theory – Analysis and Design," John Wiley & Sons, Toronto, p. 480, 1997.
- [32] J. Duncan, V. Minerva, "100:1 Bandwidth balun transformer," *Proceedings of the IRE*, , pp. 156-164, Feb 1960.
- [33] D.M. Pozar, "Microwave Engineering 2nd ed.," John Wiley and Sons, Inc., Toronto, p. 283, 1998.
- [34] M. Gans, D. Kajfez, V. Rumsey, "Frequency independent baluns" *Proc of IEEE*, pp. 647-648, Jun 1965.
- [35] E. Levine, S. Strikman, D. Treves, "Double sided printed arrays with large bandwidth," *IEE Proceedings*, vol. 135, pt. H, no. 1, Feb 1988.
- [36] H. Wheeler, "Transmission Line properties of parallel strips separated by a dielectric sheet," *IEEE Transactions on Microwave Theory and Techniques*, vol. MTT-13, no. 2, Mar. 1965.
- [37] P.S. Hall and C.M. Hall, "Coplanar corporate feed effects in microstrip patch array design," *Proc. IEE*, vol. 135, pt. H, pp. 180-186, Jun 1988.
- [38] M. Ammann, "Design of Rectangular Microstrip Antennas for the 2.4 GHz Band," *Applied Microwave and Wireless*
- [39] D.M. Pozar and D.H. Schaubert, "Microstrip Antennas- The Analysis and Design of Microstrip Antennas and Arrays," IEEE Press, New York, 1995.
- [40] G.J. Stern and R.S. Elliott, "The design of microstrip dipole arrays including mutual coupling, Part II: experiment," *IEEE Transactions on Antennas and Propagation*, vol. AP-29, no. 5, pp 761-765, Sep 1981.
- [41] P.B. Katehi, "A generalized method for the evaluation of mutual coupling in microstrip arrays," *IEEE Transactions on Antennas and Propagation*, vol. AP-35, no. 2, , pp 125-133, Feb 1987.

[42] D.M. Pozar, "Input impedance and mutual coupling of rectangular microstrip antennas," *IEEE Transactions on Antennas and Propagation*, vol. AP-30, no. 6, pp. 1191-1196, Nov. 1982.

[43] N. Alexopoulos and I. Rana, "Mutual impedance computation between printed-dipoles," *IEEE Transactions on Antennas and Propagation*, vol. AP-29, no. 1, pp 106-111, Jan 1981.

[44] P. Darwood, P.N. Fletcher, G.S. Hilton, "Mutual coupling compensation in small planar array antennas," *IEE Proc. Microwave Antennas Propagation*, vol. 145, no. 1, pp 1-6, Feb. 1998.

[45] A.C. Ludwig, "The definition of cross polarization," *IEEE Transactions on Antennas and Propagation*, vol. AP-21, pp. 116-119, Jan 1973.

[46] G. Evans, "Antenna Measurement Techniques," Artech House, Boston, 1990.

[47] C. Balanis, "Antenna Theory, Analysis and Design," John Wiley and Sons, Toronto, 1997.

[48] C.J. Brochu, G.A. Morin and J.W. Moffat, "Gain Measurement of a Cavity-Backed Spiral antenna from 4 to 18 GHz using the Three-Antenna Method," DREO Report No. 1337, Ottawa, Nov. 1998.

[49] R. A. Sainati, "CAD of Microstrip Antennas for Wireless Applications," Artech House, Norwood, MA, 1996.

APPENDIX A *MATLAB® PROGRAM*
FOR GAIN TRANSFER
CALCULATION

The following program was used to derive the absolute gain of the AUT through comparison with the gain of a known antenna.

```

%%%%%%%%%%%%%%%%%%%%%%%%%%%%%%%%%%%%%%%%%%%%%%%%%%%%%%%%%%%%%%%%%%%%%%%%
%%%%%%%%%%%%%%%%%%%%%%%%%%%%%%%%%%%%%%%%%%%%%%%%%%%%%%%%%%%%%%%%%%%%%%%%
%
%                               Title:          gainxfer_9
%                               %
%
%                               %
%                               This program calculates the gain of an antenna by the "gain
transfer method" %
%                               %
%                               %
%
%                               %
%%%%%%%%%%%%%%%%%%%%%%%%%%%%%%%%%%%%%%%%%%%%%%%%%%%%%%%%%%%%%%%%%%%%%%%%
%%%%%%%%%%%%%%%%%%%%%%%%%%%%%%%%%%%%%%%%%%%%%%%%%%%%%%%%%%%%%%%%%%%%%%%%
%
%                               For the gain transfer method two antenna measurements are made:
%                               - one measurement of the AUT
%                               - a second measurement of a reference antenna(REFANT) of
known gain.
%
%                               Both measurements must use the same RF circuitry (cable, amps and
probe)so that the gain of % the AUT can be indirectly calculated by comparison of both
measurements (AUT and REFANT)wrt % the known gain of the reference antenna.
%                               If the separation distances between each antenna and the probe used
to measure it are
%                               different, a correction factor must be added to the calculation.
%
%                               The gain array of the REFANT antenna is a 2-Column array of Frequency
and Gain
%                               listed in a text file of the following format:
%                               1. A few lines of textual header information
%                               2. The last line of the header starting with
%                               "***" followed by the
%                               column titles of the gain array such as:
%                               **Freq (GHz) Gain (dB)
%                               3. A two column array of Frequency and Gain
%
%                               ALGORITHM
%                               1- READ Wiltron AUT measurement get FREQAUT
%                               and MAGAUT
%                               2- READ Wiltron REFANT measurement get FREQREFANT
%                               and MAGREFANT
%                               3- READ REFANT gain file
%                               get REFANT
%
%                               It is assumed that the frequency values for the AUT and
REFANT (FREQAUT and
%                               FREQREFANT) are identical. As the frequencies in the
REFANT gain file
%                               probably don't match those of the measured data, it is
necessary to
%                               interpolate the gain values to match the measurement
frequencies. The gain
%                               can be interpolated only for frequencies inside the REFANT
frequency range.
%                               For frequencies outside this range, Matlab will make the
gain values NAN
%                               (or Not a Number), thus avoiding an error in the PLOT
routines
%
%                               4- Interpolate REFANT into REFANTI .
%                               REFANTI will be the REFANT gain interpolated
%                               with the restriction as described above.
%                               REFANTI = interp1(REFANT(:,1), REFANT(:,2),
%                               FREQAUT
%                               5- The gain is calculated: AUTGAIN = MAGAUT-
MAGREFANT + REFANTI'

```

```

%
%           IF the distances AUT-probe and REFANT-probe are different
then a correction           is required.
%
%           6-           the corrected gain is:   AUTGAIN = AUTGAIN
+ 20*log10( distAUT/distREFANT )
%
%           7-           the theoretical gain curve is calculated
based on the entered aperture           size.
%
%
%           Mfiles used by this program:
%
%           ascanfp           Read a (TEXT) data
array file                               (Self
%           contained function, it selects a file and reads data)
%           wi_read           Wiltron file read
%
%           Callbacks:
%           cstedit           Annotations text editing
%           calbckgen           Generic call back functions
%
%           Claude Brochu
%           Rev 4: Change all references to SGH for
REFANT           22 Feb 1999
%           5: Write more annotations on the
graphs           23 Feb 1999
%           6: Add colors to second graph &
More comments           24 Feb 1999
%           7: Reformat graphs and add Print
to file menu           1 Mar 1999
%           Blaine Duffley
%           Rev 9: Automatic positioning of annotations
%           3 Mar 1999
%           92: Save header information to file
%           4 Mar 1999
%
%
%%%%%%%%%%%%%%%%%%%%%%%%%%%%%%%%%%%%%%%%%%%%%%%%%%%%%%%%%%%%%%%%%%%%%%%%
%
errrtile='Error Reading File';

%           User enters Get AUT filename

[autfname autpath]=uigetfile('*.*.dat',' Specify the AUT Measurement File');
if autfname==0  errmsg ={'File Selection Cancelled';'';'ABORTING'};
  errordlg(errmsg, ' File Selection'); return, end

disp(['AUT Measurement File           :           ' autpath autfname]); cd(autpath);

%           User enters REFANT filename

[REFANTfname REFANTpath]=uigetfile('*.*.dat',' Specify the Reference Antenna Measurement
File');
if REFANTfname==0  errmsg ={'File Selection Cancelled';'';'ABORTING'};
  errordlg(errmsg, ' File Selection'); return, end

disp(['Reference Antenna Measurement File           :           ' REFANTpath REFANTfname]);
cd(REFANTpath);

%           User enters REFANT gain filename

[REFANT, count, gpath, gfname] = ascanfp(' Specify the Reference Antenna GAIN
File','**',1);

%           Read AUT measurement from Wiltron File

[freq, AUTMAG, Phase, ERR_INDEX, AUTIdent]=wi_read([autpath autfname],'freq');

```

```

if      ERR_INDEX ~= 0

    errmsg={'  ERROR  ' int2str(ERR_INDEX) ' reading file:  '};[autpath aufname];...
        '';'  ABORTING'';
    errorldg(errmsg, errtitle); return; end;

disp(sprintf('%s%s','VNA Identification:          ', AUTIdent'))

%      Read REFANT measurement from Wiltron File

[freq, REFANTMAG, Phase, ERR_INDEX, REFANTIdent]=wi_read([REFANTpath
REFANTfname], 'freq');
if      ERR_INDEX ~= 0
    errmsg={'  ERROR  ' int2str(ERR_INDEX) ' reading file:  '};[REFANTpath
REFANTfname];...
        '';'  ABORTING'';
    errorldg(errmsg, errtitle); return; end;

disp(sprintf('%s%s','VNA Identification:          ', REFANTIdent'))

% REFANT gain interpolated to match the measurement frequency values
REFANTI=interp1(REFANT(:,1),REFANT(:,2),freq);

%      Gain Transfer Calculation
AUT_Gain=REFANTI-REFANTMAG+AUTMAG;

%      Get probe-AUT and probe-reference antenna separation distances
Prompt={'Distance Probe-AUT:', 'Distance Probe-Reference Antenna:'};
titre='Antenna Separation Distances';
Dist_AUT_REFANT=str2num(char(inputdlg(Prompt,titre,1,{3.9,3.9})));

%      Gain correction due to distances applied
AUT_Gain_C=AUT_Gain +20*log10(Dist_AUT_REFANT(1)/Dist_AUT_REFANT(2));

%
disp_dist=[char(Prompt) [' '];' ' ] num2str(Dist_AUT_REFANT) [' m';' m'];
disp(disp_dist)

%      Uniform Distribution Aperture on Ground Plane
%      Ref: Balanis pg 597

prompt={'Enter the aperture width (mm) ', 'Enter the aperture length (mm) '};
titre='Aperture Size';
def={'90','130'};
AP_Size=str2num(char(inputdlg(prompt,titre,1,def)));
Ap_width= AP_Size(1);           % width of aperture in mm
Ap_length=AP_Size(2);          % length of aperture in mm
c=2.88e11;                      % speed of light in mm
lamda=c./(freq .*1e9);         % array of wavelengths in mm
x=4*pi*Ap_width*Ap_length;
Theoretical_Gain=10.*log10(x./lamda.^2);

%      Generate the Gain plot

SSZ=get(0,'screensize'); SSZ([1 2])=SSZ([3 4]);
pos1=SSZ.*[.1 .1 .75 .75]; pos2=SSZ.*[.12 .07 .75 .75];% Cascade plots

figure('number','off','name',[blanks(20) 'Antenna Gain by "Gain Transfer Method"'], ...
'pos',pos1)
plot(freq, AUT_Gain_C)
set(gca,'pos',[.11 .13 .775 .77])
title(char('\bfAntenna Gain by "Gain Transfer Method"', ...
'AUT Gain - Ref Antenna Gain - 100% Aperture Efficient Gain'), ...
'button', 'calbckgen(''Title''))
xlabel('\bfFrequency (GHz)', 'button', 'calbckgen(''Xlabel''))
ylabel('\bfGain (dBi)', 'button', 'calbckgen(''Ylabel''))

```

```

grid
%
%           Activate GUI menus
axesmenu, textmenu, linemenu
hm=uimenu('label','&Annotations');
uimenu(hm,'label','New','callback','calbckgen(''Annotations''))
uimenu(hm,'label','Edit','callback','cstedit')
hm=uimenu('label','Print to &File');
uimenu(hm,'label','&jpeg Format','callback','calbckgen(''PrintJPEG''))
uimenu(hm,'label','&tiff Format','callback','calbckgen(''PrintTIFF''))

%           Plot Graph 1
%           Add Uniform Distribution Aperture to the gain graph
hold on
plot (freq, Theoretical_Gain, '-r')
plot (freq, REFANTI, 'k')

%           Add Annotations in relative positions

a=axis;
posx=.55*(a(2)-a(1))+a(1);
posy=.70*(a(4)-a(3))+a(3);
text('position',[posx posy],'string','AUT Gain','color','b')
disp_dist_AS=char('AUT Equivalent Aperture Size', ...
    ['      Width:  ' num2str(Ap_width) ' mm'], ...
    ['      Length: ' num2str(Ap_length) ' mm'], ...
    disp_dist);
posx=.03*(a(2)-a(1))+a(1);
posy=.90*(a(4)-a(3))+a(3);
text('position',[posx posy],'string',disp_dist_AS,'color','r')
posx=.75*(a(2)-a(1))+a(1);
posy=.95*(a(4)-a(3))+a(3);
text('position',[posx posy],'string','Theoretical Curve','color','r')
posx=.3*(a(2)-a(1))+a(1);
posy=.45*(a(4)-a(3))+a(3);
text('position',[posx posy],'string','Reference Antenna Interpolated Gain','color','k')
File_Ident=char(['AUT S21 File:      ' autfname], sprintf('%s',AUTIdent'), ...
    ['Reference Antenna S21 File:    ' REFANTfname], sprintf('%s',REFANTIdent'), ...
    ['Reference Antenna Gain File:   ' gfname]);
posx=.3*(a(2)-a(1))+a(1);
posy=.09*(a(4)-a(3))+a(3);
text('position',[posx posy],'string',File_Ident,'color','k')

drawnow                                     %           Bring "Save Data" window to
the foreground

%           Save annotations, frrequency and gains to a text file

[dfile,dpath] = uiputfile('*.txt','Save the AUT Gain Array to File',5,5);
if ~(size(dpath,2) == 1) & (size(dfile,2) == 1)
    fid = fopen([dpath,dfile],'wt');
    disp(['Output Array Filename:      ' dpath,dfile]);
    %           Write header information to file
    fprintf(fid,'%s%s\n','AUT S21 File:      ', autfname);
    fprintf(fid,'%s%s\n','Reference Antenna S21 File: ', REFANTfname);
    fprintf(fid,'%s%s\n','Reference Antenna Gain File: ', gfname);
    fprintf(fid,'%s%s\n','Equivalent Aperature Width (mm): ', num2str(Ap_width));
    fprintf(fid,'%s%s\n','Equivalent Aperature Length (mm): ', num2str(Ap_length));
    fprintf(fid,'%s%s\n','Distance Probe - AUT (m):      ',
num2str(Dist_AUT_REFANT(1)));
    fprintf(fid,'%s%s\n','Distance Probe - Referance Antenna (m): ',
num2str(Dist_AUT_REFANT(2)));
    %           Write frequency and gain data to file
    GainARRAY= [freq AUT_Gain C Theoretical_Gain];
    TitleRow = [' FREQ      AUT Gain(dB) Theoretical Gain(dB)'];
    fprintf(fid,'%s\n', ['**' TitleRow]);
    fprintf(fid,'%12.4f %12.4f %12.4f \n', GainARRAY);
    fclose(fid);
end

%           Trace Input Measurement DATA to a second graph

```

```

hs=figure('number','off','name',[blanks(20) 'Measurement Data for "Gain Transfer
Method"'], ...
    'pos',pos2);
set(gca,'pos',[.11 .13 .775 .77])
title(char('\bfMeasured S21 of the AUT and Reference Antenna', ' '), ...
    'button', 'calbckgen(''Title'')')
xlabel('\bfFrequency (GHz)', 'button', 'calbckgen(''Xlabel'')')
ylabel('\bfS21 (dB)', 'button', 'calbckgen(''Ylabel'')')
grid
hold on
%
%           Activate GUI menus
axesmenu, textmenu, linemenu
hm=uimenu('label','&Annotations');
uimenu(hm,'label','New','callback','calbckgen(''Annotations'')')
uimenu(hm,'label','Edit','callback','cstedit')
hm=uimenu('label','&Print to File');
uimenu(hm,'label','&jpeg Format','callback','calbckgen(''PrintJPEG'')')
uimenu(hm,'label','&tiff Format','callback','calbckgen(''PrintTIFF'')')

%           Plot Graph 2

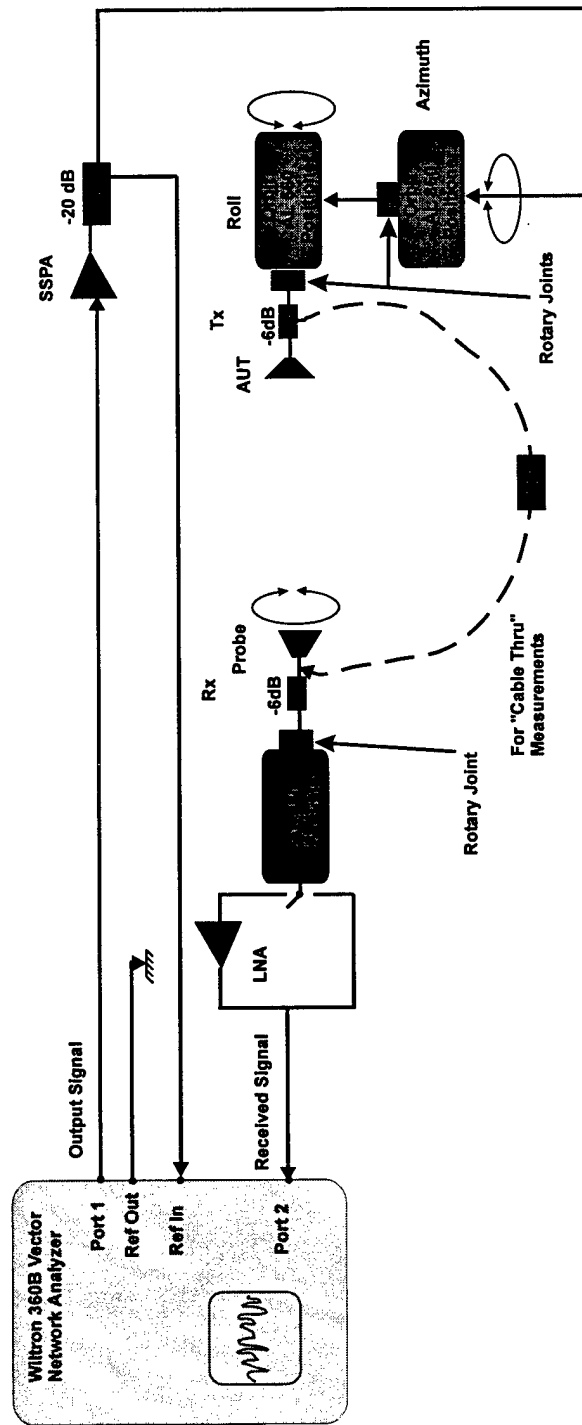
figure(hs)
plot (freq,REFANTMAG,'k')
plot (freq,AUTMAG,'b')

%           Add Annotations in relative positions

a=axis;
posx=.2*(a(2)-a(1))+a(1);
posy=.5*(a(4)-a(3))+a(3);
text('position',[posx posy],'string','Reference Antenna Measurement','color','k')
posx=.4*(a(2)-a(1))+a(1);
posy=.95*(a(4)-a(3))+a(3);
text('position',[posx posy],'string','AUT Measurement','color','b')
posx=.3*(a(2)-a(1))+a(1);
posy=.09*(a(4)-a(3))+a(3);
text('position',[posx posy],'string',File_Ident(1:4,:),'color','k')
%           %%%%%%%%%%%%%%%%%%%%%%%%%%%%%%%%%%%%%%%%%%%%%%%%%%%%%%%%%%%%%%%%%%%%%%%%%

```

APPENDIX B *ANECHOIC* *CHAMBER MEASUREMENT SETUP*



APPENDIX C ROHACELL 31 HF™

MATERIAL DATA

As stated in the manufacturer's specifications, *Rohacell*™ is a closed-cell rigid expanded plastic material or more accurately, polymethacrylimide foam (PMI). The following are the properties of *Rohacell 31 HF*™.

Property	Value	Property	Value
Density lbs/ft ³ (kg/m ³)	2.0 (32)	Shear Strength psi (N/mm ²)	57 (0.4)
Tensile Strength psi (N/mm)	142 (1.0)	Modulus of Elasticity psi (N/mm ²)	5120 (36)
Compressive Strength psi (N/mm ²)	57 (0.4)	Shear Modulus psi (N/mm ²)	1990 (14)
Flexural Strength psi (N/mm ²)	114 (0.8)	Elongation at Break %	3.5
Dimensional Stability under Heat °F (°C)	356 (180)		

Table 7. Physical Properties of Rohacell 31 HF™

Property	Frequency (GHz)			
	2.0	5.0	10.0	26.0
Dielectric Constant	1.08	1.05	1.05	1.06
Loss Tangent	.0001	.0004	.0008	.003

Table 8. Electrical Properties of Rohacell 31 HF™

APPENDIX D *ARLON CUCLAD 217™*

MATERIAL DATA

CuClad 217™ is a PTFE/woven fibreglass laminate substrate manufactured by **Arlon®**. The strength vs dielectric constant tradeoff is based on the ratio of fibreglass to PTFE.. The crossplied laminates provide good electrical and mechanical isotropy.

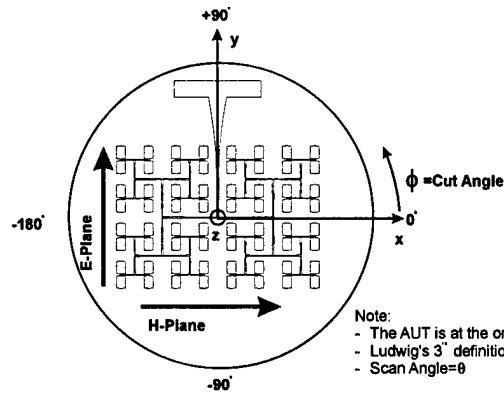
Property	Value	Property	Value
Dielectric Constant @10 GHz	2.17,2.20	Tensile Modulus (kpsi)	275
Loss Tangent @10 GHz	.0009	Compressive Modulus (kpsi)	237
Volume Resistivity (M Ω -cm)	2.3 x 10 ⁸	Flexural Modulus (kpsi)	357
Surface Resistivity (M Ω)	3.4 x 10 ⁶		
Dielectric Breakdown (kv)	>45		
Copper Thickness	½ ounce		

Table 9. Physical and Electrical Properties of Arlon CuLad 217™

APPENDIX E *U OF B* ARRAY

(5.77MM) E- AND H-PLANE CUTS

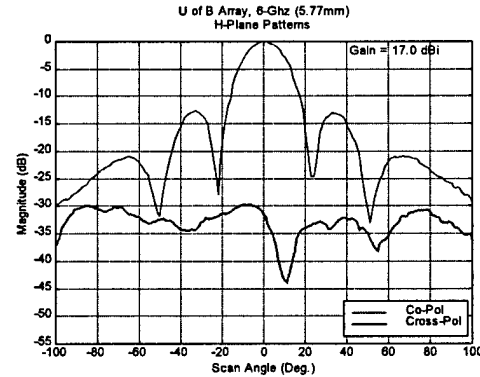
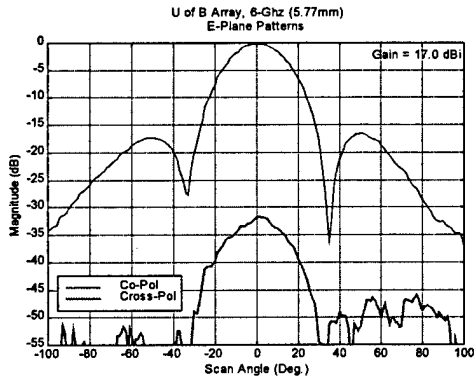
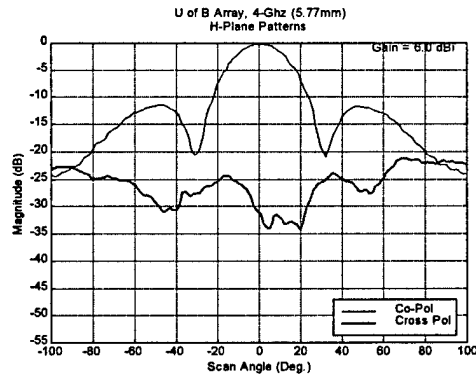
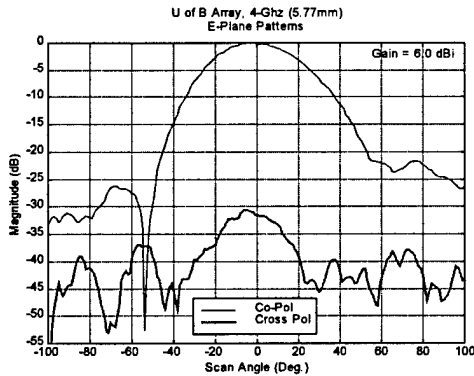
FOR VARIOUS FREQUENCIES

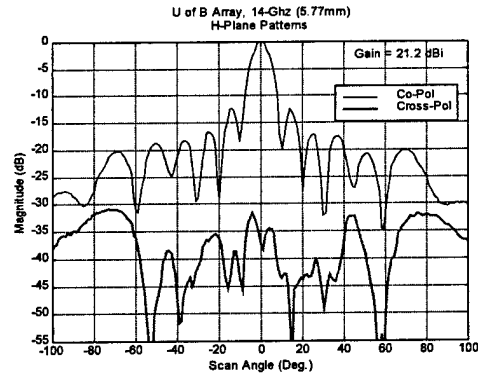
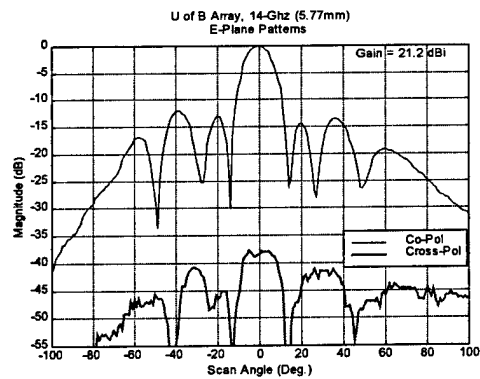
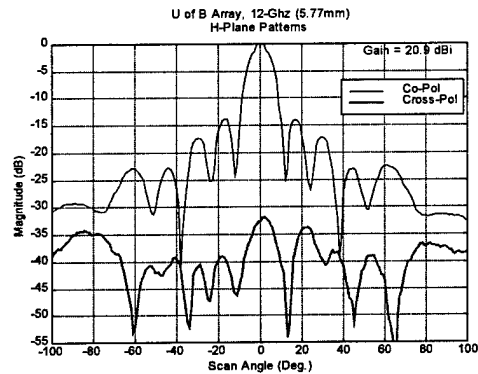
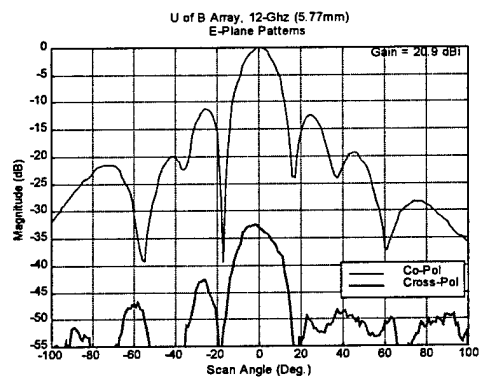
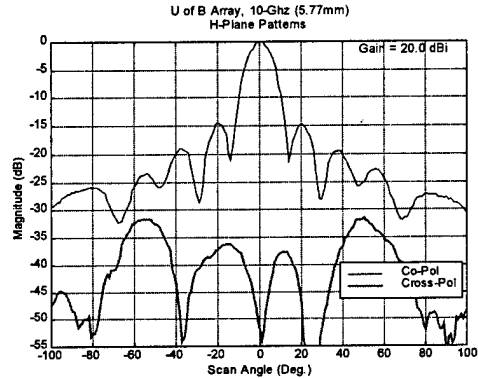
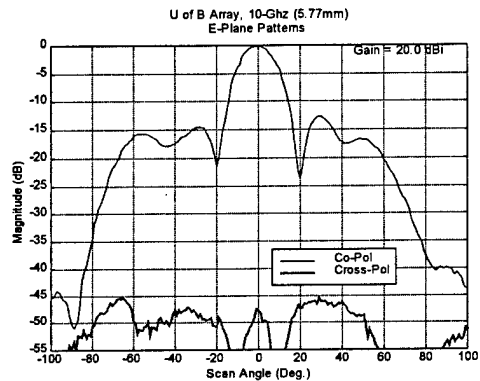
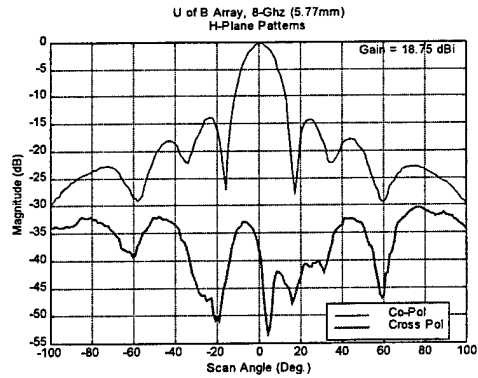
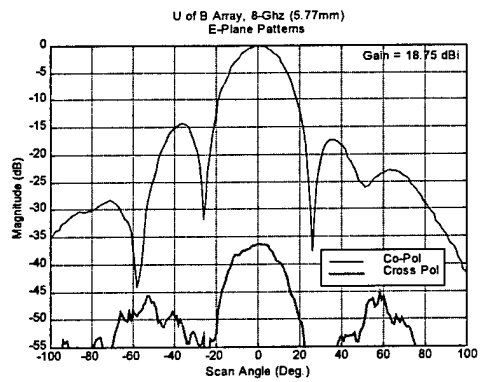


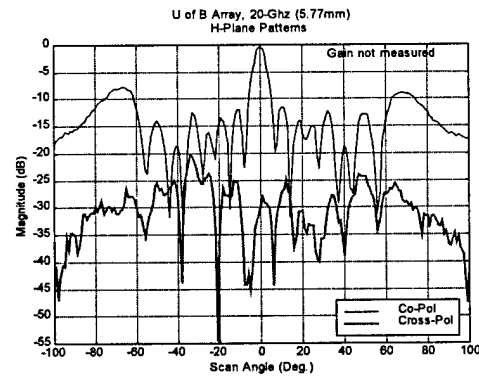
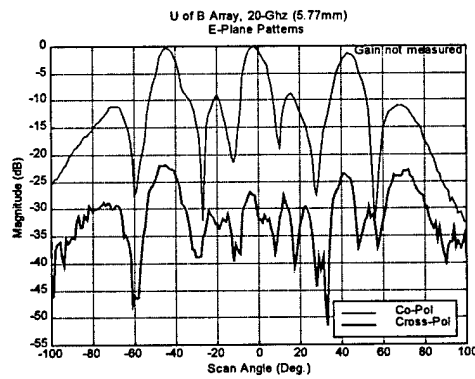
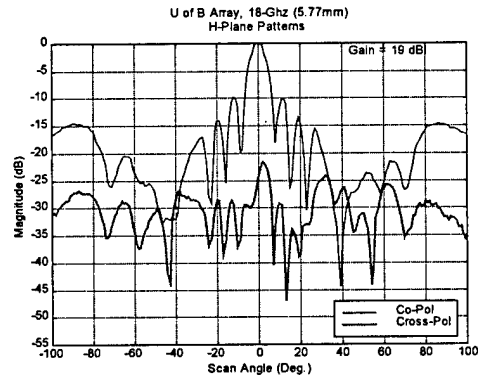
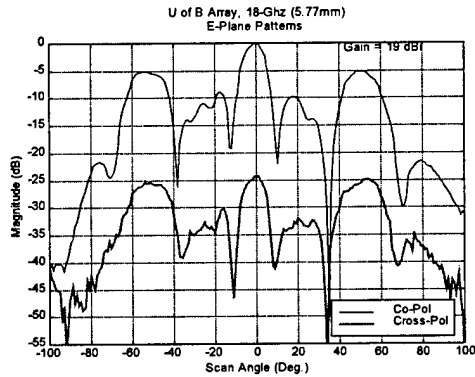
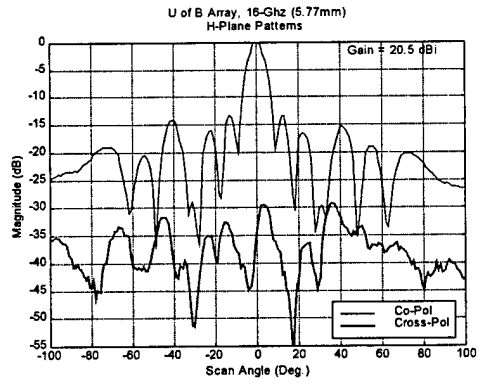
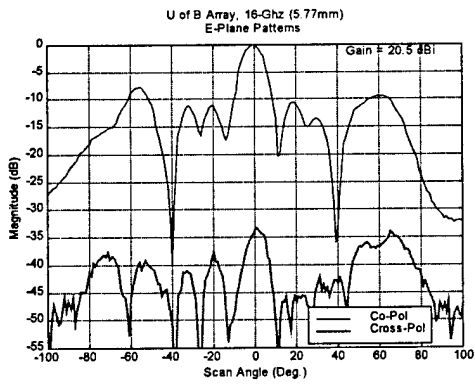
Note:
 - The AUT is at the origin of the far field spherical co-ordinate system.
 - Ludwig's 3' definition of polarization is used.
 - Scan Angle= θ

E-Plane Patterns ($\phi = 90^\circ$)

H-Plane Patterns ($\phi = 0^\circ$)



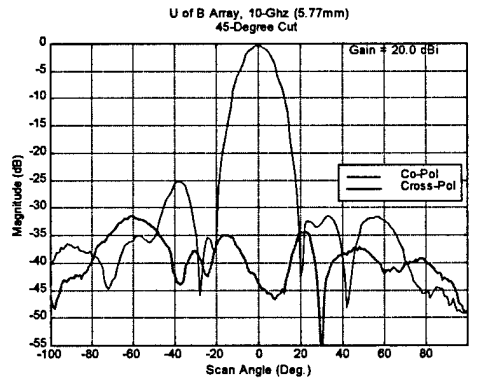
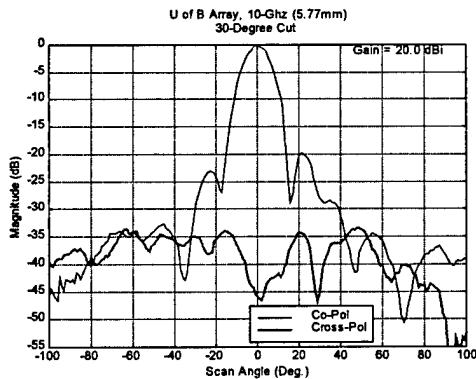
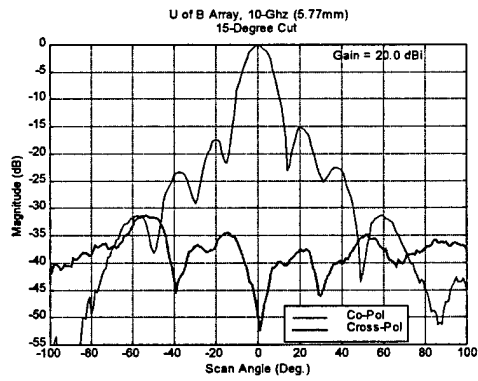
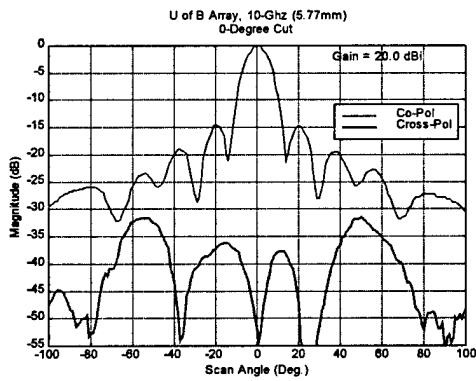
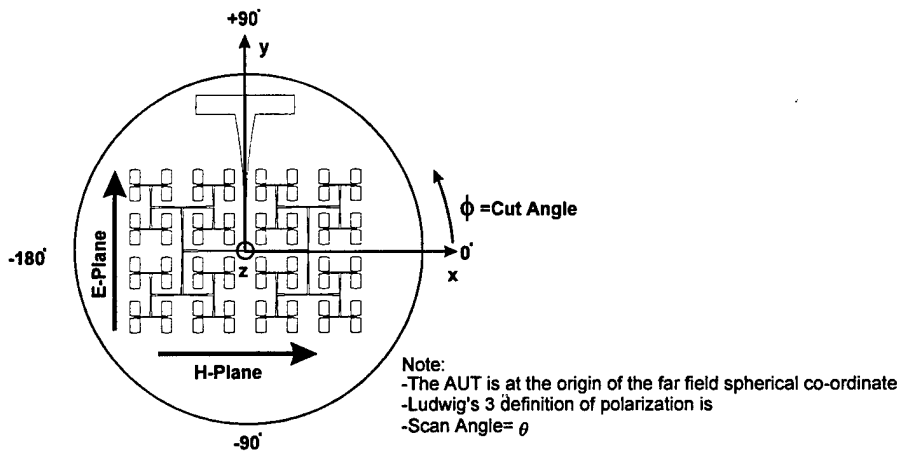


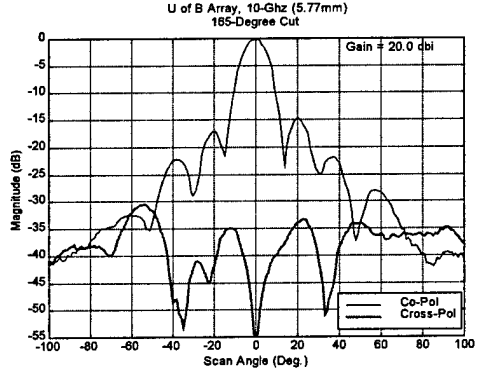
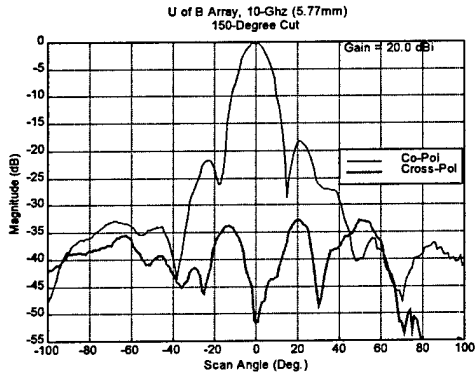
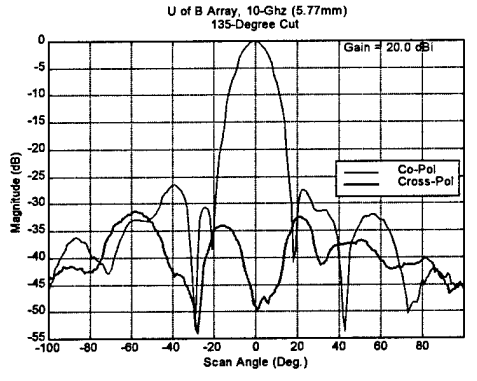
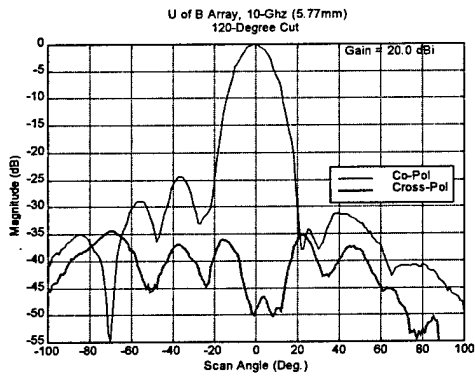
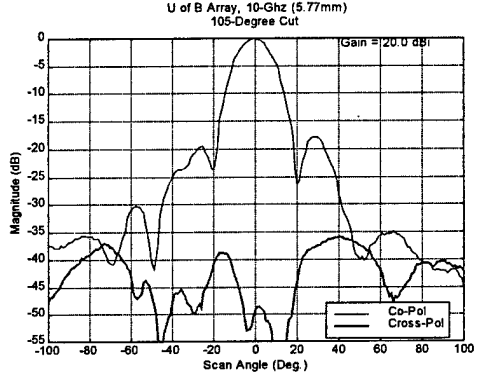
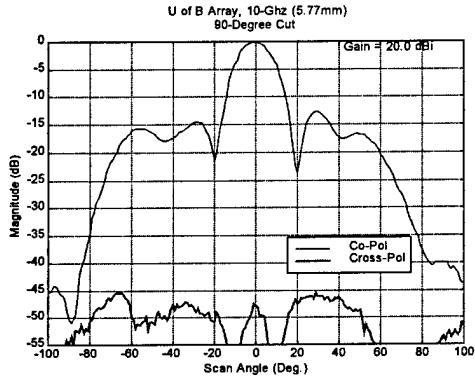
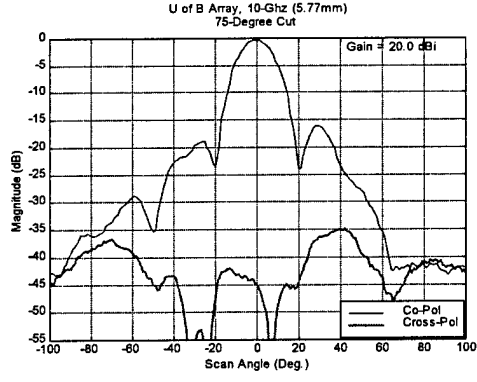
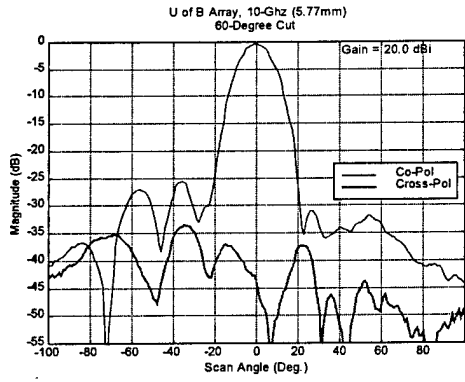


APPENDIX F *U OF B* ARRAY

(5.77MM) *VARIOUS PATTERN CUTS*

AT 10 GHZ

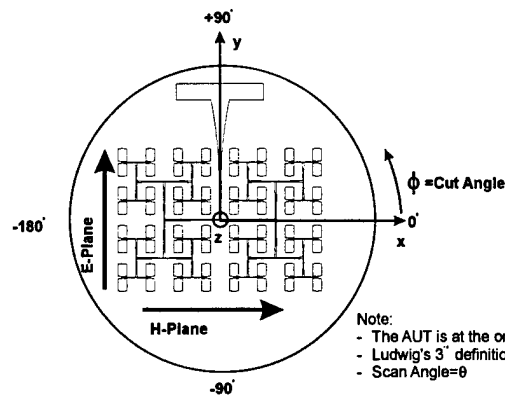




APPENDIX G OPTIMIZED ARRAY-1

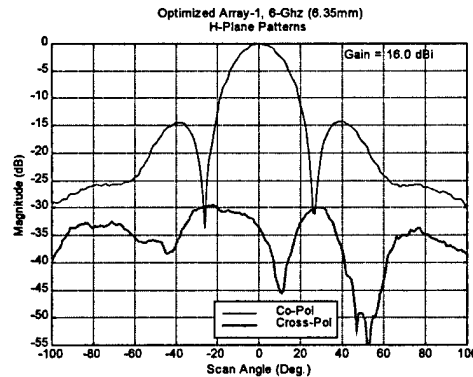
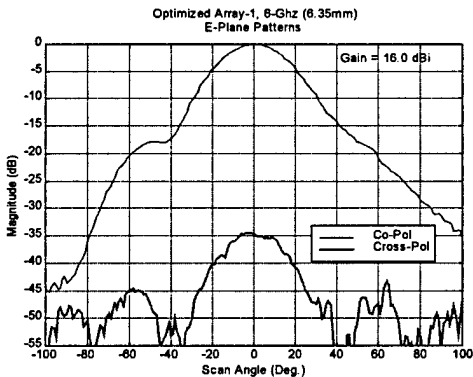
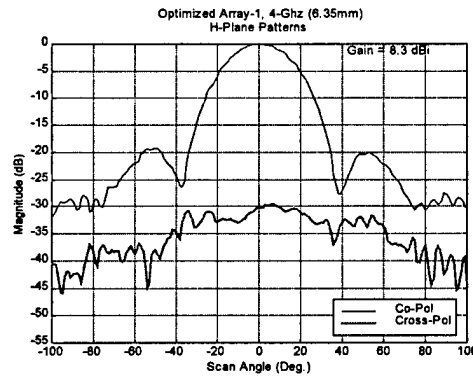
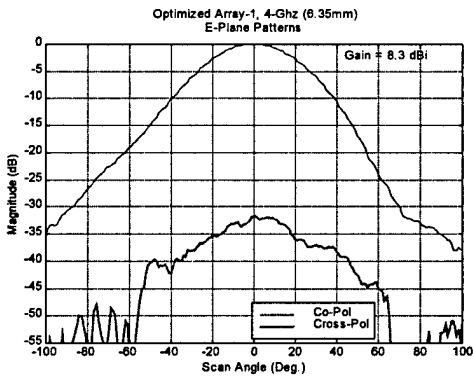
(6.35MM) E- AND H-PLANE CUTS

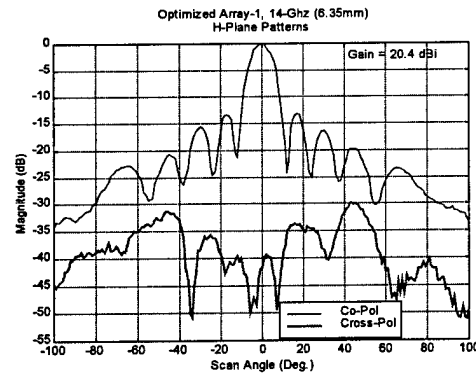
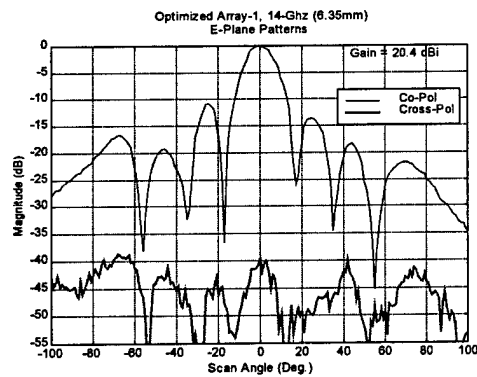
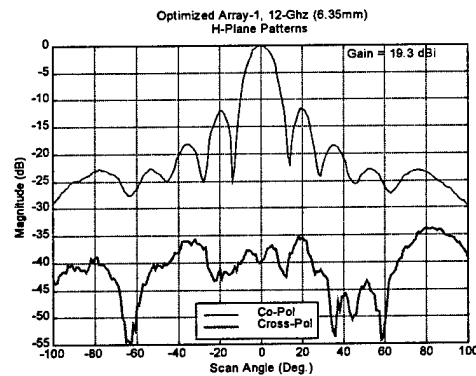
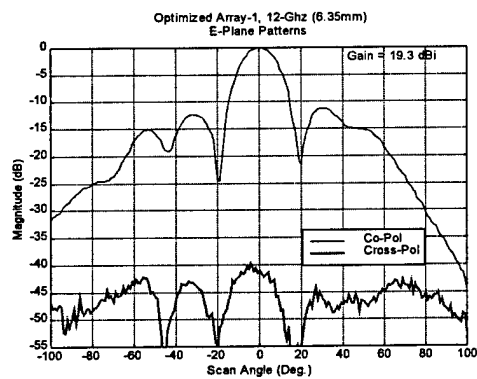
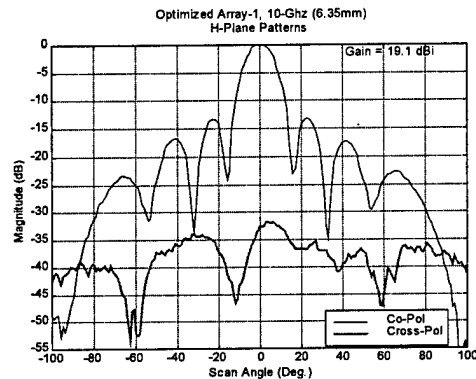
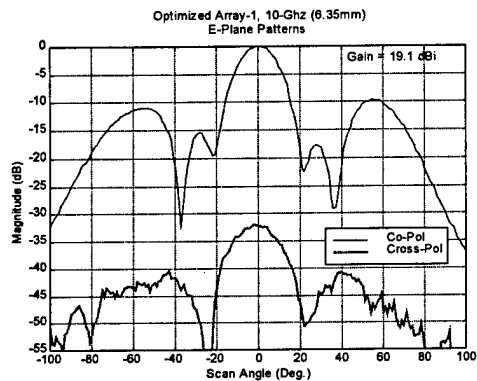
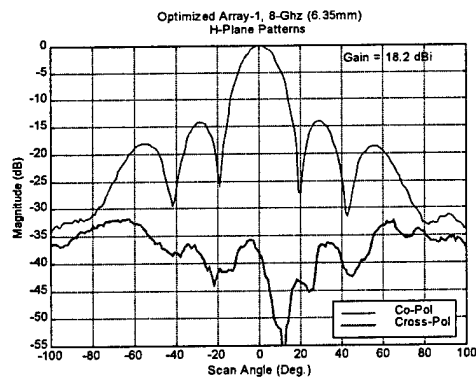
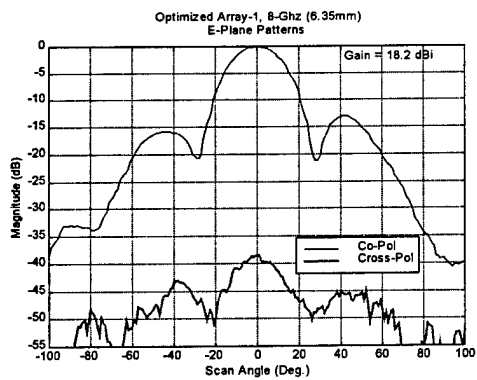
FOR VARIOUS FREQUENCIES

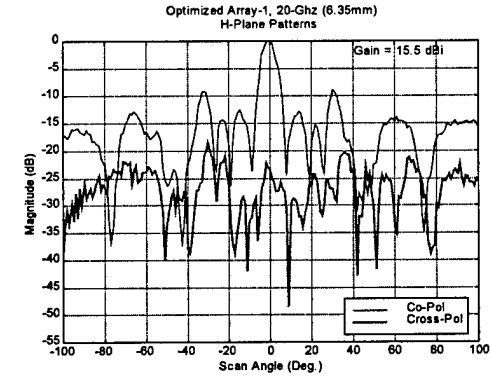
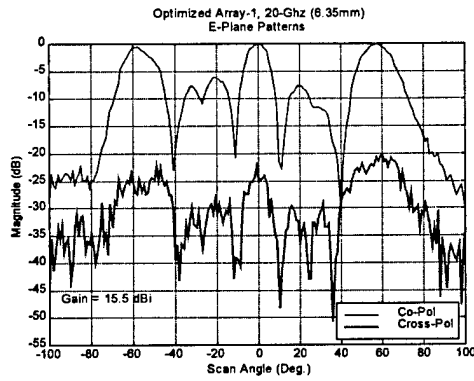
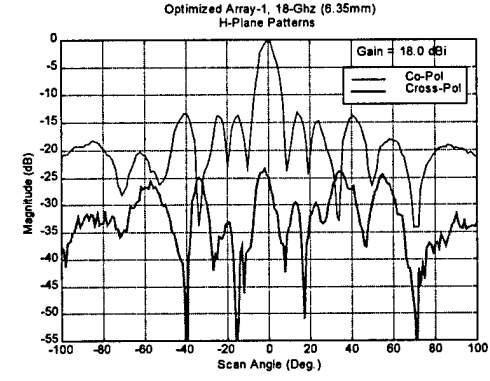
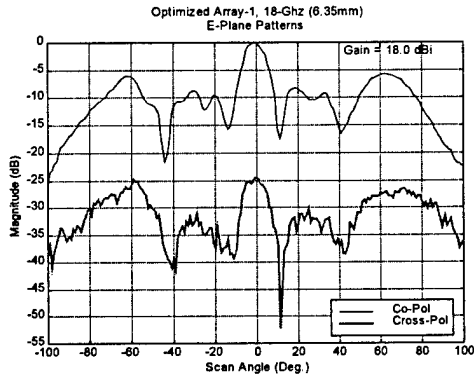
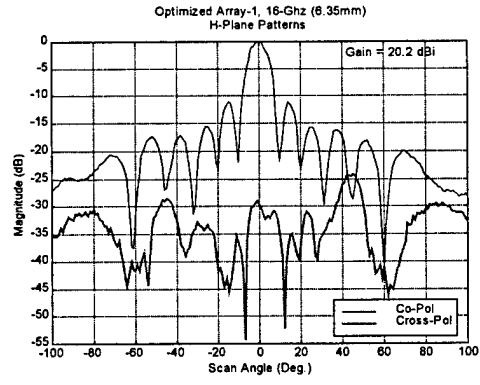
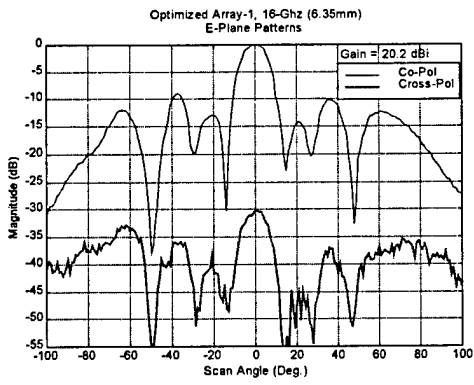


E-Plane Patterns ($\phi = 90^\circ$)

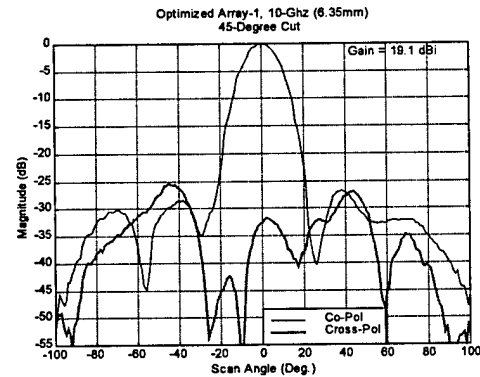
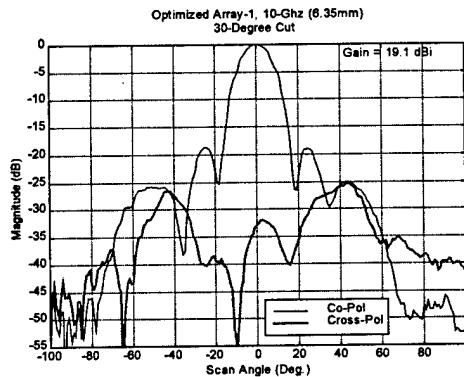
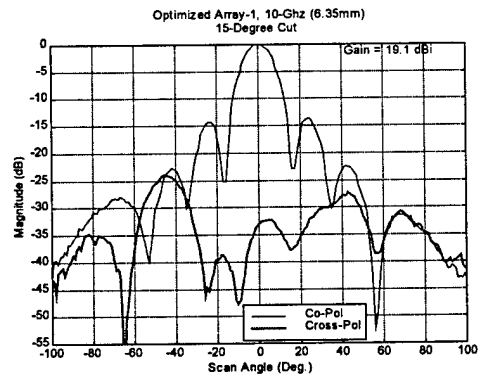
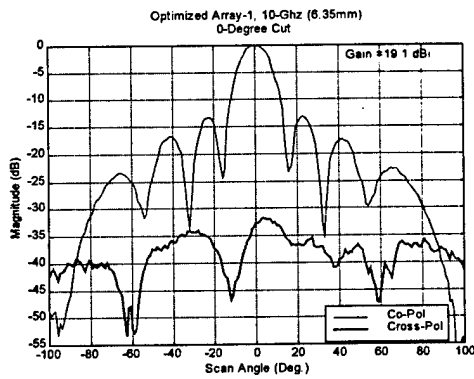
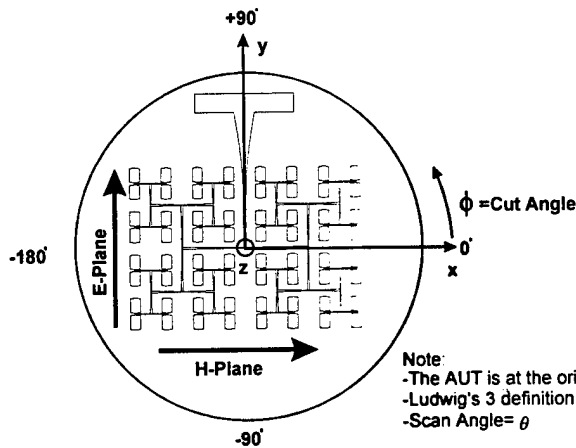
H-Plane Patterns ($\phi = 0^\circ$)

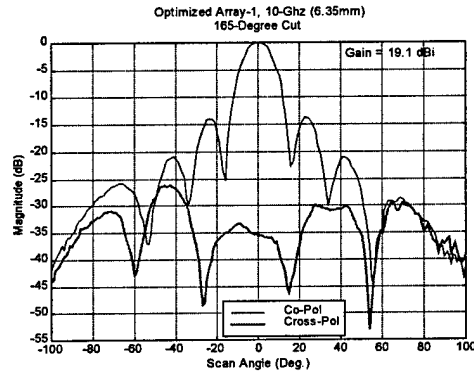
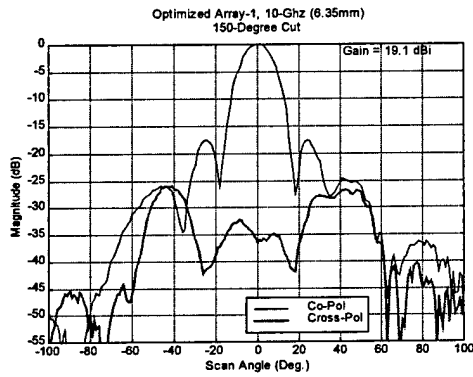
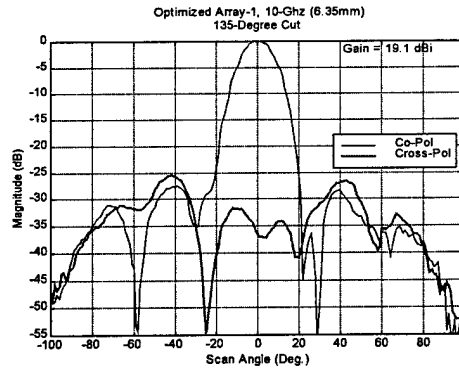
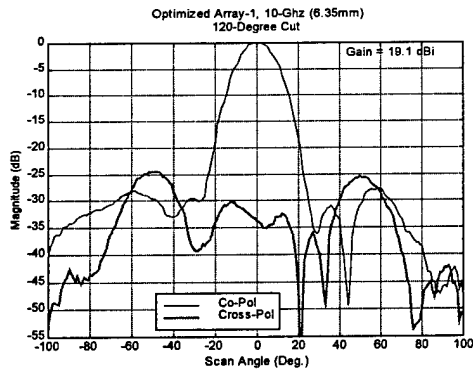
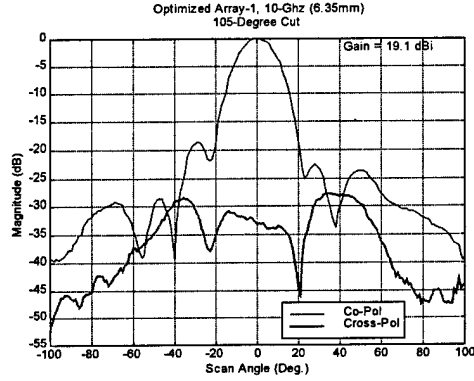
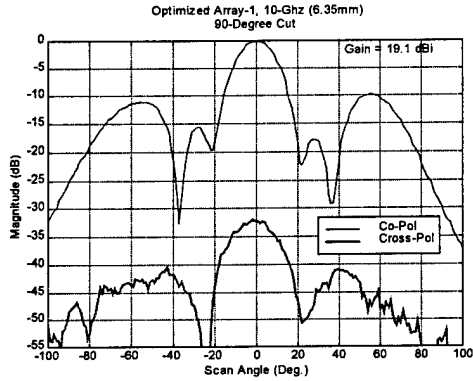
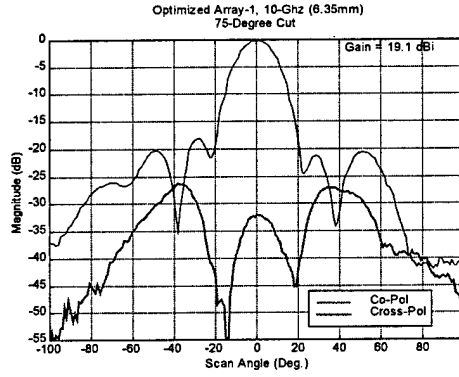
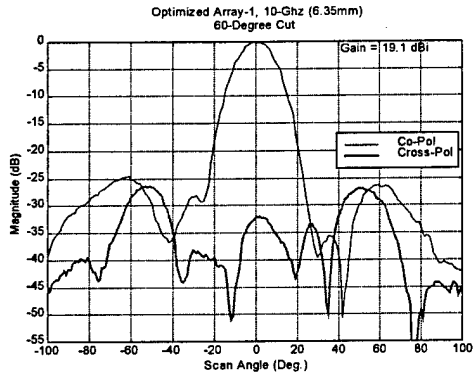






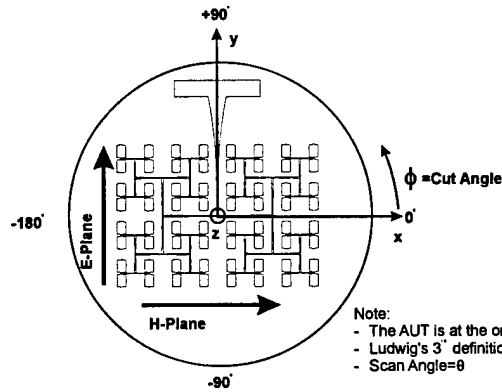
APPENDIX H OPTIMIZED ARRAY-1 (6.35MM) VARIOUS PATTERN CUTS AT 10 GHZ





APPENDIX I U OF B ARRAY (8.0 MM)

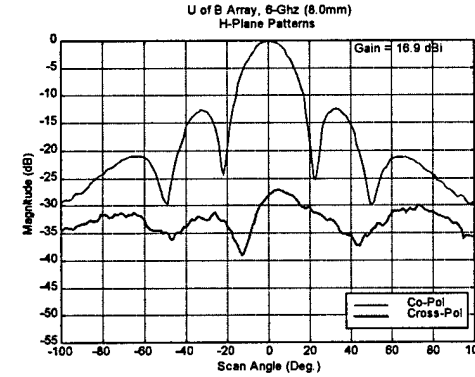
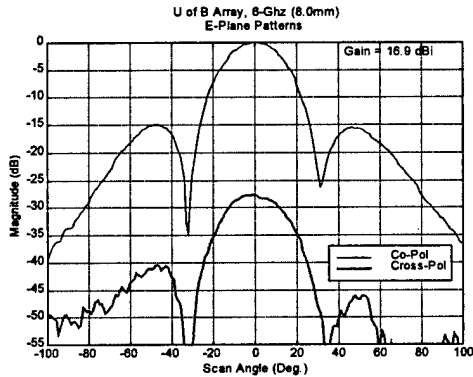
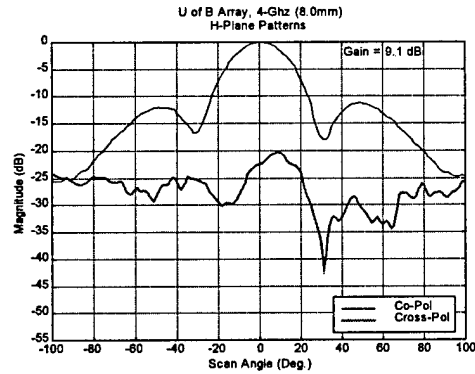
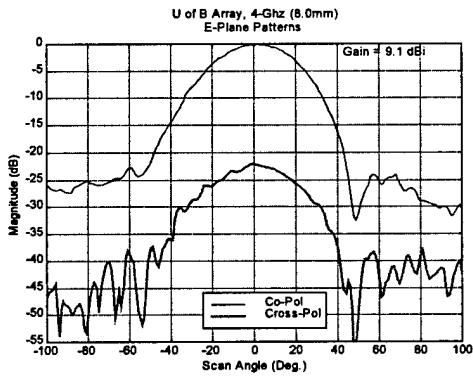
E- AND H-PLANE CUTS FOR VARIOUS FREQUENCIES

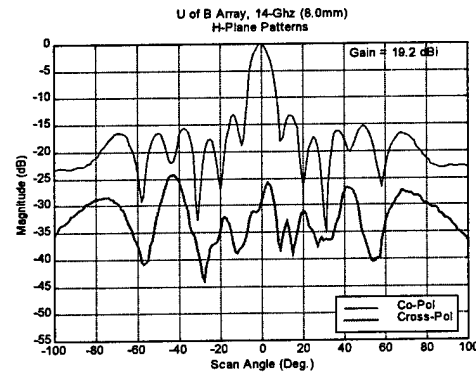
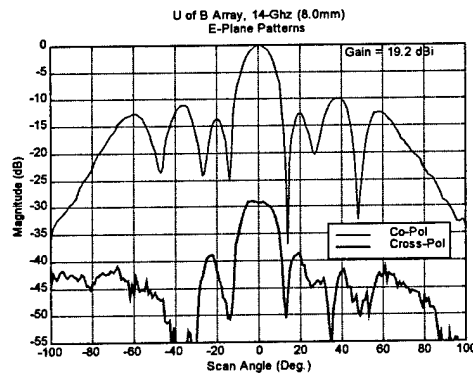
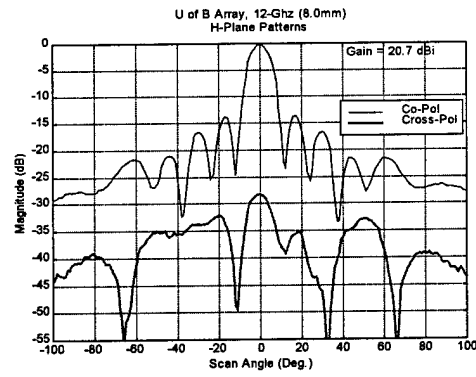
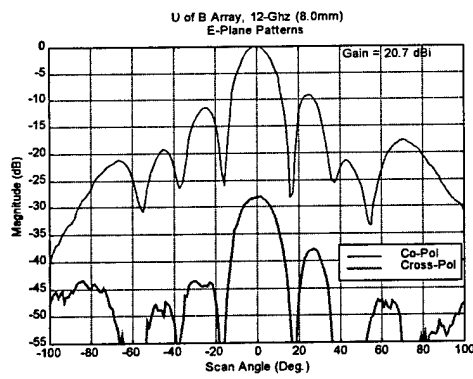
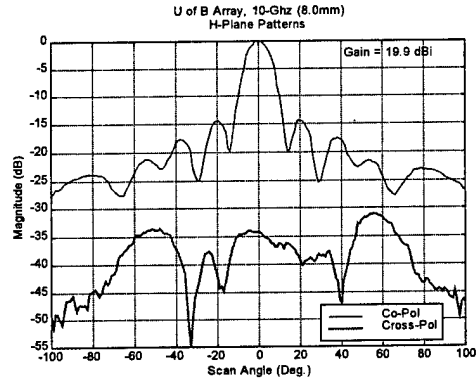
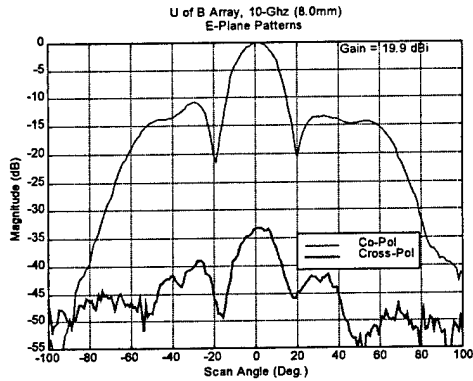
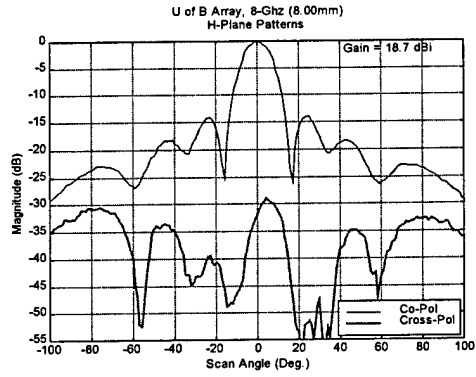
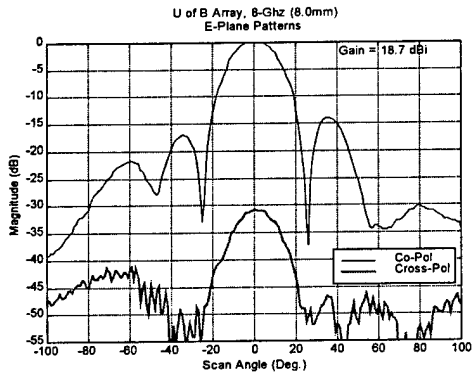


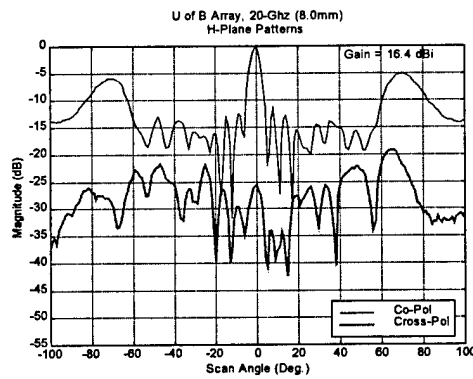
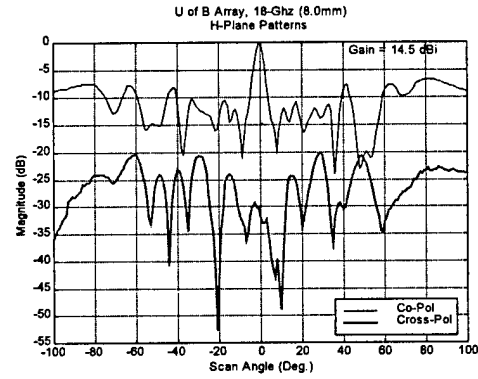
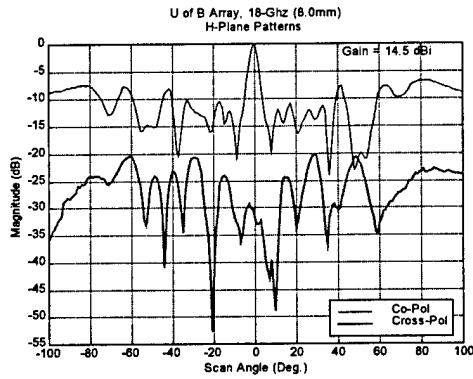
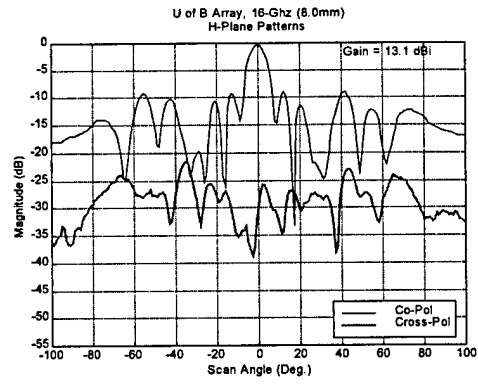
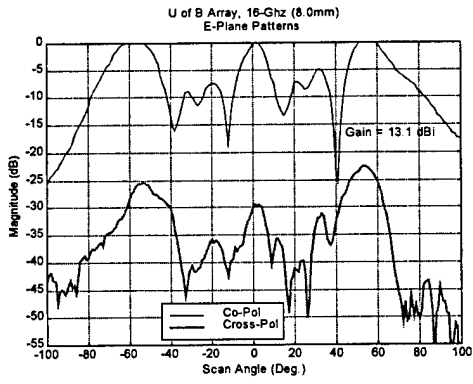
Note:
 - The AUT is at the origin of the far field spherical co-ordinate system.
 - Ludwig's 3rd definition of polarization is used.
 - Scan Angle=0

E-Plane Patterns ($\phi = 90^\circ$)

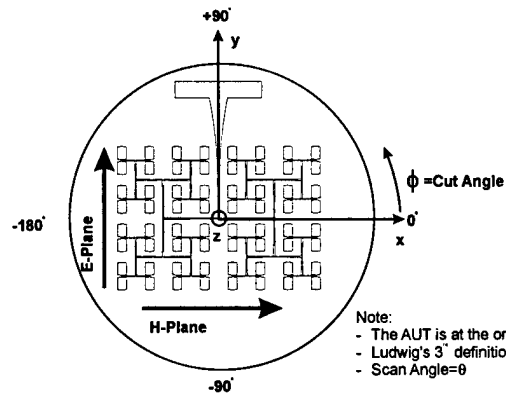
H-Plane Patterns ($\phi = 0^\circ$)





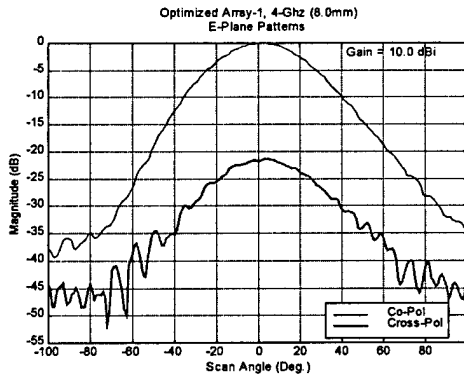


APPENDIX J OPTIMIZED ARRAY-1 (8.0MM) E- AND H-PLANE CUTS FOR VARIOUS FREQUENCIES

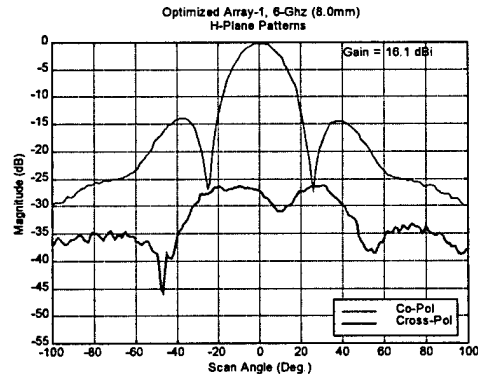
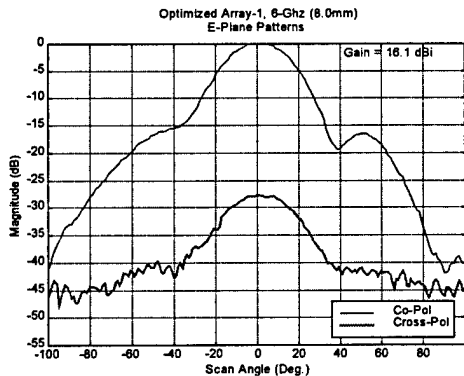
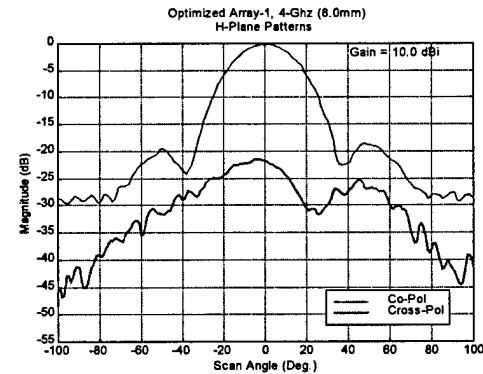


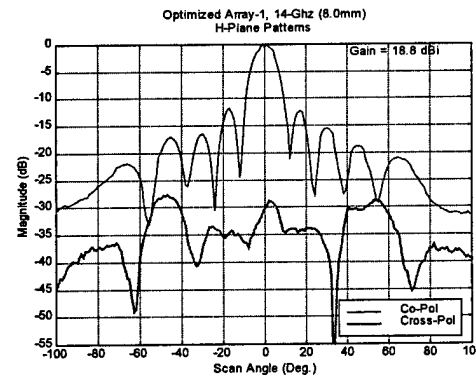
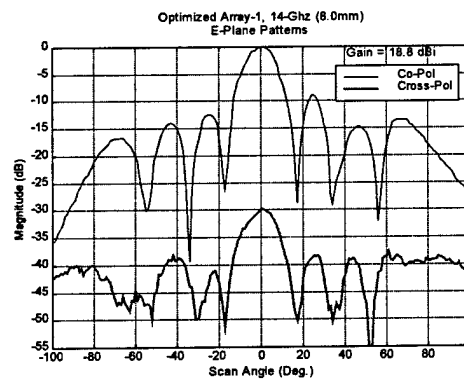
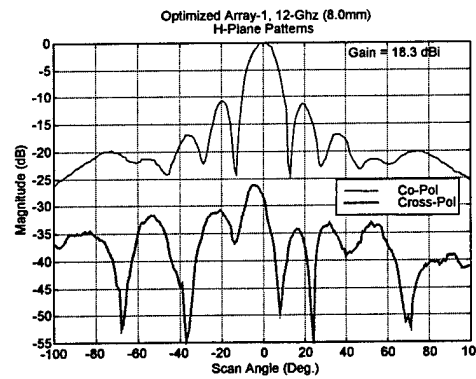
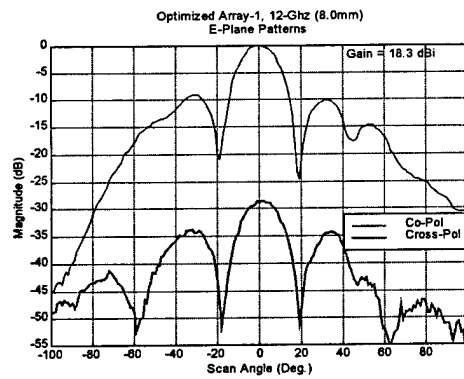
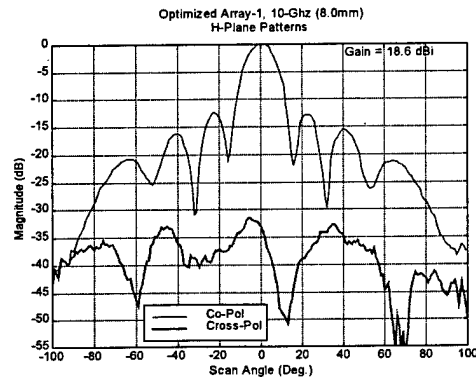
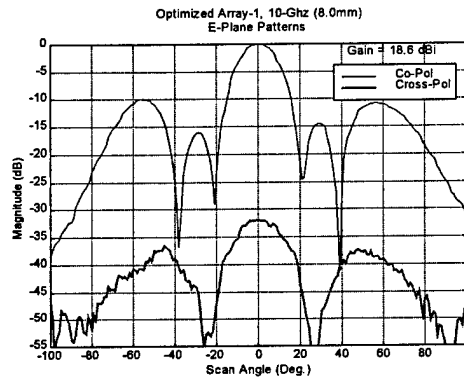
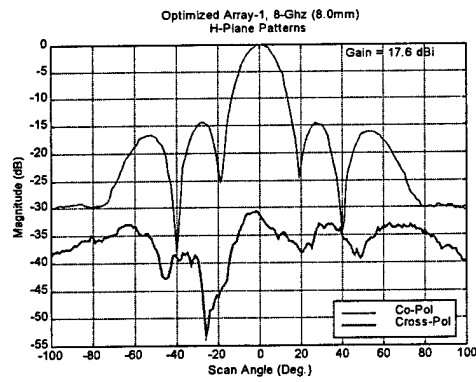
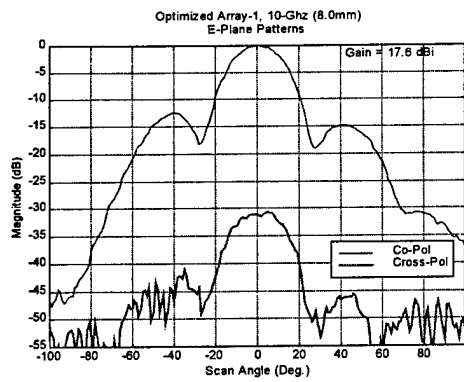
Note:
 - The AUT is at the origin of the far field spherical co-ordinate system.
 - Ludwig's 3rd definition of polarization is used.
 - Scan Angle=θ

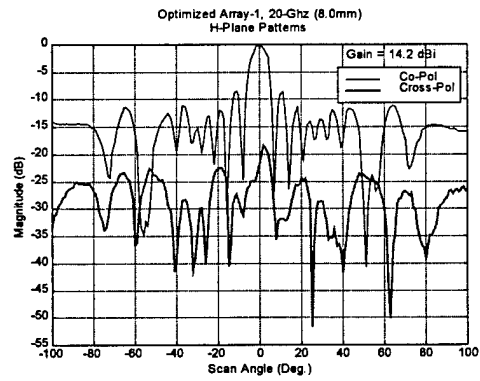
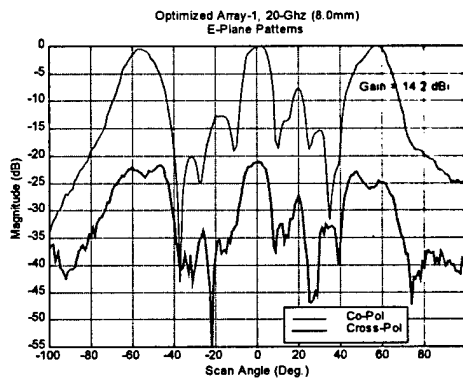
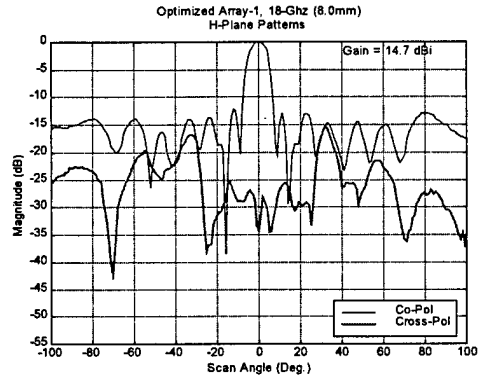
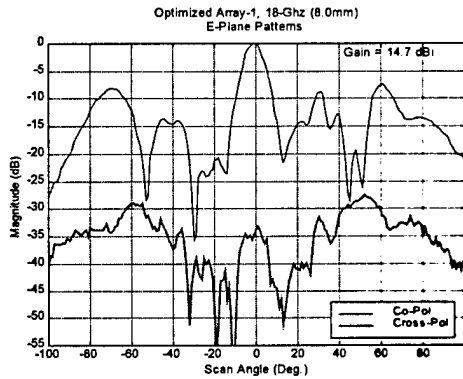
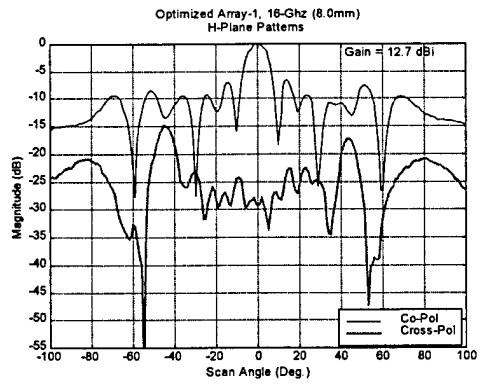
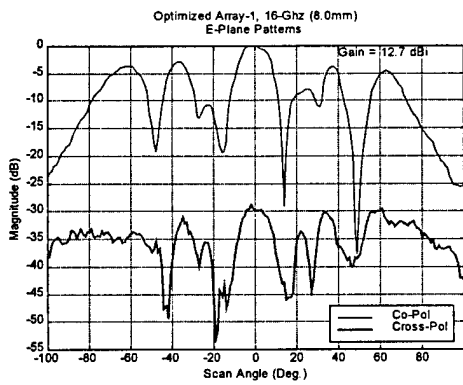
E-Plane Patterns ($\phi = 90^\circ$)



H-Plane Patterns ($\phi = 0^\circ$)







DOCUMENT CONTROL DATA

(Security classification of title, body of abstract and indexing annotation must be entered when the overall document is classified)

1. ORIGINATOR (the name and address of the organization preparing the document. Organizations for whom the document was prepared, e.g. Establishment sponsoring a contractor's report, or tasking agency, are entered in section 8.) <p style="text-align: center;">Royal Military College of Canada</p>		2. SECURITY CLASSIFICATION (overall security classification of the document, including special warning terms if applicable) <p style="text-align: center;">UNCLASSIFIED</p>	
3. TITLE (the complete document title as indicated on the title page. Its classification should be indicated by the appropriate abbreviation (S,C or U) in parentheses after the title.) <p style="text-align: center;">Design and Optimization of a Wideband Printed-Dipole Array (U)</p>			
4. AUTHORS (Last name, first name, middle initial) <p style="text-align: center;">Duffley, B.G., Morin, G.A., Antar, Y.M.M.</p>			
5. DATE OF PUBLICATION (month and year of publication of document) <p style="text-align: center;">November 1999</p>	6a. NO. OF PAGES (total containing information. Include Annexes, Appendices, etc.) <p style="text-align: center;">135</p>	6b. NO. OF REFS (total cited in document) <p style="text-align: center;">49</p>	
7. DESCRIPTIVE NOTES (the category of the document, e.g. technical report, technical note or memorandum. If appropriate, enter the type of report, e.g. interim, progress, summary, annual or final. Give the inclusive dates when a specific reporting period is covered.) <p style="text-align: center;">Technical Report</p>			
8. SPONSORING ACTIVITY (the name of the department project office or laboratory sponsoring the research and development. Include the address.) <p style="text-align: center;">Defence Research Establishment Ottawa</p>			
9a. PROJECT OR GRANT NO. (if appropriate, the applicable research and development project or grant number under which the document was written. Please specify whether project or grant) <p style="text-align: center;">5ca12</p>	9b. CONTRACT NO. (if appropriate, the applicable number under which the document was written)		
10a. ORIGINATOR'S DOCUMENT NUMBER (the official document number by which the document is identified by the originating activity. This number must be unique to this document.) <p style="text-align: center;">DREO TECHNICAL REPORT 1999-122</p>	10b. OTHER DOCUMENT NOS. (Any other numbers which may be assigned this document either by the originator or by the sponsor)		
11. DOCUMENT AVAILABILITY (any limitations on further dissemination of the document, other than those imposed by security classification) <input checked="" type="checkbox"/> Unlimited distribution <input type="checkbox"/> Distribution limited to defence departments and defence contractors; further distribution only as approved <input type="checkbox"/> Distribution limited to defence departments and Canadian defence contractors; further distribution only as approved <input type="checkbox"/> Distribution limited to government departments and agencies; further distribution only as approved <input type="checkbox"/> Distribution limited to defence departments; further distribution only as approved <input type="checkbox"/> Other (please specify):			
12. DOCUMENT ANNOUNCEMENT (any limitation to the bibliographic announcement of this document. This will normally correspond to the Document Availability (11). However, where further distribution (beyond the audience specified in 11) is possible, a wider announcement audience may be selected.) <p style="text-align: center;">Full unlimited</p>			

13. **ABSTRACT** (a brief and factual summary of the document. It may also appear elsewhere in the body of the document itself. It is highly desirable that the abstract of classified documents be unclassified. Each paragraph of the abstract shall begin with an indication of the security classification of the information in the paragraph (unless the document itself is unclassified) represented as (S), (C), or (U). It is not necessary to include here abstracts in both official languages unless the text is bilingual).

Modern satellite and mobile communications systems continue to push the bandwidth requirement of antenna subsystems. Printed microstrip architectures have been widely investigated and are attractive for their conformability, small size and cost effectiveness. While vigorous research activity over the past two decades has improved the bandwidth of microstrip elements to upwards of 30%, this may not be adequate for the future system demands of multipurpose antennas. In this report, printed-dipole arrays are investigated. They have the advantage of large bandwidths, up to 100%. Arrays of this type were described in the literature, however, no detailed analysis or measurements were provided. For this report, a 32-element wideband printed-dipole array was fabricated, analyzed from 4 to 20 Ghz and successfully optimized for improved bandwidth performance in excess of an octave. The important design parameters were extracted and their effect on performance were demonstrated.

14. **KEYWORDS, DESCRIPTORS or IDENTIFIERS** (technically meaningful terms or short phrases that characterize a document and could be helpful in cataloguing the document. They should be selected so that no security classification is required. Identifiers such as equipment model designation, trade name, military project code name, geographic location may also be included. If possible keywords should be selected from a published thesaurus. e.g. Thesaurus of Engineering and Scientific Terms (TEST) and that thesaurus-identified. If it is not possible to select indexing terms which are Unclassified, the classification of each should be indicated as with the title.)

Phased arrays, wideband arrays, printed-dipole arrays

The Defence Research
and Development Branch
provides Science and
Technology leadership
in the advancement and
maintenance of Canada's
defence capabilities.

Leader en sciences et
technologie de la défense,
la Direction de la recherche
et du développement pour
la défense contribue
à maintenir et à
accroître les compétences
du Canada dans
ce domaine.



www.crad.dnd.ca

